The role of Breast Cancer Antiestrogen Resistance 3 (BCAR3) in breast tumor cell adhesion and motility

Ashley Lauren Wilson
Aberdeen, Maryland

M.S., University of Virginia, 2010
M.S., University of Maryland, Baltimore County, 2007
B.S., University of Maryland, Baltimore County, 2006

A Dissertation presented to the Graduate Faculty
of the University of Virginia in Candidacy for the Degree of
Doctor of Philosophy

Department of Microbiology, Immunology and Cancer Biology

University of Virginia
May, 2015

ABSTRACT

The 5-year survival rate for patients diagnosed with metastatic breast cancer is only 25%. As we move further into the era of personalized medicine, it is critical that we gain a better understanding of the molecular drivers and cell signaling pathways that underlie breast tumor progression and metastasis in order to improve patient survival. The adaptor molecule Breast Cancer Antiestrogen Resistance 3 (BCAR3) functions in cellular processes that contribute to tumor cell adhesion, motility and invasion. Data presented in this thesis demonstrate that BCAR3 localizes to adhesions, promotes Rac1 activity and drives several critical facets of cell motility in invasive breast tumor cells, including membrane protrusion and adhesion disassembly. Interestingly, BCAR3-mediated adhesion disassembly was found to be contingent on its ability to interact with its well-established binding partner, the adaptor molecule $p130^{Cas}$ (Cas). The requirement for BCAR3 in driving this pro-migratory phenotype was underscored by the fact that, when BCAR3 was selectively depleted from invasive breast tumor cells, the cells failed to migrate/invade efficiently or respond properly to growth factor stimuli. Instead, RhoA signaling predominated under these conditions, as evidenced by an increase in RhoA-mediated tension, ROCK-mediated phosphorylation of myosin light chain II, the presence of actin-rich stress fibers, and large, stable ROCK/mDia1-dependent focal adhesions. Together, these data establish that BCAR3 functions as a positive regulator of actin cytoskeletal remodeling and adhesion disassembly in invasive breast tumor cells through its ability to influence the balance between Rac and Rho signaling. Furthermore, while disruption of BCAR3/Cas interaction had no effect on BCAR3 or Cas localization to adhesions, blockade of BCAR3/Cas phenocopied the loss of BCAR3 in that rates of adhesion disassembly were significantly reduced. This suggests that, when in complex with Cas in invasive breast cancer cells, BCAR3 may

drive Rac1 activity in adhesions, thus promoting breast tumor cell motility/invasion. Conversely, Rac/Rho reciprocity may be tipped in favor of RhoA signaling in the presence of a BCAR3 molecule that cannot bind to Cas, ultimately leading to deficient adhesion turnover and reduced cell motility.

BCAR3 expression, which is a robust biomarker of a cell signaling axis comprised of Cas and the non-receptor tyrosine kinase c-Src (Src), is upregulated in invasive, triple-negative breast cancer cell lines. Overexpression of BCAR3 in breast cancer cells promotes Src activity, invasive tumor cell behaviors and therapeutic resistance. However, BCAR3 protein expression in human breast tumors had not been reported. To determine the expression pattern of BCAR3 in human breast cancers, 74 human breast tumors and 8 normal breast tissue specimens were analyzed immunohistochemically for BCAR3 expression. BCAR3 protein levels were elevated in high-grade ductal carcinoma *in situ* (DCIS) and invasive ductal carcinoma (IDC) compared to normal mammary ductal epithelial cells. Moreover, BCAR3 was expressed across multiple subtypes of human breast cancer including triple-negative breast tumors. While BCAR3 protein levels did not correlate with tumor invasiveness or a particular breast cancer subtype, these studies revealed the immense heterogeneity of BCAR3 expression within each tumor subtype. Taking into account these findings, a re-evaluation of the therapeutic and prognostic potential of BCAR3 is put forth that addresses the possible implications of targeting BCAR3, including clinical resistance and the challenges that exist given the heterogeneity of its expression within and between patients. Finally, this work provides a foundation for future studies that aim to determine whether elevated BCAR3 protein levels drive breast tumor progression and/or correlate with clinical outcomes, and

whether they can serve as a biomarker to identify tumors that exhibit aggressive subtypes of DCIS and/or high Src activity.

TABLE OF CONTENTS

Abstract i

Table of Contents iv

List of Figures ix

List of Abbreviations xii

Acknowledgments xviii

Chapter 1. Introduction 1

1.1. Normal mammary gland architecture and breast cancer development 1

1.2. Breast cancer pathology and progression 4

1.3. Molecular profiling of human breast tumors 9

1.4. Tumor heterogeneity, personalized medicine and therapeutic challenges 10

1.5. Clinical resistance and metastasis 11

1.6. Cell motility: the basis of metastasis 14

1.6.1. Chemotaxis 15

1.6.2. Rho-family GTPases: master regulators of cell motility 18

1.6.3. Polarity and protrusion 21

1.6.4. Adhesion establishment and turnover 24

1.6.5. Adhesion maturation and tension 28

1.6.6. Rear retraction 30

1.7. Adhesion/adaptor proteins regulate Rac1 and RhoA 30

1.7.1. FAK 31

1.7.2. Paxillin 32

1.7.3. Src 35

1.7.4. Cas 36

1.7.5. BCAR3 40

1.8. Significance and overview 42

Chapter 2. BCAR3 promotes cell motility by regulating actin cytoskeletal and adhesion remodeling in invasive breast cancer cells 44

2.1. Introduction 44

2.2. Results 45

2.2.1. BCAR3 promotes membrane protrusiveness 45

2.2.2. BCAR3 promotes membrane protrusiveness through activation of Rac1 50

2.2.3. BCAR3 alters actin cytoskeletal and adhesion remodeling 53

2.2.4. Growth factor-induced cytoskeletal remodeling is regulated by BCAR3 . 58

2.2.5. RhoA-mediated contractility predominates upon loss of BCAR3..... 59

2.3. Discussion 67

2.3.1. Regulation of Rac1 by BCAR3 70

2.3.2. BCAR3 and breast cancer progression 72

Chapter 3. Direct interaction between BCAR3 and Cas promotes adhesion disassembly in invasive breast cancer cells 74

3.1. Introduction 74

3.2. Results 75

3.2.1. BCAR3 co-localizes with Cas in adhesions 75

3.2.2. Localization of BCAR3 to adhesions does not require direct interaction with Cas 75

3.2.3. Direct interaction between BCAR3 and Cas is required for efficient dissociation of BCAR3 from adhesions 78

3.2.4. BCAR3 promotes adhesion disassembly via its direct interaction with Cas 88

3.3. Discussion 96

3.3.1. BCAR3/Cas interactions are required for efficient BCAR3-medicated adhesion disassembly 96

3.3.2. BCAR3/Cas complexes may regulate the molecular switch between adhesion turnover and maturation in invasive breast cancer cells 100

3.3.3. When and where is BCAR3 present along the adhesion continuum? ... 101

Chapter 4. BCAR3 protein levels are upregulated in multiple subtypes of human breast cancer 104

4.1. Introduction 104

4.2. Results 106

4.2.1. BCAR3 protein levels are upregulated in tumor cells compared to normal ductal epithelial cells 106

4.2.2. BCAR3 is expressed across multiple subtypes of human breast cancer 116

4.2.3. BCAR3 protein is expressed at the highest levels within regions of high-grade DCIS 116

4.2.4. BCAR3 protein levels are not altered in response to varying matrix rigidity 119

4.3. Discussion 122

4.3.1. BCAR3 protein levels correlate with high-grade DCIS 127

4.3.2. Heterogeneity of BCAR3 protein expression in human breast cancer .. 129

4.3.3. Is BCAR3 a good therapeutic target for breast cancer? 130

Chapter 5. Perspectives 133

5.1. Do BCAR3/Cas complexes exist in 3D adhesions and what function do they serve in 3D cell motility/invasion? 134

5.1.1. Adhesion and motility in 3D 134

5.1.2. Future studies: Visualizing BCAR3 and Cas in 3D adhesions 136

5.1.3. Future studies: BCAR3/Cas complexes and regulation of Rac/Rho signaling in 3D 139

5.1.4. Future studies: BCAR3/Cas signaling in invadopodia 141

5.1.5. Future studies: In vivo mouse models of breast cancer 142

5.2. Is BCAR3 a developmentally regulated gene that is aberrantly re-expressed during breast tumor progression? 144

5.2.1. BCAR3: A regulatory switch for motility and invasion 144

5.2.2. BCAR3 as a potential regulator of the epithelial-mesenchymal transition (EMT) 147

5.2.3. BCAR3 and mammary gland development 148

5.3. Is BCAR3 a viable biomarker and/or therapeutic target for breast cancer? 150

5.3.1. BCAR3 as a therapeutic target 150

5.3.2. BCAR3 as a biomarker 153

Chapter 6. Materials and Methods 155

6.1. Antibodies and reagents 155

6.2. Plasmids and cloning strategies 155

6.2.1. L744E/R748E GFP-BCAR3 cloning 156

6.2.2. mCherry-Cas cloning 156

6.3. Cell culture 156

6.4. Small-interfering RNA and plasmid transfection 157

6.5. Immunoprecipitation, immunoblotting, and immunofluorescence 157

6.6. Live-cell imaging 158

6.6.1. Protrusion dynamics 158

6.6.2. Adhesion dynamics 159

6.7. GTP-bound GTPase pull-down assays 160

6.8. Immunohistochemistry 160

6.9. Collagen-coated polyacrylamide substrates 161

6.10. Statistical analysis 162

Appendix 1. Potential regulation of signaling pathways downstream of epidermal growth factor receptor by BCAR3 and Cas 163

A1.1. Introduction 163

A1.2. Results 165

A1.2.1. Cas may regulate ligand-induced EGFR auto-phosphorylation, while both BCAR3 and Cas may regulate AKT, but not ERK, signaling downstream of EGFR 165

A1.2.2. BCAR3 may regulate cofilin activity in invasive breast cancer cells 177

A1.2.3. BCAR3 may regulate p190RhoGAP phosphorylation in invasive breast cancer cells 181

A1.3. Discussion 184

List of References 187

LIST OF FIGURES

Figure 1.1. Normal mammary gland architecture and transition to invasive carcinoma 2

Figure 1.2. Pro-tumor features of the tumor microenvironment 7

Figure 1.3. The metastatic cascade 12

Figure 1.4. Breast tumor cell chemotaxis is mediated by tumor-associated macrophages 16

Figure 1.5. Regulation of Rho-family GTPases by GEFs and GAPs 19

Figure 1.6. Actin-driven protrusion, adhesion establishment, and adhesion maturation 22

Figure 1.7. The EGF-cofilin pathway 25

Figure 1.8. Structural features of FAK, paxillin and Src 33

Figure 1.9. Structural features of Cas and BCAR3 38

Figure 2.1. BCAR3 promotes membrane protrusiveness in breast cancer cells 46

Figure 2.2. BCAR3 overexpression increases migration distance 48

Figure 2.3. BCAR3 promotes Rac1 activity 51

Figure 2.4. BCAR3 alters actin organization and adhesion size and distribution in invasive breast cancer cells 54

Figure 2.5. BCAR3 regulates adhesion disassembly 56

Figure 2.6. BCAR3 regulates actin cytoskeletal and adhesion remodeling in response to growth factor 60

Figure 2.7. Loss of BCAR3 elevates RhoA activity and ROCK-mediated phosphorylation of MLC II 63

Figure 2.8. RhoA effector signaling mediates adhesion length in BCAR3-depleted invasive breast cancer cells 65

Figure 2.9. BCAR3 regulates the balance between Rac1 and RhoA signaling in invasive breast cancer cells 68

Figure 3.1. BCAR3 co-localizes with endogenous Cas in adhesions 76

Figure 3.2. Localization of BCAR3 to adhesions does not require direct interaction with Cas 79

Figure 3.3. BCAR3 localizes to vinculin-containing adhesions in Cas-/- MEFs 81

Figure 3.4. Direct interaction between BCAR3 and Cas is required for efficient dissociation of BCAR3 from adhesions 84

Figure 3.5. Direct interaction between BCAR3 and Cas is required for efficient dissociation of talin from adhesions 89

Figure 3.6. Direct interaction between BCAR3 and Cas is required for efficient dissociation of α-actinin from adhesions 93

Figure 3.7. BCAR3/Cas interactions control efficient BCAR3-mediated adhesion disassembly 97

Figure 4.1. BCAR3 expression is readily detectable in human breast cancer cells via immunohistochemistry 107

Figure 4.2. BCAR3 protein levels are upregulated in breast tumor cells compared to normal ductal epithelial cells 110

Figure 4.3. BCAR3 protein levels are upregulated in DCIS 112

Figure 4.4. BCAR3 protein levels are upregulated in invasive ductal carcinoma (IDC) 114

Figure 4.5. BCAR3 protein levels are expressed across multiple subtypes of human breast cancer 117

Figure 4.6. Highest BCAR3 protein levels are observed within regions of high-grade DCIS 120

Figure 4.7. Ductal epithelial cells adjacent to regions of high collagen content and desmoplastic stroma express high levels of BCAR3 123

Figure 4.8. BCAR3 protein levels in invasive breast cancer and non-tumorigenic mammary epithelial cells are unaltered in response to differing matrix rigidities 125

Figure A1.1. Effect of Cas and BCAR3 on EGFR signaling pathways; 30-minute EGF stimulation 166

Figure A1.2. Effect of Cas and BCAR3 on EGFR signaling pathways; 15-minute EGF stimulation 169

Figure A1.3. Effect of Cas and BCAR3 on EGFR signaling pathways; 5-30 minute EGF stimulation 172

Figure A1.4. Effect of Cas and BCAR3 on EGFR signaling pathways; 5-30 minute EGF stimulation with double Cas knockdown 175

Figure A1.5. BCAR3 may regulate cofilin activity in invasive breast cancer cells 179

Figure A1.6. BCAR3 may regulate p190RhoGAP phosphorylation in invasive breast cancer cells 182

LIST OF ABBREVIATIONS

Acceptor photobleaching fluorescence resonance energy transfer = apFRET

Actin-related protein 2/3 = ARP2/3

Adenosine triphosphate = ATP

Alpha-actinin = α-actinin

Amino-terminal = N-terminal

Analysis of variance = ANOVA

Arginine = Arg or R

Atypical ductal hyperplasia = ADH

Atypical lobular hyperplasia = ALH

Beta-mercaptoethanol = BME

Breast cancer antiestrogen resistance 1 = BCAR1 or Cas

Breast cancer antiestrogen resistance 3 = BCAR3

C-terminal domain = CTD

Calf intestinal alkaline phosphatase = CIP

Cancer stem cell = CSC

Cancer-associated fibroblast = CAF

Carboxy-terminal = C-terminal

Cas-null = Cas-/-

Cdc42/Rac interactive binding domain = CRIB

Cell derived matrix = CDM

Cellular Src kinase or c-Src = Src

Chinese hamster ovary = CHO

Circulating tumor cell = CTC

Colony-stimulating factor-1 = CSF-1

Colony-stimulating factor-1 receptor = CSF-1R

Cyan fluorescent protein = CFP

Dedicator of cytokinesis 180 = DOCK180

Deoxyribonucleic acid = DNA

Differential interference contrast = DIC

Doxycycline = Dox

Ductal carcinoma *in situ* = DCIS

Engulfment and cell motility = ELMO

Enhanced green fluorescent protein = EGFP

Epidermal growth factor = EGF

Epidermal growth factor receptor = EGFR or ERBB

Epithelial-mesenchymal transition = EMT

Essential light chain = ELC

Estrogen receptor = ER

Estrogen receptor-negative = ER^-

Estrogen receptor-positive = ER^+

Extracellular matrix = ECM

Extracellular signal-regulated kinase = ERK

Fetal bovine serum = FBS

Filamentous actin = F-actin

Fluorescein isothiocyanate = FITC

Fluorescence lifetime imaging microscopy = FLIM

Fluorescence recovery after photobleaching = FRAP

Fluorescence resonance energy transfer = FRET

Focal adhesion kinase = FAK

Focal adhesion-targeting = FAT

Four point one ezrin radixin moesin = FERM

G-protein coupled receptor kinase-interacting protein = GIT1

Glutamic acid = Glu or E

Green fluorescent protein = GFP

GTPase-activating protein = GAP

Guanine nucleotide exchange factor = GEF

Guanosine diphosphate = GDP

Guanosine triphosphate = GTP

Heavy chain = HC

Hematoxylin and eosin = H&E

HER2-amplified = $HER2^{+}$

HER2-negative = $HER2^{-}$

HER2/neu = HER2

Hydrogen chloride = HCl

Hypoxia-inducible factor = HIF

Immunohistochemistry = IHC

Invasive carcinoma = IC

Invasive ductal carcinoma = IDC

Leucine = Leu or L

Leucine/aspartate = LD

LIM kinase = LIMK

Lin-11 isL-1 mec-3 = LIM

Lobular carcinoma *in situ* = LCIS

Mammalian diaphanous 1 = mDia1

Mammary epithelial cell = MEC

Mammary intraepithelial neoplasia = MIN

Matrix metalloprotease = MMP

Messenger ribonucleic acid = mRNA

Mouse embryonic fibroblast = MEF

Mouse mammary tumor virus = MMTV

Myeloid-derived suppressor cell = MDSC

Myosin light chain = MLC

Neural precursor cell expressed, developmentally downregulated protein 9 = NEDD9

Non-muscle myosin II = myosin II

Novel SH2 domain-containing protein = NSP

Nucleation-promoting factor = NPF

$p130^{Crk\text{-}associated\ substrate}$ = Cas

p21 activated kinase = PAK

PAK interacting exchange factor = PIX

Pascal = Pa

Phenylalanine = Phe or F

Phosphatidylinositol-4,5-bisphosphate 3-kinase = PI3K

Phosphorylated myosin light chain = pMLC

Polyacrylamide gel electrophoresis = PAGE

Polyoma middle T oncoprotein = PyMT

Progesterone receptor = PR

Progesterone receptor-negative = PR^-

Proline-rich tyrosine kinase 2 = PYK2

Protein tyrosine phosphatase alpha = PTPα

Protein-protein interaction = PPI

Radioimmune precipitation assay = RIPA

Ras superfamily and interacting protein chimeric unit = Raichu

Receptor tyrosine kinase = RTK

Red fuorescent protein = RFP

Regulatory light chain = RLC

Regulatory T cell = T_{reg}

Rho-associated coiled coil-containing kinase = ROCK

Rhotekin binding domain = RBD

Rotations per minute = rpm

Selective estrogen receptor modulator = SERM

Serine = Ser or S

Short-hairpin ribonucleic acid = shRNA

Small-interfering ribonucleic acid = siRNA

Sodium chloride = NaCl

Sodium dodecyl sulfate = SDS

Src-binding domain = SBD

Src-family kinase = SFK

Src-homology = SH

Standard error of the mean = SEM

Substrate domain = SD

T-cell lymphoma invasion and metastasis 1 = Tiam1

Terminal duct lobular units = TDLU

Three-dimensional = 3D

Threonine = Thr or T

Total internal reflective fluorescence = TIRF

Transforming growth factor-beta = TGF-β

Triple-negative = TN

Triple-negative breast cancer = TNBC

Tumor microenvironment = TME

Tumor microenvironment for metastasis = TMEM

Tumor-associated macrophage = TAM

Tumor-node-metastasis = TNM

Two-dimensional = 2D

Tyrosine = Tyr or Y

Tyrosine-x-x-proline = YxxP

University of Virginia = UVA

Valine = Val or V

Vascular endothelial growth factor = VEGF

Wildtype = WT

Yellow fluorescent protein = YFP

ACKNOWLEDGMENTS

First and foremost, I dedicate this work to my family. Without their endless support and encouragement, this work would not have been possible. SMR, it is nearly impossible to articulate in words how much you mean to me (however, I will surely find a way to say it gracefully on 10/17/15, wink). You brighten every single one of my days with your smile, your sense of humor and a bottle of wine (obviously). I cannot wait for all of life's future adventures, but I find serenity in knowing that I will share them all with you. To my parents, Doug and Nancy, and my sister, Shannon, I love you all dearly. I do not think I would have made it through graduate school without your pump-up calls, love and support. I cannot thank you enough. Finally, to my dearest friends, near and far, you have been amazing cheerleaders. I look forward to many more movie/game nights, costume parties, and of course, tailgates! Go 'hoos!

I would also like to acknowledge my mentor, Dr. Amy Bouton. Thank you for your optimism and guidance when I needed them most. Your enthusiasm for research and science is inspiring. You have helped me to grow as a scientist, and have always encouraged me to think about the "burning" questions. I would further like to thank my thesis committee members, Drs. Tom and Sally Parsons, Dr. Ulrike Lorenz and Dr. Peggy Shupnik, for their wonderful feedback and advice throughout the years. I would also like to give special thanks to past and present members of the Bouton lab, especially Bri, Randy, the Michaels, Allison, Ryan and Keena. Thank you all for providing support and creating a fun and lighthearted work environment.

Finally, I would like to acknowledge Dr. Kristen Atkins for analyzing our human breast tumor samples and teaching me the fundamentals of clinical breast pathology, Dr. Pat Pramoonjago for performing our tissue IHC, and the laboratory of Dr. Rick Horwitz

(especially Kris, Jessica and Alexia) for providing countless reagents and assistance with live-cell TIRF imaging and data analysis.

CHAPTER 1: Introduction*

This chapter contains excerpts from Wilson et al., PLOS One, 2013

Breast cancer is a leading cause of cancer death among women, second only to lung cancer. Advancements in screening technology and mammography have made breast cancer one of the most frequently diagnosed cancers in women, with over 231,000 new cases of invasive breast cancer estimated in 2015 (American Cancer Society, 2015). Despite improved detection, approximately 40,000 women will succumb to the disease annually (American Cancer Society, 2015).

1.1 Normal mammary gland architecture and breast cancer development

Normal mammary gland architecture consists of an inner, luminal epithelial cell layer surrounded by a myoepithelial cell layer [1]. These structures are highly organized and polarized, such that the luminal epithelial cells face a hollow ductal lumen and the surrounding myoepithelial cells directly contact an encapsulating basement membrane (**Fig 1.1A and B**) [1, 2]. Branched ductal epithelial structures form terminal duct lobular units (TDLU), which produce breast milk [3]. Mammary glands reside in a rich stromal microenvironment consisting mainly of adipose and connective tissue, blood vessels, as well as extracellular matrix (ECM) proteins [1].

The steroid hormone estrogen is a critical regulator of normal mammary gland development and differentiation. Estrogen receptor (ER)-mediated signaling can become deregulated in cell types that comprise normal mammary glands, resulting in aberrant cell proliferation and the development of breast cancer [1]. There are two subtypes of the ER, ERα and ERβ, which are normally expressed at differing levels in mammary glands of pre- and post-menopausal women. In pre-menopausal women,

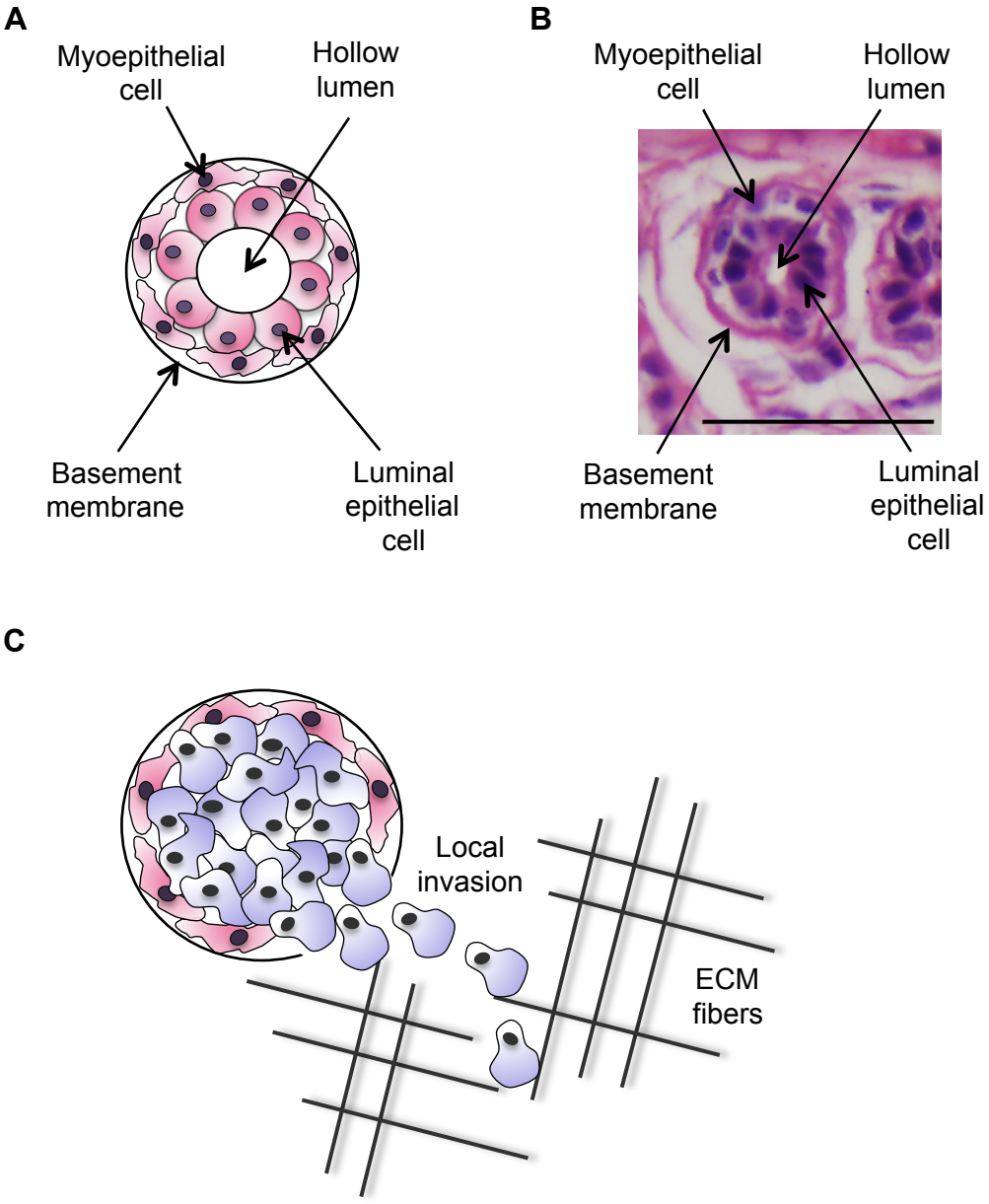
A
Myoepithelial cell
Hollow lumen
Basement membrane
Luminal epithelial cell
B
Myoepithelial cell
Hollow lumen
Basement membrane
Luminal epithelial cell
C
Local invasion
ECM fibers

Figure 1.1. Normal mammary gland architecture and transition to invasive carcinoma. (**A**) Schematic illustration of normal mammary gland architecture. A normal mammary gland consists of an inner, luminal epithelial cell layer surrounded by a myoepithelial cell layer. The luminal epithelial cells face a hollow ductal lumen and the surrounding myoepithelial cells directly contact an encapsulating basement membrane. Arrows point to these major structures. (**B**) Representative image of a mammary gland from a normal human breast tissue specimen immunohistochemically stained for H&E as described in the methods. Arrows point to the architectural features described in (A). Scale bar=50μm. (**C**) Epithelial cell invasion through the basement membrane marks the transition from *in situ* carcinoma to invasive carcinoma. This figure is adapted from Nelson and Bissell (2005) and Weigelt and Bissell (2008) [4, 5].

ERα is abundantly expressed in luminal epithelial cells, while ERβ is expressed in both epithelial and stromal cells [6]. In contrast, in post-menopausal women, ERα is expressed in less than 10% of luminal epithelial cells, while ERβ is expressed in greater than 50% of epithelial and stromal cells [6]. Knockout mice have helped to reveal the discrete roles of ERα and ERβ in normal mammary gland and breast tumor development. ERα knockout mice fail to develop differentiated mammary glands in response to estrogen and progesterone stimulation, while ERβ knockout mice form normal mammary glands [7]. These data underscore the necessity of ERα in normal mammary gland development. ERα plays an essential role in cell proliferation, while ERβ can function as an antagonist of ERα and is suggested to potentially have a tumor-suppressive role [6, 8].

1.2 Breast cancer pathology and progression

Historically, breast cancer progression has been pathologically defined by a discrete set of stages beginning with ductal epithelial cell hyperplasia, followed by *in situ* carcinoma, and finally invasive carcinoma [1, 9]. These stages have been studied extensively using mouse models of mammary tumor progression. For example, the mouse mammary tumor virus (MMTV)-polyoma middle T oncoprotein (PyMT) model of breast carcinogenesis defines 4 specific stages of breast tumor progression, including hyperplasia, adenoma/mammary intraepithelial neoplasia (MIN), early carcinoma and late carcinoma [10]. These stages mimic those observed in human disease. In humans, breast hyperplasia is defined by an over-proliferation of epithelial cells, resulting in lobules densely packed with cells and/or filling of the intraductal luminal space [11]. Although considered benign lesions, atypical ductal hyperplasia (ADH) and atypical lobular hyperplasia (ALH) describe the proliferation of “dysplastic” epithelial cells with

altered features, for example irregularly shaped nuclei with enlarged nucleoli [11]. These hyperplastic lesions are thought to transition to ductal or lobular carcinoma *in situ* (DCIS or LCIS), where tumor cells are still confined within ducts or lobules. Epithelial cell invasion through the basement membrane marks the transition from *in situ* carcinoma to invasive carcinoma (IC, **Fig. 1.1C**).

There are standard pathological criteria that pathologists use for breast cancer diagnosis and metastatic prognosis, including tumor size, histological grade, steroid receptor status and nodal status [12]. Diagnostic imaging (e.g. mammography, ultrasound, magnetic resonance imaging) is useful for assessing "tumor-node-metastasis" (or TNM) staging, which includes an evaluation of primary tumor size, axillary lymph node involvement, and metastasis [13, 14]. Tumor grade is typically determined from a core needle biopsy obtained from the primary tumor mass. Pathologists assign histological grade by evaluating three major features of a breast tumor: (1) nuclear shape/morphology, (2) mitotic activity, and (3) tubule formation. A numerical score is assigned to each of these features. When cells in the tumor exhibit irregularly shaped or enlarged nuclei, a higher score is assigned. Mitotic figures are a rough estimate of how quickly a tumor is proliferating. When a tumor exhibits a high number of mitoses, it is assigned a higher score. Tubule formation is an assessment of the level of differentiation of cells within the tumor. If less than 25% of the tumor exhibits cells forming ducts (or tubules), it is considered poorly differentiated and assigned a higher score. Finally, tumor grade is determined by adding up the numerical scores for all three of these features; a higher total score typically denotes a higher tumor grade.

Hormone receptor status is a primary criterion used when determining breast cancer prognosis and personalized therapeutic strategies. Generally, early-stage, low-grade breast tumors are ER-positive (ER^+). ER^+ tumors are attractive candidates for

hormone-targeted therapies, including selective estrogen receptor modulators (SERMs) (e.g. the antiestrogen tamoxifen) and aromatase inhibitors [15]. However, as breast cancer progresses, there is typically a decrease in ER expression accompanied by an increase in oncogenic growth factor receptor signaling [16]. In particular, the epidermal growth factor receptor (EGFR, also known as ERBB) family of receptor tyrosine kinases (RTKs) is frequently overexpressed in human breast cancer. Constitutive activation of EGFR and/or ERBB2 (also known as HER2/neu or simply HER2) promotes tumor cell proliferation and survival and drives tumor progression [17]. Small molecule inhibitors and monoclonal antibodies have been developed to target aberrant RTK signaling in advanced solid tumors, however many of these therapies have failed in clinical trials due to resistance [18].

While factors promoting breast tumor progression are often attributed to tumor cells themselves and their aberrant signaling/behaviors, it is important to acknowledge the emerging role of the tumor microenvironment (TME) in regulating progression and metastasis (**Fig 1.2**). For over the past decade, the TME has been shown to play both pro-tumor and anti-tumor roles. Recently, much attention has been given to the pro-tumor aspects of the TME that support primary tumor growth, dissemination and metastasis, as well as secondary outgrowth in distant metastatic niches [19]. Notable pro-tumor features of the TME include (1) tumor-associated macrophages (TAMs) and their local release of growth factors and cytokines to promote tumor cell growth, chemotaxis, motility and invasion, (2) cancer-associated fibroblasts (CAFs) and their ability to secrete new ECM components, (3) regulatory T cell and myeloid-derived suppressor cell infiltration to drive an immunosuppressive environment, and lastly (4) tumor vascularization as a result of stromal cells releasing pro-angiogenic factors (e.g.

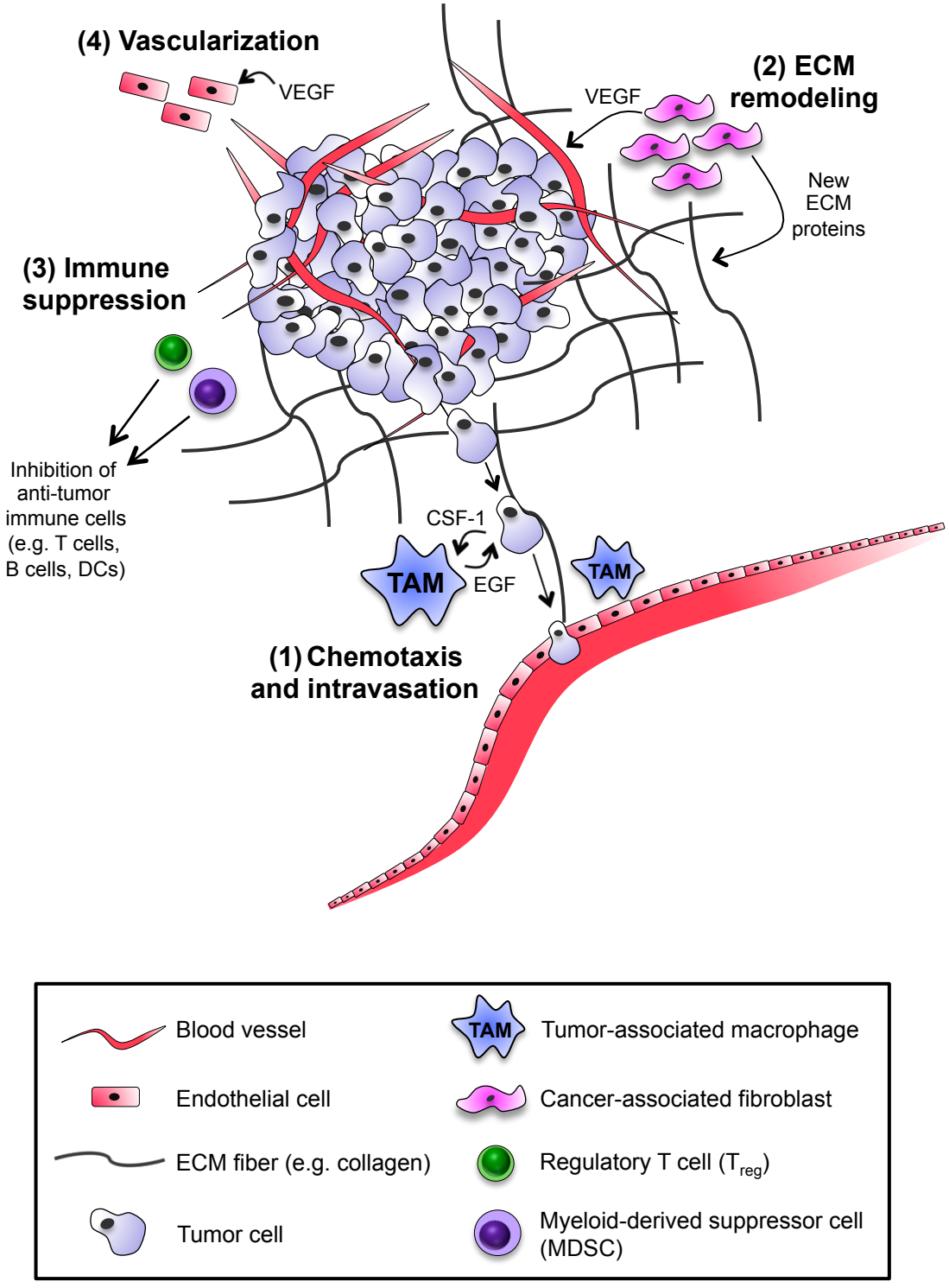
(4) Vascularization
VEGF
VEGF
(2) ECM remodeling
New ECM proteins
(3) Immune suppression
Inhibition of anti-tumor immune cells (e.g. T cells, B cells, DCs)
CSF-1
EGF
TAM
TAM
(1) Chemotaxis and intravasation
Blood vessel
Endothelial cell
ECM fiber (e.g. collagen)
Tumor cell
TAM
Tumor-associated macrophage
Cancer-associated fibroblast
Regulatory T cell (T_{reg})
Myeloid-derived suppressor cell (MDSC)

Figure 1.2. Pro-tumor features of the tumor microenvironment. Four major roles of the tumor microenvironment (TME) in promoting breast tumor progression and metastasis are shown. Specifically, (1) Tumor-associated macrophages (TAMs) promote breast tumor cell chemotaxis and intravasation through their local release of growth factors (e.g. EGF) and cytokines. In turn, breast tumor cells attract TAMs through secretion of CSF-1. (2) Cancer-associated fibroblasts (CAFs) promote ECM remodeling through secretion of new ECM components. (3) Regulatory T cell and myeloid-derived suppressor cell infiltration facilitates an immunosuppressive microenvironment. Finally, (4) tumors become highly vascularized as a result of stromal cells releasing pro-angiogenic factors (e.g. vascular endothelial growth factor, or VEGF). CAFs are a notable source of VEGF in the TME. This figure is adapted from Quail and Joyce (2013) [19].

vascular endothelial growth factor, or VEGF) [19]. Many aspects of this so-called "reactive tumor stroma" have become attractive targets for therapeutic intervention [20].

1.3 Molecular profiling of human breast tumors

While the pathological "stages" of breast cancer progression are fairly well defined, they are vastly oversimplified. Human breast cancer pathology is far more complex, and during the past decade a greater appreciation of breast tumor heterogeneity has emerged. Clinical evidence and molecular profiling have given rise to a new era of thought that breast cancer is not a single entity, rather it is an amalgam of multiple disease states [2, 21]. No one stage is necessarily a precursor for another. Instead breast cancer manifests as a continuum, where whole tumors may exhibit regions of both DCIS and IC.

The advent of gene microarray-based molecular profiling has helped to better define breast tumor subtypes. Most of this work has been led by Charles Perou's group, who have identified four "intrinsic" subtypes of human breast cancer, including (1) Luminal A, (2) Luminal B, (3) HER2-enriched and (4) Basal-like, as well as an unusually distinctive, normal breast-like group [22-24]. Luminal A and B subtypes are both ER^+ [25]. Luminal A tumors are regarded as having the best prognosis due to the fact that they are usually low-grade, express the highest levels of ER, and are predicted to be most susceptible to adjuvant hormonal therapy with tamoxifen [25-27]. Luminal B tumors tend to be more aggressive given they express lower levels of ER and are accompanied by additional mutations in tumor suppressor genes, e.g. p53, and Cyclin D1 amplification [25]. HER2-enriched tumors are also aggressive due to amplification and hyper-activation of the HER2 growth factor signaling cascade. HER2-amplified breast tumors are currently treated with anti-HER2 monoclonal antibodies in the clinic,

for example Trastuzumab and Pertuzumab [18, 28]. Lastly, the basal-like subtype of breast tumors tend to be histologically high-grade and are comprised mostly of triple-negative breast cancers (TNBC), owing to their lack of expression of ER, progesterone receptor (PR), and a lack of overexpression of HER2 [25, 29]. However, not all basal-like tumors are triple-negative. TNBC is notoriously difficult to treat because patients are not suitable candidates for endocrine therapy or trastuzumab, and while chemotherapy remains the standard-of-care for treatment of TNBC, most patients still have a poor clinical outcome [29]. Finally, claudin-low tumors comprise a distinct subset of TNBC. They express low levels of tight junction proteins (i.e. claudins 3, 4 and 7) as well as E-cadherin [30]. Claudin-low tumors are frequently associated with a poor prognosis given that they express molecular markers of epithelial-mesenchymal transition (EMT) and cancer stem cells, and exhibit immense immune cell infiltration [31].

1.4 Tumor heterogeneity, personalized medicine and therapeutic challenges

The inherent genetic signatures of different breast cancer subtypes hold great prognostic value. These genetic signatures (along with the standard parameters of tumor size, grade, hormone receptor and nodal status) can be used to better predict treatment response, relapse-free survival, and clinical outcome [32]. While significant advances have been made in molecular profiling, however, breast tumor heterogeneity proves to be a major therapeutic challenge. Many studies that have molecularly classified tumors use biopsy specimens from single tumors, which may not necessarily be an accurate representation of a larger cohort of tumors [33]. Furthermore, it is possible that within a single primary tumor, distinct regions of tumor cells can exhibit different genetic signatures, and this clonal diversity may alter drug sensitivity and result in clinical resistance [33]. In addition to clonal diversity, research has revealed the

unique role of cancer stem cells (CSCs) in contributing to tumor heterogeneity and therapeutic resistance. Cancer stem cells represent a rare population of undifferentiated, self-renewing cells that are suggested to have an intrinsic capacity to drive tumor progression and resistance [34]. Targeted therapies directed against CSCs aim to induce their differentiation and inhibit self-renewal [35].

1.5 Clinical resistance and metastasis

Clinical resistance of breast cancer can be *de novo* or acquired. *De novo* or "intrinsic" resistance refers to a complete failure to respond to a drug, while acquired resistance is marked by an initial therapeutic response followed by tumor progression over time [8]. Breast cancer resistance often manifests as local recurrence and/or distant metastasis. Metastatic disease is the result of a defined series of events including (1) tumor cell escape from the primary tumor mass and local invasion, (2) intravasation into the bloodstream and/or lymphatics, (3) tumor cell survival in the circulation, (4) arrest at a distant organ site and extravasation out of the bloodstream, and finally (5) colonization of tumor cells in the new metastatic niche to give rise to micro-metastases, which eventually develop into clinically detectable metastases (**Fig 1.3**) [36]. Distant metastases are considered incurable and are largely responsible for breast cancer patient mortality. In fact, the 5-year survival rate for patients with metastatic breast cancer compared to localized disease plummets from 99% to merely 25%; a staggering statistic (American Cancer Society, 2015).

A significant amount of work has contributed to our understanding of the molecular events underlying the reputed "invasion-metastasis cascade" described above [36]. This canonical model suggests metastasis is an "acquired" behavior of tumor cells and it may be many years before distant metastases arise post-treatment [12]. While

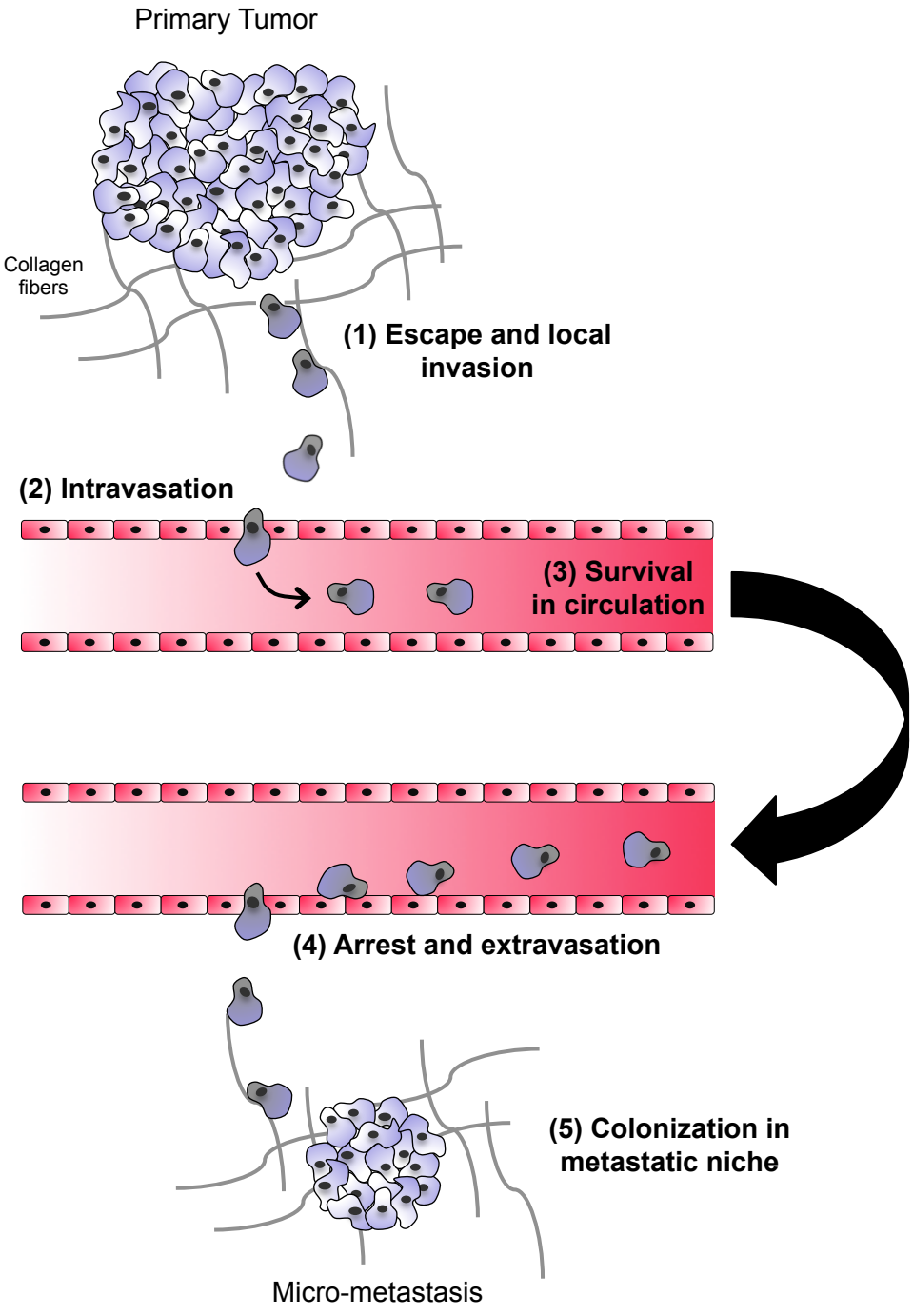
Primary Tumor
Collagen fibers
(1) Escape and local invasion
(2) Intravasation
(3) Survival in circulation
(4) Arrest and extravasation
(5) Colonization in metastatic niche
Micro-metastasis

Figure 1.3. The metastatic cascade. The metastatic cascade consists of five major steps including, (1) tumor cell escape from the primary tumor mass and local invasion, (2) intravasation into the bloodstream and/or lymphatics, (3) tumor cell survival in the circulation, (4) arrest at a distant organ site and extravasation out of the bloodstream, and finally (5) colonization of tumor cells in the new metastatic niche to give rise to micro-metastases. This figure is adapted from Valastyan and Weinberg (2011) [36].

this model is likely accurate for many patients, it is important to note that, like tumor progression, breast cancer metastasis is also heterogeneous [12]. Metastatic lesions can arise very early, even within a couple of years post-treatment. By genetically profiling primary human breast tumors, new models of metastasis have emerged suggesting that breast tumor cells may have an "inherent" capacity to disseminate and may express certain organ-specific pro-metastatic gene signatures [12, 36-41]. Furthermore, circulating tumor cells (or CTCs) can be detected in peripheral blood of both early- and late-stage breast cancer patients, and the presence of CTCs correlates with poor distant disease-free survival, poor breast cancer-specific survival and poor overall survival [42, 43].

1.6 Cell motility: the basis of metastasis

Cell motility is inherent to metastasis. High-resolution multiphoton microscopy has demonstrated that tumor cells use different types of cell motility *in vivo*. Studies have revealed tumor cells move either "collectively" as sheets or individually as single cells [44]. When tumor cells move individually, they exhibit amoeboid-like or mesenchymal motility. In amoeboid-like motility, tumor cells are only loosely attached to the ECM and move rapidly, whereas, in mesenchymal motility, polarized tumor cells can form focal adhesions and move more slowly [44]. Invasive breast tumor cells have been shown to adopt amoeboid-like motility *in vivo* when moving along collagen fibers within the microenvironment [45]. However, it has recently been demonstrated that, depending on cues within the microenvironment, breast tumor cells can also adopt a slower type of motility characterized by invasive protrusions polarized toward blood vessels [46]. Interestingly, only breast tumor cells that adopt this slower form of motility are capable of disseminating [46]. Despite these more recent *in vivo* findings, most of our mechanistic

understanding of cell adhesion and motility has been learned using two-dimensional *in vitro* models of mesenchymal cell motility.

Cell motility involves a complex, yet tightly regulated, series of events that promote remodeling of cellular adhesions and the actin cytoskeleton. Cells move directionally by first establishing protrusions toward a given stimulus. The actin-rich protrusions at the leading edge are then stabilized by nascent adhesions that are reinforced by tension generated by the actin crosslinking ability of myosin II. This rise in intracellular tension promotes adhesion disassembly in the rear and provides the force required to move cells along substrates within their microenvironment [47]. These major steps of cell motility, and their key molecular regulators, are described in further detail below.

1.6.1 Chemotaxis

Chemotaxis, or the directional movement of cells toward extracellular stimuli, has three major phases including (1) chemosensation, (2) polarization and (3) locomotion [48]. Tumor cell chemotaxis is mediated by the release of small signaling molecules, such as growth factors and chemokines, by different cell types within the tumor microenvironment [48]. Growth factor receptors and chemokine receptors expressed on the surfaces of tumor cells can detect and bind to these chemoattractant molecules. Ligand-bound receptors then activate downstream intracellular signaling cascades that lead to dynamic reorganization and polarization of the actin cytoskeletal network toward the extracellular cue. Perhaps the most well established growth factor involved in breast cancer cell chemotaxis is epidermal growth factor (EGF). John Condeelis' group has shown that EGF produced by TAMs can elicit invasive protrusions, i.e. invadopodia, in breast cancer cells expressing EGFR (**Fig 1.4**) [48-50]. Concurrently, invasive breast

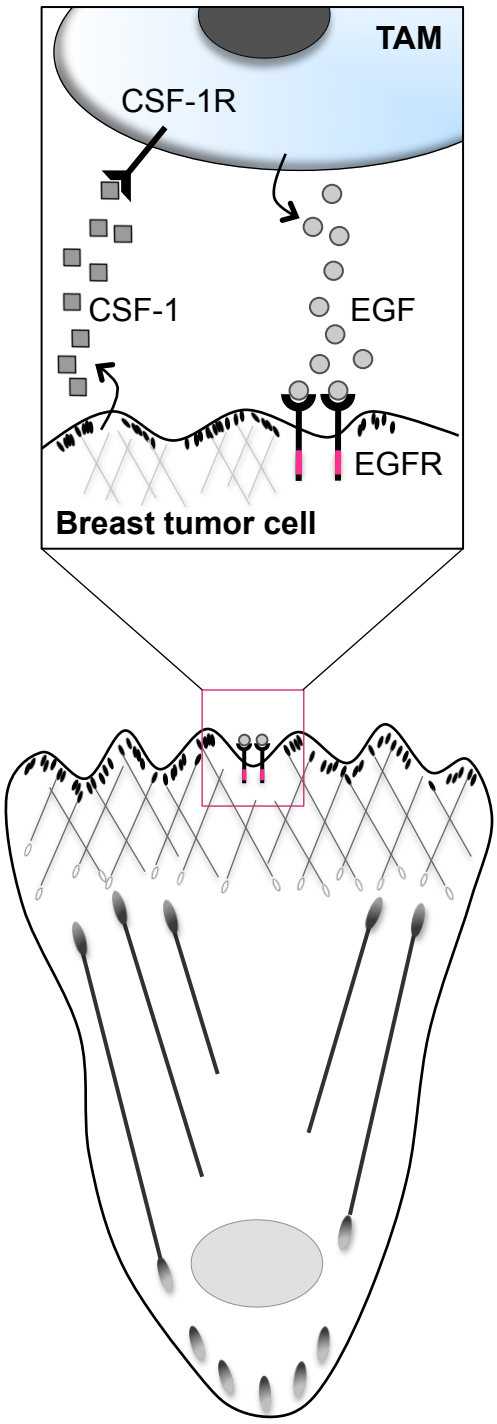
TAM
CSF-1R
CSF-1
EGF
EGFR
Breast tumor cell

Figure 1.4. Breast tumor cell chemotaxis is mediated by tumor-associated macrophages. Epidermal growth factor (EGF) produced by tumor-associated macrophages (TAMs) can elicit invasive protrusions in breast cancer cells expressing the EGF receptor (EGFR). Concurrently, invasive breast tumor cells attract macrophages by producing colony-stimulating factor-1 (CSF-1), which binds to the CSF-1 receptor (CSF-1R) expressed on TAMs. This paracrine-signaling loop between breast tumor cells and TAMs results in breast tumor cell polarization and chemotaxis. Schematic of migrating cell (bottom) adapted from Parsons *et al*. (2010) [51]; inset box (top) adapted from Roussos *et al*. (2011) [48].

cancer cells attract macrophages by producing colony-stimulating factor-1 (CSF-1), which binds to the CSF-1 receptor (CSF-1R) expressed on TAMs. This chemotactic "paracrine loop" between breast cancer cells and TAMs results in rapid, polarized migration of tumor cells along collagen fibers away from the primary tumor toward blood vessels [48, 50, 52]. Upon arrival at the endothelium, a "tumor microenvironment for metastasis" (or TMEM) consisting of polarized breast tumor cells, TAMs, and endothelial cells becomes established [52]. Within TMEM structures, TAMs promote tumor cell intravasation into the bloodstream, thus facilitating dissemination [52, 53]. Very recently, TMEMs have been shown to be good predictors of metastatic risk in human breast tumors [52, 54].

1.6.2 Rho-family GTPases: master regulators of cell motility

Rho-family GTPases function as molecular "switches" that control cell motility [55]. Two major types of proteins regulate Rho GTPases: guanine nucleotide exchange factors (GEFs) and GTPase-activating proteins (GAPs) (**Fig 1.5**). GEFs turn on Rho GTPases by facilitating exchange of GDP for GTP. In their GTP-bound form, Rho GTPases are considered active and able to interact with their downstream effector molecules [55]. Conversely, GAPs turn off Rho GTPases by promoting reversion of GTP back to GDP. Cdc42, Rac1 and RhoA are three well-established Rho GTPase family members with roles in cell polarity, actin cytoskeletal dynamics, tension and contractility. Biosensor studies indicate that all three are activated at the leading edge of protrusive cells and their coordination is critical for efficient motility [56].

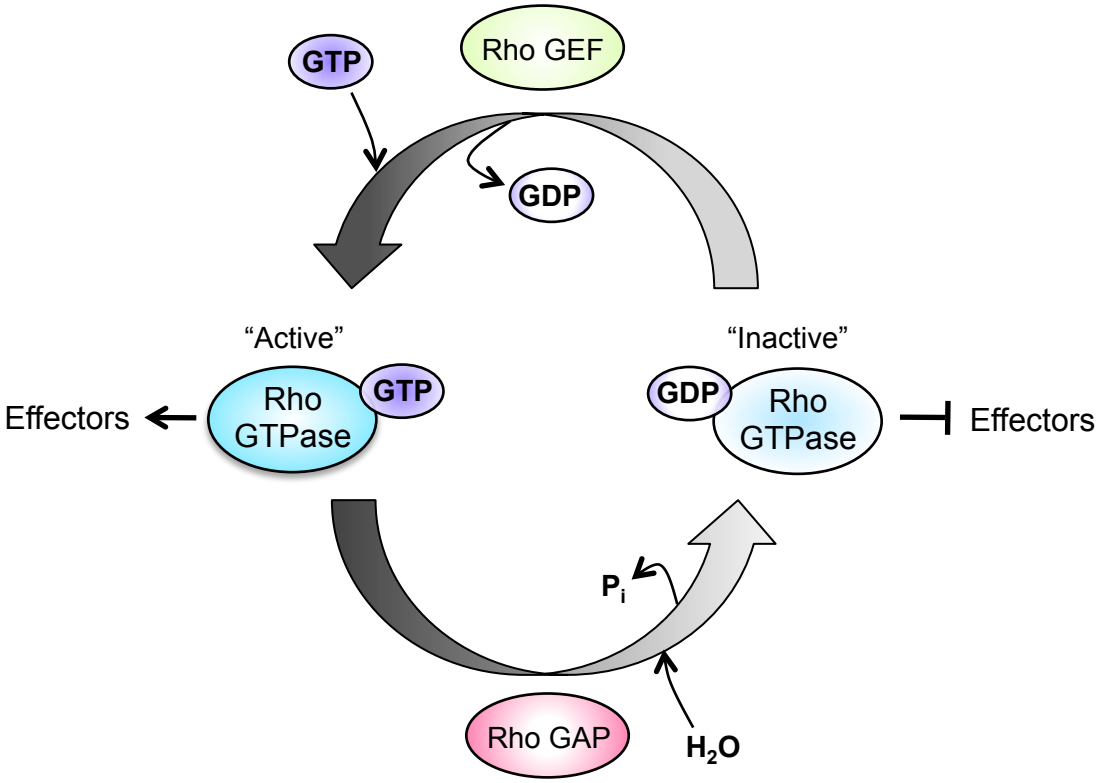
GTP
Rho GEF
GDP
"Active"
"Inactive"
Effectors
Rho GTPase
GTP
GDP
Rho GTPase
Effectors
P_i
Rho GAP
H_2O

Figure 1.5. Regulation of Rho-family GTPases by GEFs and GAPs. Two major types of proteins regulate Rho GTPases: guanine nucleotide exchange factors (GEFs) and GTPase-activating proteins (GAPs). GEFs turn on Rho GTPases by facilitating exchange of GDP for GTP (top). In their GTP-bound form, Rho GTPases are considered active and able to interact with their downstream effector molecules (left). Conversely, GAPs turn off Rho GTPases by promoting hydrolysis of GTP to GDP (bottom). In their GDP-bound form, Rho GTPases are inactive and unable to interact with their effectors (right). This figure is adapted from Raftopoulou and Hall (2004) [55].

1.6.3 Polarity and protrusion

Membrane protrusion is the first step of cell motility. Protrusions help to establish front-to-back polarity in migrating cells [57]. There are different types of protrusions, including lamellipodia, filopodia, and in the case of certain tumor cells, specialized structures called invadopodia. Lamellipodia are broad protrusions driven by a dendritic actin network and can support cell movement over long distances [58]. Filopodia are thin, actin-rich projections that function as exploratory sensors for a cell to get a feel for its surrounding microenvironment [58]. Cdc42 induces filopodia and helps to establish and maintain cell polarity. Invadopodia are unique to tumor cells and these proteolytic, actin-rich extensions promote invasion by locally releasing matrix metalloproteases (MMPs) to degrade ECM proteins [59, 60].

Rac1 is required for lamellipodial protrusion (**Fig 1.6**, inset box A). Rac1 controls actin-related protein 2/3 (ARP2/3), the major actin nucleator that initiates and promotes actin polymerization. More specifically, active GTP-bound Rac1 can recruit and bind a pentameric nucleation-promoting factor (NPF) called WAVE, a close relative of the Wiskott Aldrich Syndrome Protein (WASP)-family of proteins that regulates actin assembly [61, 62]. Interaction between Rac1 and WAVE is believed to expose a sequestered ARP2/3-activating domain in the WAVE complex [61]. Activated ARP2/3 complexes, in collaboration with other nucleators, NPFs and formins, create new, branched actin filaments off the sides of pre-existing filaments [62, 63]. Actin filament branching generates a so-called “dendritic” actin network that drives membrane protrusion.

The dendritic actin network extends from the leading edge of the cell, throughout the lamellipodium, to a region known as the transition zone [51]. In the transition zone, actin filaments undergo depolymerization or severing. Actin severing is critical for

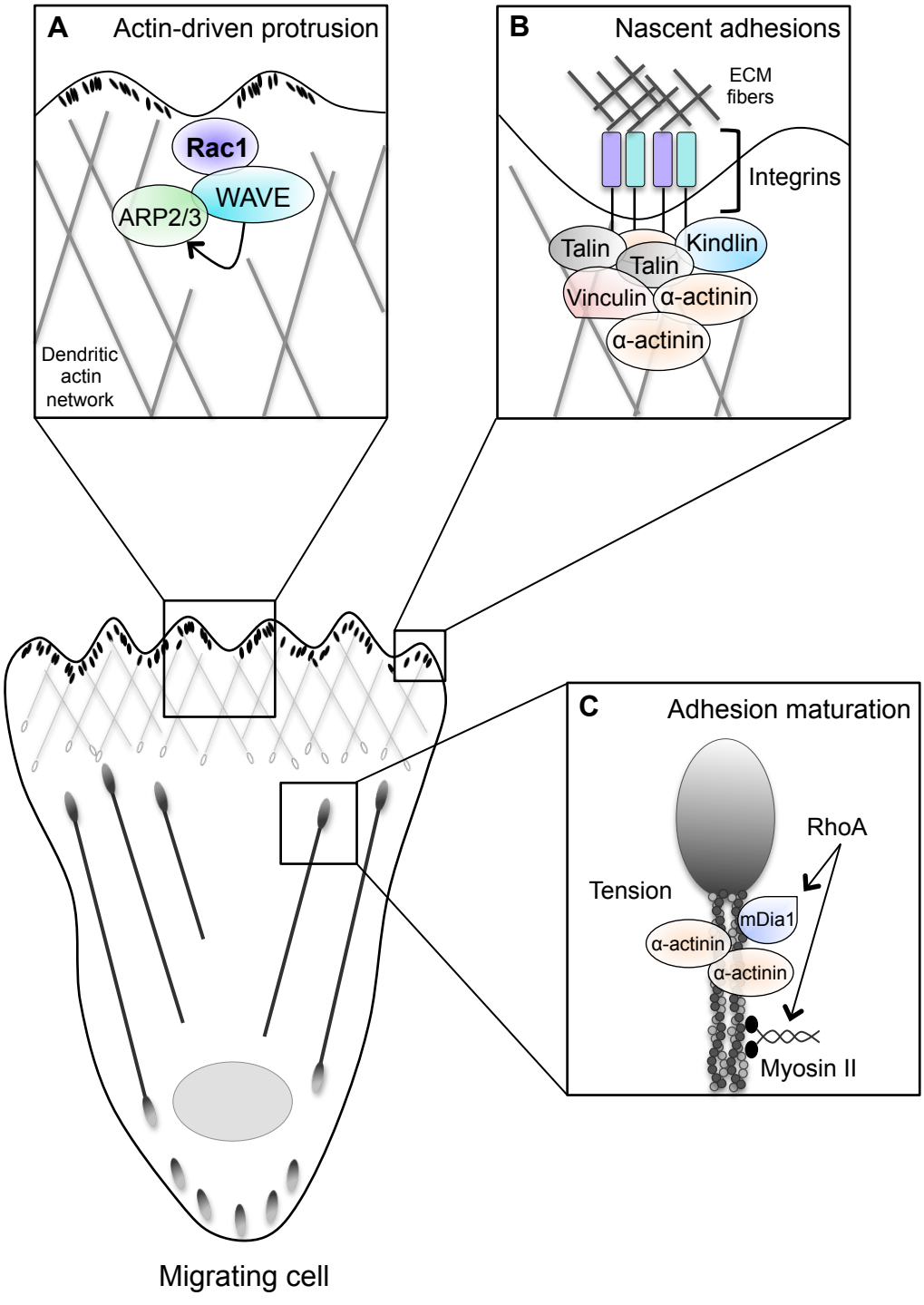
A
Actin-driven protrusion
Rac1
WAVE
ARP2/3
Dendritic actin network
B
Nascent adhesions
ECM fibers
Integrins
Talin
Talin
Kindlin
Vinculin
α-actinin
α-actinin
C
Adhesion maturation
RhoA
Tension
mDia1
α-actinin
α-actinin
Myosin II
Migrating cell

Figure 1.6. Actin-driven protrusion, adhesion establishment, and adhesion maturation. (**A**) Interaction between Rac1 and the nucleation-promoting factor WAVE activates the ARP2/3 complex. Activated ARP2/3 initiates and promotes actin polymerization by creating new, branched actin filaments off the sides of pre-existing filaments. This generates a "dendritic" actin network that drives membrane protrusion. (**B**) Actin-rich protrusions are stabilized by nascent adhesions. Kindlin, talin, vinculin and α-actinin are four major proteins responsible for anchoring integrin receptors to actin in nascent adhesions. (**C**) Adhesion maturation requires tensional force and a structural actin template upon which adhesions can elongate. RhoA signaling promotes myosin II-dependent tension, while the actin-crosslinking abilities of myosin II and α-actinin, along with the actin nucleator mDia1, mediate actin template assembly. Schematic of migrating cell and inset box (B) adapted from Parsons *et al*. (2010) [51]; inset box (C) adapted from Choi *et al*. (2008) [64].

persistent protrusion and is mediated by the EGF-stimulated cofilin pathway [65]. Cofilin severs filamentous actin (or F-actin) into smaller fragments, thereby generating actin filaments with free barbed ends [65]. These filaments support nucleation at the protruding edge of a cell, and if available, actin monomers polymerize onto the free barbed ends (**Fig 1.7**). Cofilin is negatively and positively regulated by kinases and phosphatases. For example, LIM kinase (LIMK) is a well-established negative regulator of cofilin. LIMK, which is activated by a downstream effector of RhoA GTPase, can phosphorylate cofilin and inhibit its actin severing ability [66]. A delicate balance between actin assembly and disassembly is required for efficient protrusion/motility, and deregulated cofilin pathway signaling is a major determinant of breast cancer cell invasion and metastasis [65].

1.6.4 Adhesion establishment and turnover

Actin-rich protrusions are stabilized by newly formed, or nascent, adhesions. Adhesions are linkages between the intracellular actin cytoskeleton and the ECM. Integrins are a major family of cell surface adhesion receptors and each receptor consists of a heterodimeric alpha and beta subunit. There are many combinations of alpha and beta subunits, creating a diverse array of integrin receptors capable of binding different ECM components with varying affinity [67]. Integrins are critical mechanotransducers; they relay information about the surrounding mechanical microenvironment by activating signaling cascades within the cell.

Integrin-associated nascent adhesions are the earliest adhesions visible at the leading edge of cells and they have very fast turnover rates (about 60 seconds) [51]. Nascent adhesions are small, multi-protein complexes that have recently been shown to arrange in a hierarchical fashion (**Fig 1.6**, inset box B) [68]. As nascent adhesions first

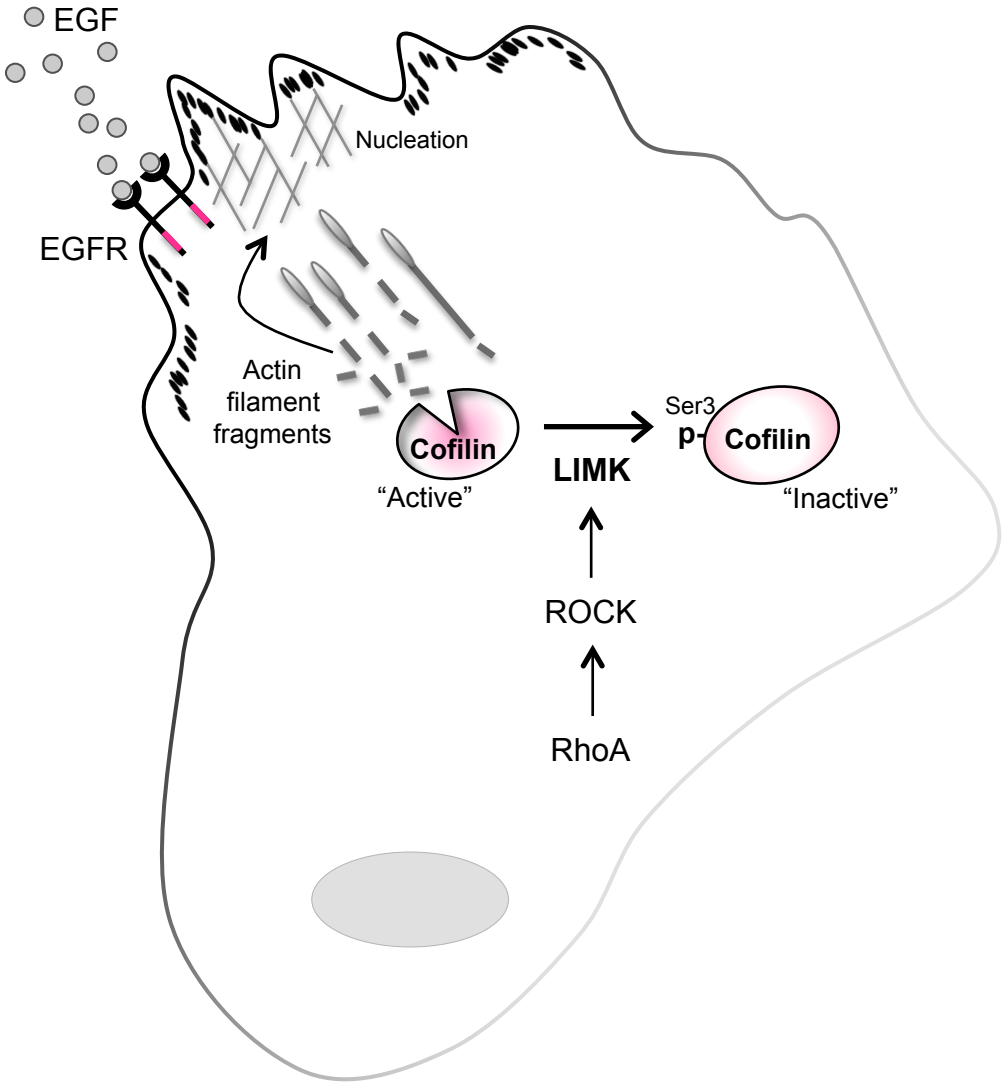
EGF
Nucleation
EGFR
Actin
filament
fragments
Cofilin
"Active"
LIMK
Ser3
P
Cofilin
"Inactive"
ROCK
RhoA

Figure 1.7. The EGF-cofilin pathway. In response to EGF stimulation, the actin-severing protein, cofilin, breaks down filamentous actin into smaller fragments, thereby generating actin filaments with free barbed ends. These filaments support nucleation at the protruding edge of a cell, and if available, actin monomers polymerize onto the free barbed ends. Cofilin is negatively regulated by LIM kinase (LIMK), a downstream effector of RhoA/ROCK signaling. LIMK can phosphorylate cofilin on serine 3 (pSer3), thus inhibiting its actin severing ability. This figure is adapted from Wang *et al*. (2007) [65].

become established, two of the earliest proteins recruited are kindlin and talin. Both kindlin (arrives first) and talin (arrives second) directly bind to integrin beta subunit cytoplasmic tails via their FERM (4.1 ezrin radixin moesin) domain-containing "head" regions and are required to help cluster and fully activate integrins [68-72]. In addition to its N-terminal "head" region, talin has a mechanosensing C-terminal rod that directly binds F-actin and another notable actin-binding protein, vinculin [72]. Vinculin is actually associated with talin prior to its interaction with integrin, and vinculin is believed to boost talin-mediated integrin activation [68, 73]. Vinculin itself is mechanosensing and its structure consists of a head, neck and tail region that can bind talin, ARP2/3 and actin, respectively [74]. Furthermore, directed mutagenesis of different vinculin domains has shown that vinculin is important for recruiting many other core adhesion proteins, like paxillin, focal adhesion kinase (FAK), and p130$^{\text{Crk-associated substrate}}$ (Cas) [74]. Lastly, another key protein that can interact with integrin as well as the head region of vinculin is α-actinin. α-actinin has a well-established role in binding and crosslinking actin filaments to promote nascent adhesion assembly. Recently, α-actinin has been shown to exhibit a very unique spatial periodicity in adhesions and it can even be detected in complex with integrin prior to integrin-talin association or nascent adhesion assembly [68]. These data suggest that α-actinin may also help to nucleate nascent adhesions. Studies have also demonstrated that α-actinin is an early constituent of maturing adhesions, and its roles in adhesion maturation are discussed further below. Taken together, kindlin, talin, vinculin and α-actinin are four major proteins responsible for anchoring integrins to actin and establishing nascent adhesions.

The rate of nascent adhesion formation is directly related to the rate of actin assembly at the leading edge [51]. At the back of the lamellipodium (in the transition zone), nascent adhesions reach a critical decision point where they can either turnover

(disassemble) or mature into structures called focal complexes. Turnover can be driven by Rac1 activation and occurs when there is a lack of tension to reinforce the adhesion. Actin filament depolymerization diminishes tension. Also, kinases and adaptor molecules present in adhesions, such as FAK, Src, Cas and paxillin, can locally activate Rac1 and inhibit RhoA signaling thereby reducing tension and promoting nascent adhesion disassembly [75, 76]. In fact, inhibiting tension with myosin II-specific siRNAs or blebbistatin promotes nascent adhesion turnover and prevents maturation [64]. While tension is generally thought to not be required for nascent adhesion turnover, this may be a little oversimplified because recent data indicate that incorporation of certain constituents into assembling adhesions (i.e. talin) requires myosin II activity [68].

1.6.5 Adhesion maturation and tension

Nascent adhesions can mature into focal complexes and eventually focal adhesions as part of a continuum [51]. Focal complexes are slightly larger than nascent adhesions and can persist for a few minutes, while mature focal adhesions are very stable, elongated, and situated at the tips of bundled actin filaments (also known as stress fibers) (**Fig 1.6**, inset box C). Adhesion maturation requires both tensional force and a structural actin template upon which adhesions can elongate.

The major force-generating protein involved in cell motility is non-muscle myosin II (simply referred to as myosin II). Myosin II is a member of the myosin superfamily of molecular motor proteins and is composed of two heavy chains (HCs), two essential light chains (ELCs), and two regulatory light chains (RLCs) [77]. The two HCs create a coiled-coil rod-like structure, while the ELCs and RLCs form “levers” that link the heavy chains to their head domains [77]. The head domains bind directly to actin filaments and contain the ATP-dependent motors (i.e. ATPases). Myosin II is regulated by

phosphorylation of its RLCs. When the RLCs are not phosphorylated, myosin II is in a closed conformation, however upon phosphorylation of the RLCs, myosin II opens up and the head domains are then able to bind actin, exert tension and promote contraction [77]. Many kinases can phosphorylate the RLCs of myosin II, including the well-defined Rho-associated coiled coil-containing kinase (or ROCK). ROCK is a serine/threonine kinase and one of the two major downstream effectors of RhoA GTPase. ROCK can directly phosphorylate the RLC of myosin II (referred to as phosphorylated myosin light chain, or pMLC, from here on out) at residues threonine 18 and serine 19, thereby triggering myosin II activation.

The contractile activity of myosin II allows it to generate tension. This force can be translated into "stretching" of various mechanosensing proteins within an adhesion, such as talin, vinculin, or Cas [74, 78, 79]. The stretching of these proteins opens them up, revealing docking sites to recruit additional proteins to reinforce the adhesion. Conformational changes also expose critical phosphorylation sites that upon phosphorylation recruit Rho GEFs and GAPs to locally promote RhoA-mediated myosin II-dependent tension and/or decrease Rac1-mediated turnover. Recently, and mechanistically distinct from its actin crosslinking ability, α-actinin has also been shown to transmit forces through integrins to promote adhesion maturation [80]. It does this in part through its ability to compete with talin for binding to the integrin tail.

While force generation is important for adhesion maturation, it is not sufficient. α-actinin and myosin II have been shown to support maturation by creating a structural actin "template" along which adhesions can mature [64]. This is independent of myosin II's motor activity, and instead requires the actin crosslinking abilities of myosin II and α-actinin. More specifically, overexpression of α-actinin or a motor-deficient mutant of myosin II that retains its ability to bind to actin was able to rescue adhesion maturation in

myosin II-depleted CHO.K1 cells [64]. More recently, the second major downstream effector of RhoA, mammalian diaphanous 1, or mDia1, has been shown to be required for actin stress fiber template assembly [81]. mDia1 is a formin molecule with established roles in actin nucleation and elongation [82]. Taken together, these data support a model whereby mDia1, α-actinin and myosin II work together to nucleate, reinforce and elongate actin stress fibers from nascent adhesions. These stress fibers serve as templates to coordinate the hierarchical recruitment of proteins to maturing adhesions [64]. Perturbation of template assembly, for example by inhibiting mDia1, can lead to a decreased accumulation of proteins present in maturing adhesions, including phosphorylated FAK and paxillin [81].

1.6.6 Rear retraction

In order for a cell to move forward, adhesions in the rear of the cell must undergo disassembly. While it is well established that RhoA-dependent myosin II-generated tension is important for rear retraction, other forces may play a role as well, including forces generated from actin depolymerization [83]. Additionally, tension at the leading edge of the cell is coupled to retraction in the cell rear, such that, the inward force generated by actin polymerization at the leading edge of a cell essentially “pulls” the cell rear forward [84].

1.7 Adhesion/adaptor proteins regulate Rac1 and RhoA

Coordination of Rho GTPase crosstalk is necessary for efficient cell motility and wound repair [85, 86]. Rac1 and RhoA frequently act in opposition to one another, thus it is critical to achieve a balance through their localized activation and inhibition. Kinases and adaptor molecules mediate this balance by creating platforms to locally recruit and

stimulate Rho GEFs and GAPs. Several of these kinases and adaptor proteins are described in further detail below.

1.7.1 FAK

Focal adhesion kinase (or FAK) and proline-rich tyrosine kinase 2 (PYK2) comprise the FAK-family of non-receptor protein tyrosine kinases [87]. FAK is ubiquitously expressed across many normal tissue types and is frequently overexpressed in human cancers. FAK has diverse roles in tumor cell survival, proliferation, adhesion, motility and invasion, and has been extensively studied for over 20 years. Tissue-specific knockout mouse models combined with different cancer predispositions have highlighted the diverse roles of FAK in tumor development and progression. More specifically, conditional knockout of FAK in mammary epithelial cells (MECs) has been shown to block breast tumor progression, suppress lung metastasis, and disrupt the tumorigenic capacities of a small population of CSCs in the MMTV-PyMT mouse model of human breast cancer [88-90]. Also, conditional FAK deletion in intestinal epithelial cells has been demonstrated to suppress Wnt-mediated tumorigenesis *in vivo* [91]. Furthermore, FAK signaling in endothelial cells, TAMs and CAFs has also been implicated in the TME as a key regulator of tumor progression and metastasis, making it a promising clinical target [92]. In fact, Jean *et al.* recently demonstrated that inhibition of FAK in endothelial cells prevents VEGF-enhanced tumor cell extravasation and metastasis using conditional kinase-dead FAK knock-in mouse models of ovarian cancer and melanoma [93]. This study, in particular, highlights the role of FAK kinase activity in controlling vascular permeability by directly phosphorylating a tyrosine residue on an adherens junction protein in endothelial cells.

While the kinase activity of FAK plays a role in tumor progression, it is also important to note that the adaptor function of FAK controls many aspects of tumor cell motility, including membrane protrusion and adhesion turnover at the leading edge [75]. FAK consists of an N-terminal FERM domain, which can directly bind ARP2/3, a central kinase domain, followed by proline-rich domains and a C-terminus that contains a focal adhesion-targeting (FAT) domain (**Fig 1.8A**) [92]. As an adaptor, FAK can recruit several other downstream kinases and scaffolding molecules that modulate Rho GTPase signaling, some of which are described in further detail below.

1.7.2 Paxillin

Paxillin is a scaffolding, or adaptor, molecule and an early marker of assembling nascent adhesions. Its structure consists of an N-terminal signaling domain containing five leucine/aspartate-rich (LD1-5) sequence motifs and a C-terminal domain with four lin-11 isL-1 mec-3 (LIM) double zinc finger domains that are required for targeting paxillin to adhesions (**Fig 1.8B**) [94]. Paxillin has an established role in regulating nascent adhesion disassembly downstream of FAK and it does this through its ability to locally enhance Rac1 activation. Paxillin recruits a G-protein coupled receptor kinase-interacting protein (GIT)-PAK interacting exchange factor (PIX)-p21 activated kinase (PAK) complex (simply referred to as a GIT1-PIX-PAK complex) when it is phosphorylated on serine 273 in its LD4 domain [95]. PIX and PAK work together downstream of paxillin to locally promote Rac1 activity and suppress RhoA. PIX, a Rac1 GEF, directly activates Rac1, while PAK can negatively regulate several RhoA GEFs (e.g. p115-RhoGEF) [85]. FAK/Src-mediated tyrosine phosphorylation of paxillin at two major tyrosine residues, Y31 and Y118, can also promote subsequent recruitment of SH2 domain-containing proteins, such as Crk, to recruit Rac1 GEFs. Depletion of

A FAK

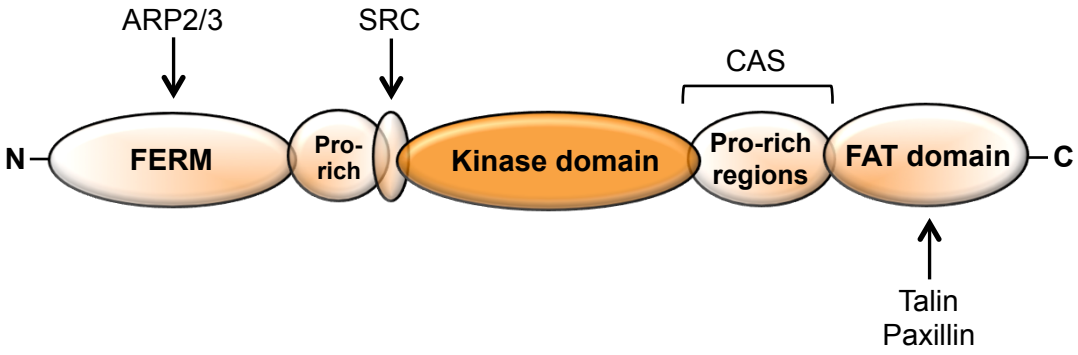

B Paxillin

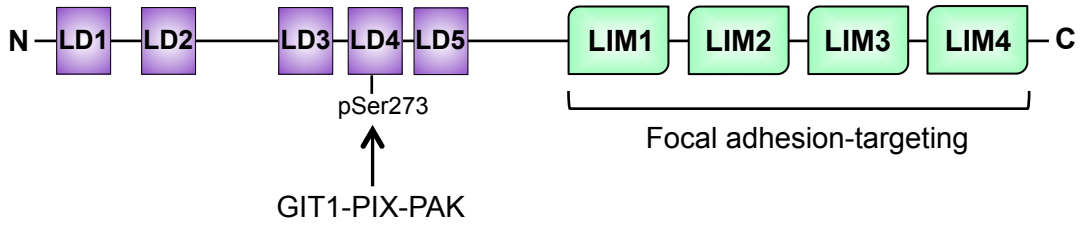

C SRC

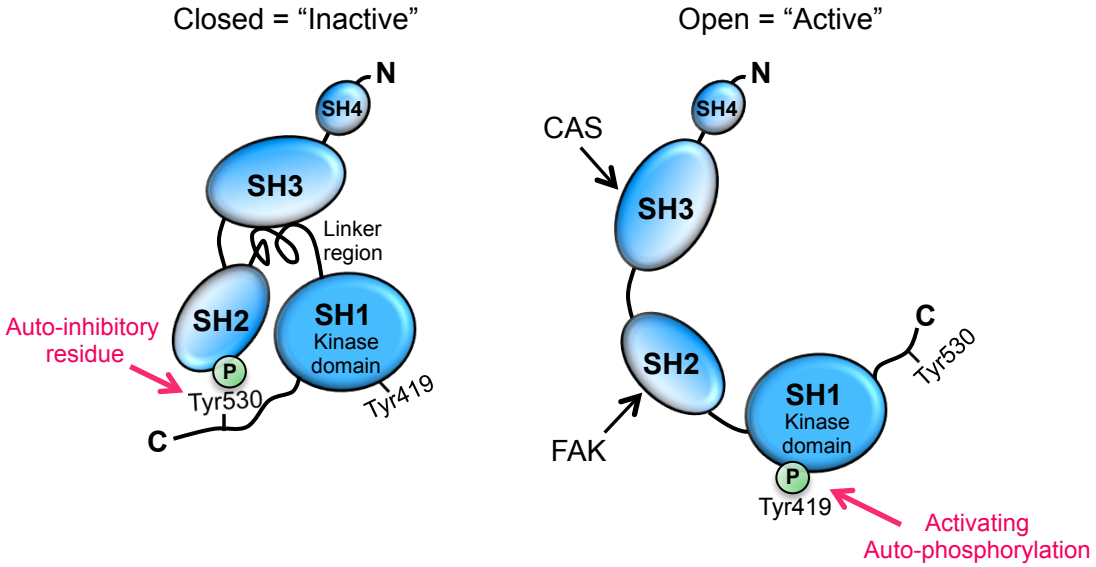

Figure 1.8. Structural features of FAK, paxillin and Src. (**A**) The structural domains of FAK include an N-terminal 4.1 ezrin radixin moesin (FERM) domain, a proline-rich (Pro-rich) region, a central kinase domain, additional proline-rich domains, and a C-terminus that contains a focal adhesion-targeting (FAT) domain. FAK interacts with the various proteins shown at the indicated sites. Schematic adapted from Sulzmaier *et al*. (2014) [92]. (**B**) The structure of paxillin consists of an N-terminal domain containing five leucine/aspartate-rich (LD1-5) sequence motifs and a C-terminal domain with four lin-11 isL-1 mec-3 (LIM) double zinc finger domains (LIM1-4) that are required for targeting paxillin to adhesions. When serine 273 in the LD4 domain is phosphorylated, paxillin recruits a Rac1-activating complex known as GIT1-PIX-PAK. Schematic adapted from Deakin and Turner (2008) [94]. (**C**) Src consists of four Src homology (SH) domains (SH1-4). The SH1 domain contains the kinase, and therefore is referred to as the kinase domain. When phosphorylated, an auto-inhibitory tyrosine residue in the C-terminal domain of Src, Tyr530, binds to the SH2 domain within Src, orchestrating a closed, catalytically inactive Src molecule (left panel, pink arrow). Under these conditions, a linker domain also interacts with the SH3 domain within Src, reinforcing the closed conformation. Activation of Src can be achieved through removal of the inhibitory phosphate on Tyr530, followed by autophosphorylation of tyrosine residue 419, Tyr419, in the kinase domain of Src (right panel, pink arrow). These signaling events drive Src into an open, catalytically active conformation. FAK and Cas can also activate Src by directly binding to the SH2 and SH3/2 domains of Src, respectively, thus blocking adoption of the closed, inhibitory conformation. Part (C) adapted from Yeatman (2004) [96].

paxillin in MDA-MB-231 cells inhibits breast cancer cell extravasation and lung metastasis *in vivo*, thus underscoring the role of paxillin in promoting breast tumor progression [97].

1.7.3 Src

c-Src (referred to herein as Src) is the human cellular equivalent of v-Src, the prototypical viral oncogene discovered in Rous-sarcoma virus over a century ago [96]. Src encodes a non-receptor protein tyrosine kinase that is frequently overexpressed and/or hyper-activated in numerous human cancers, including breast cancer [98, 99]. Like FAK, Src has been implicated in many biological activities that promote tumor progression, including tumor cell survival, proliferation, adhesion, motility and metastasis. Gene expression profiling has further implicated Src activity to be associated with aggressive breast tumor subtypes (i.e. TNBC), and thus patients diagnosed with TNBC may be good candidates for treatment with the clinical Src inhibitor dasatinib [100, 101].

Src consists of four Src homology (SH) domains (SH1-4). The SH1 domain contains the kinase and is also referred to as the kinase domain (**Fig 1.8C**). The activity of Src is negatively regulated by the presence of an auto-inhibitory tyrosine residue, Tyr530, in its C-terminal domain [96]. More specifically, when Tyr530 is phosphorylated, it binds to the SH2 domain within Src, orchestrating a closed, catalytically inactive structure. Also, under these conditions, a secondary linker domain interacts with the SH3 domain within Src, further contributing to the auto-inhibitory conformation. Full activation of Src can be achieved through distinct mechanisms. One mechanism involves removal of the inhibitory phosphate on Tyr530, followed by autophosphorylation of a second critical tyrosine residue, Tyr419, in the kinase domain of Src [96]. These

events drive Src into an open conformation that is catalytically active. A second mechanism involves binding of a heterologous protein to the SH2 and SH3 domains of Src, thereby blocking the adoption of the auto-inhibitory conformation. By preventing the auto-inhibitory conformation, full activation of Src can then be achieved via autophosphorylation of Tyr419 and removal of the phosphate on Tyr530. FAK and Cas can bind directly to Src via the SH2 and SH3/2 domains, respectively and, in doing so, activate Src kinase activity [102].

Activated Src promotes localized Rac1 activity through several mechanisms. These include its ability to facilitate Cas/Crk coupling and subsequent recruitment of the Rac1 GEF DOCK180/ELMO (discussed further below), as well as direct phosphorylation of the Rac1 GEF Tiam1 (T-cell lymphoma invasion and metastasis 1) in adhesions [103]. Src also indirectly promotes Rac1 activity by inhibiting RhoA signaling. More specifically, Src phosphorylates a notable Rho GAP, p190RhoGAP, downstream of EGFR [104]. Src-mediated activation of p190RhoGAP suppresses RhoA, tipping the scale in favor of Rac1.

1.7.4 Cas

Crk-associated substrate, Cas (also known as $p130^{Cas}$ or Breast Cancer Antiestrogen Resistance 1; BCAR1), is an adaptor molecule with major roles in cell adhesion, motility, invasion and metastasis. BCAR1 was originally discovered in a functional screen whose gene product conferred resistance of ER^+ human breast cancer cells to antiestrogens [105, 106]. Cas is a member of the Cas-family of adaptor proteins that includes three other proteins, most notably NEDD9 (neural precursor cell expressed, developmentally downregulated protein 9), which has been shown to promote metastasis in many human cancers, including melanoma and breast cancer

[107]. Although overexpression of Cas alone is not sufficient to induce mammary epithelial cell transformation, it has been shown that FAK promotes breast tumorigenesis through its ability to bind to Cas [108, 109]. Cas protein is ubiquitously expressed in many normal tissue cell types. However overexpression of Cas in primary human breast tumors is associated with poor tamoxifen response, poor relapse-free survival, and poor overall survival ([110, 111], The Human Protein Atlas). Furthermore, double transgenic mice that co-overexpress Cas and HER2 in mammary epithelial cells exhibit accelerated tumor formation compared to mice solely overexpressing HER2, demonstrating a role for Cas in promoting HER2-dependent breast tumorigenesis *in vivo* [112, 113].

The domain structure of Cas consists of a N-terminal SH3 domain, a long, intervening substrate domain (SD) consisting of 15 tyrosine-x-x-proline (YxxP) amino acid sequence motifs, a serine-rich region, followed by a C-terminal domain (**Fig 1.9A**) [114]. The C-terminal domain of Cas includes a Src-binding domain (SBD) and two FAT domains, which are important for recruitment of Cas to adhesions. Cas can bind directly to FAK and Src via its SH3 and SBD domains, respectively. Cas is a mechanosensor whose substrate domain extends in response to mechanical force [78]. Very recently, Cas has also been shown to bind directly to vinculin via its SH3 domain, and this Cas/vinculin interaction is required for stretch-induced activation of Cas [115].

Cas is a potent activator of Rac1. Src phosphorylates tyrosine residues within the substrate domain of Cas, providing a docking site for Crk. Cas/Crk coupling stimulates the canonical Rac1 GEF, DOCK180/ELMO, to promote Rac1 activity and cell motility [114, 116, 117].

A CAS

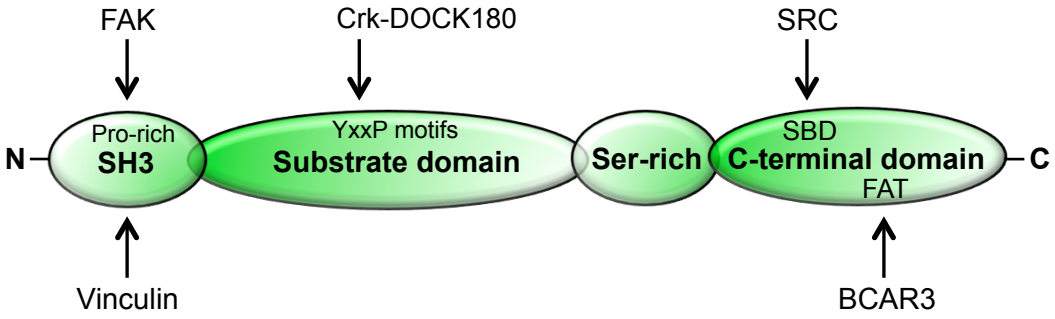
FAK
Crk-DOCK180
SRC
N
Pro-rich
SH3
YxxP motifs
Substrate domain
Ser-rich
SBD
C-terminal domain
FAT
C
Vinculin
BCAR3

B BCAR3

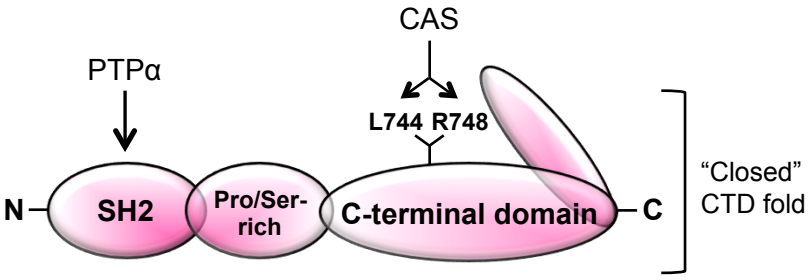
CAS
PTPα
L744 R748
N
SH2
Pro/Ser-rich
C-terminal domain
C
"Closed"
CTD fold

Figure 1.9. Structural features of Cas and BCAR3. (**A**) The structural domains of Cas include an N-terminal SH3 domain rich in proline residues (Pro-rich), a substrate domain consisting of 15 tyrosine-x-x-proline (YxxP) amino acid sequence motifs, a serine-rich (Ser-rich) region, followed by a C-terminal domain. The C-terminal domain contains a Src-binding domain (SBD) and two focal adhesion-targeting (FAT) domains. Cas interacts with the various proteins shown at the indicated sites. Notably, Cas directly interacts with BCAR3 via its C-terminal FAT domain. Schematic adapted from Cabodi *et al*. (2010) [114]. (**B**) The structural domains of BCAR3 include an N-terminal SH2 domain, a linker region rich in proline and serine residues (Pro/Ser-rich), and a C-terminal domain (CTD). The CTD of BCAR3 shares sequence homology to the Cdc25-family of Ras GEFs; however, it adopts a "closed" conformation, rendering BCAR3 catalytically inactive. BCAR3 interacts with PTPα via its N-terminal SH2 domain. BCAR3 directly interacts with Cas through two critical amino acid residues in its CTD, leucine 744 (L744) and arginine 748 (R748).

1.7.5 BCAR3

Breast cancer antiestrogen resistance 3 (BCAR3) is a cytosolic adaptor molecule that has emerged as an important regulator of breast cancer cell motility and invasion. BCAR3 mRNA and protein is weakly to moderately expressed across many normal tissue types, including but not limited to, breast, lung, liver, and colon (The Human Protein Atlas, [118]). However, BCAR3 protein levels are elevated in invasive, TNBC cells compared to cell lines representing early-stage, ER^+ breast cancer [119, 120]. BCAR3 has been shown to promote breast cancer cell motility and invasion *in vitro* [119].

BCAR3 is a member of the novel SH2 domain-containing protein (NSP) family of adaptors, and is comprised of a N-terminal region that can be alternatively spliced, an SH2 domain, and a C-terminal GEF-like domain with sequence homology to the Cdc25-family of Ras GEFs (**Fig 1.9B**) [118, 121, 122]. BCAR3 (also known as AND-34 in mice) was originally thought to function as a GEF because its overexpression promoted activation of Ras-family GTPases, such as Ral, Rap, and R-Ras, and the Rho-family GTPases, Rac1 and Cdc42, *in vitro* [123, 124]. However, recent structural data has revealed that the C-terminal GEF-like domain of BCAR3 adopts a “closed” conformation that is prohibitive for catalytic activity [125]. Therefore, it is unlikely that BCAR3 functions directly as a GEF. AND-34 knockout mice display no major developmental or phenotypic abnormalities, with the exception of a defect in ocular lens epithelial cell adhesion signaling [126].

BCAR3 was first discovered in the same functional screen as BCAR1 (Cas) that was designed to identify genes whose overexpression conferred resistance of ER^+ human breast cancer cells to antiestrogens [127]. By using well-established inhibitors of phosphatidylinositol 3-kinase (PI3K) and Rac (LY294002 and NSC23766, respectively),

Adam Lerner's group has demonstrated that BCAR3 promotes antiestrogen resistance in ZR-75-1 ER^+ breast cancer cells through a PI3K- and Rac-dependent mechanism [128]. PI3K/AKT signaling has important implications for cell proliferation and survival in the presence of antiestrogens [15, 128].

BCAR3 currently has two established binding partners, Cas and protein tyrosine phosphatase alpha (PTPα). BCAR3 and Cas bind directly to one another at their C-termini and their interaction has been well studied for over a decade. Interestingly, the "closed" conformation of BCAR3's C-terminal domain described above is instrumental for its binding to Cas [125]. BCAR3 has been shown to enhance Src kinase activity, Cas/Src interaction and Src-mediated Cas tyrosine phosphorylation [129, 130], all of which have been implicated in inducing tamoxifen resistance in ER^+ breast cancer cells [15, 131]. Recently, BCAR3/Cas interaction has been shown to promote stabilization of each protein, and their direct association is necessary for their ability to induce antiestrogen resistance [132]. More specifically, leucine 744 and arginine 748 are two critical amino acid residues in BCAR3 that are situated within the binding interface between BCAR3 and Cas (**Fig 1.9B**). When both of these residues are mutated to glutamic acid (i.e. BCAR3 L744E/R748E double mutant), BCAR3/Cas complex formation is abolished. Elena Pasquale's group has demonstrated that overexpression of wildtype BCAR3, but not L744E/R748E BCAR3, in MCF-7 ER^+ breast cancer cells enhances Cas tyrosine phosphorylation and antiestrogen resistance through an ERK1/2-dependent mechanism [132]. Together, these findings underscore the importance of BCAR3/Cas complex signaling in promoting antiestrogen resistance in ER^+ breast cancer cell lines. Interestingly, in contrast to ER^+ breast cancer cell lines, elevated BCAR3 mRNA expression in primary human ER^+ breast tumors has been shown to correlate with favorable responses to antiestrogen therapy and progression-free survival [133-135],

suggesting that BCAR3 expression may play distinct roles in mediating antiestrogen resistance in tumors compared to breast cancer cell lines.

Finally, the SH2 domain of BCAR3 has recently been shown to bind phosphorylated tyrosine 789 on PTPα [130]. PTPα is a membrane-bound protein tyrosine phosphatase and the first protein discovered to directly interact with BCAR3's SH2 domain. While the functional implications of BCAR3/PTPα interaction are less well understood, it is argued that BCAR3 serves as a "molecular bridge" between PTPα and Cas [130]. BCAR3/PTPα association may uniquely position Cas downstream of integrins so that it is primed and ready for signaling.

1.8 Significance and overview

The main focus of this dissertation is the adaptor molecule BCAR3. While our group had previously demonstrated that BCAR3 promotes breast cancer cell motility and invasion *in vitro*, several compelling questions still remained. First, it was unclear how BCAR3 promotes cell motility/invasion. Therefore, in **Chapter 2**, we set out to determine the mechanisms underlying BCAR3-mediated motility by exploring the role of BCAR3 in regulating some of the major facets of cell migration described above. Furthermore, we sought to address whether BCAR3 regulates Rac/Rho GTPase signaling in invasive breast cancer cells, similar to the kinases and other adaptor molecules mentioned herein. Second, considering the physical association between BCAR3 and Cas has been shown to be important for many of the biological activities of BCAR3, including BCAR3-induced antiestrogen resistance, we sought to determine how BCAR3/Cas interactions contribute to invasive breast cancer cell motility and invasion. Specifically, in **Chapter 3**, we explore the functional implications of BCAR3/Cas interactions in BCAR3-mediated adhesion dynamics. We examine tumor cell adhesion in particular

because it is essential for efficient cell motility, intravasation and metastasis. Furthermore, these studies will add to our understanding of the intricate relationship between BCAR3 and Cas, and provide further insight into how the BCAR3/Cas complex functions in breast cancer progression.

While many of the kinases and adaptor molecules described above (e.g. FAK, Src, Cas) are frequently overexpressed in human breast cancer, a rigorous assessment of BCAR3 protein expression in human breast tumors had never been performed. Additionally, given the inconsistent data between BCAR3 protein and mRNA levels in human breast cancer cell lines and tumors, respectively, it is critical to directly evaluate BCAR3 protein levels in tumors to determine whether BCAR3 protein expression correlates with aggressive tumor subtypes. Therefore, in **Chapter 4** we assessed BCAR3 protein expression across multiple subtypes of human breast cancer and determined whether BCAR3 correlates with a particular subtype(s) and/or tumor invasiveness. These studies may have important therapeutic implications for breast cancer patients because, if BCAR3 protein expression associates with aggressive tumor behaviors, it may be beneficial to target BCAR3 in tumors.

Finally, in **Chapter 5**, considering different modes of cell motility have been shown in tissue, we discuss the relevance of the *in vitro* motility and adhesion studies described in Chapters 2 and 3 to more physiologically relevant models. Future experiments are proposed to elucidate the role of BCAR3 in breast tumor cell motility and invasion *in vivo* using three-dimensional and animal models of breast cancer. These studies are necessary in order to determine whether BCAR3 promotes invasion and metastasis *in vivo*. If this were the case, these findings would have tremendous impact on the therapeutic and prognostic potential of BCAR3. We conclude with an evaluation of BCAR3 as a potential molecular target and/or biomarker.

CHAPTER 2: BCAR3 promotes cell motility by regulating actin cytoskeletal and adhesion remodeling in invasive breast cancer cells*

This chapter is adapted from Wilson et al., PLOS One, 2013

2.1 Introduction

Metastatic breast cancer is associated with a 5-year survival rate of only 25% (American Cancer Society, 2015). Thus, it is critical to gain a better understanding of the molecular mechanisms underlying metastasis in order to improve patient survival. Cell motility is inherent to metastasis, and previously our lab has demonstrated that elevated BCAR3 protein levels enhance breast cancer cell motility [119]. Conversely, depletion of BCAR3 reduces the migratory and invasive capacities of breast cancer cells [119]. In this work, we set out to determine the mechanism by which BCAR3 promotes breast cancer cell motility by examining its function in the regulation of membrane protrusion, adhesion turnover and contractility. We show that BCAR3 is a positive regulator of Rac1 activity, membrane protrusiveness, and adhesion turnover in invasive breast cancer cells. We further demonstrate that, in the absence of BCAR3, RhoA activity is increased, and cells exhibit a highly contractile phenotype marked by prominent actin-rich stress fibers, an increase in ROCK-mediated phosphorylation of MLC, and large ROCK/mDia1-dependent focal adhesions. Taken together, these data establish that BCAR3 functions as a positive regulator of cytoskeletal remodeling and adhesion turnover in invasive breast cancer cells through its ability to influence the balance between Rac1 and RhoA GTPase signaling. Considering that BCAR3 is elevated in advanced breast cancer cell lines and promotes cell motility, we propose that BCAR3 functions in the transition to advanced disease by triggering intracellular signaling events that are essential to the metastatic process.

2.2 Results

2.2.1 BCAR3 promotes membrane protrusiveness

Given that the establishment of membrane protrusions is a critical facet of cell migration [57] and the loss of BCAR3 has been shown to decrease breast cancer cell motility [119], we sought to determine the contribution of BCAR3 to membrane protrusiveness. BT549 cells, which are invasive breast cancer cells that express high levels of BCAR3, were transfected with control (siCtl) or BCAR3-specific (siB3-1) siRNA oligonucleotides and imaged by time-lapse video microscopy. BCAR3 protein levels were consistently reduced by greater than 90% in cells transfected with siB3-1 (**Fig 2.1A**). To visualize the protrusive area of each cell, the first and last frames of the videos were pseudo-colored gray and black, respectively (**Fig 2.1B**). Control cells developed one or more broad protrusions during the time span of the video, while BCAR3-depleted cells exhibited spiky, short-lived extensions. Both the average protrusive area per cell (**Fig 2.1C**) and the time to maximal membrane extension (**Fig 2.1D**) were significantly reduced in BCAR3-depleted cells.

Based on these results, we hypothesized that the converse should also be true, in that ectopic expression of BCAR3 in cells that normally express low levels of the protein would increase membrane protrusiveness and migration. To test this hypothesis, MCF-7 cells expressing BCAR3 under the control of a tetracycline-regulated promoter were imaged by time-lapse video microscopy (**Fig 2.1E**, top panels; **Fig 2.1F**). BCAR3 overexpression resulted in a significant increase in the average protrusive area per cell, a faster migration rate, and an increased distance traveled (**Fig 2.1 G and H; Fig 2.2**).

Membrane protrusions are generated by dynamic actin remodeling through multiple pathways, including the Cas/Crk/Rac1 signaling axis [114, 116]. Previous

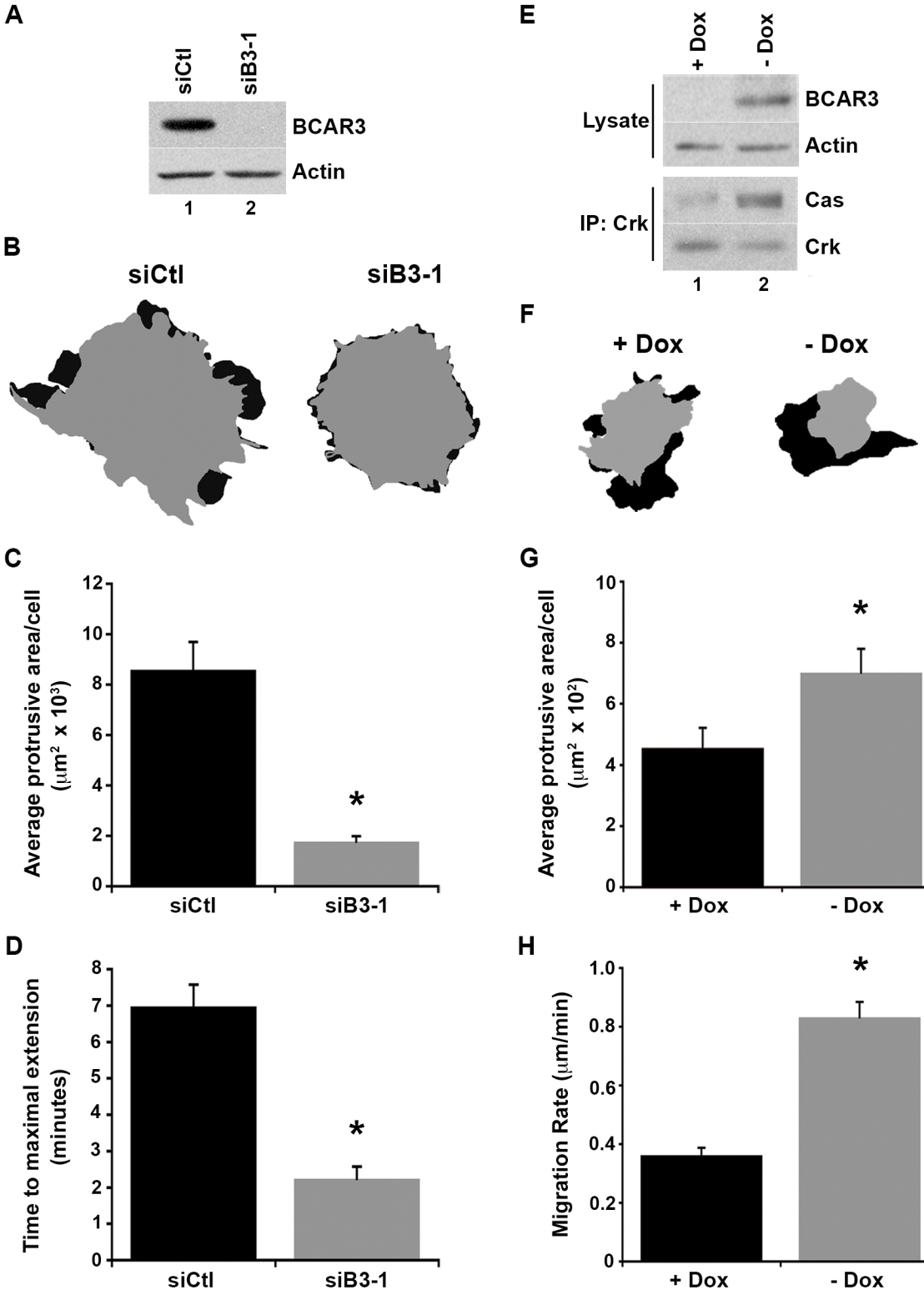
A
siCtl
siB3-1
BCAR3
Actin
1
2
B
siCtl
siB3-1
C
Average protrusive area/cell
(μm² x 10³)
12
10
8
6
4
2
0
*
siCtl
siB3-1
D
Time to maximal extension
(minutes)
8
7
6
5
4
3
2
1
0
*
siCtl
siB3-1
E
+ Dox
- Dox
Lysate
BCAR3
Actin
IP: Crk
Cas
Crk
1
2
F
+ Dox
- Dox
G
Average protrusive area/cell
(μm² x 10²)
10
8
6
4
2
0
*
+ Dox
- Dox
H
Migration Rate (μm/min)
1.0
0.8
0.6
0.4
0.2
0
*
+ Dox
- Dox

Figure 2.1. BCAR3 promotes membrane protrusiveness in breast cancer cells. (**A**) BT549 cells were transfected with control (siCtl; lane 1) or BCAR3-specific (siB3-1; lane 2) siRNA oligonucleotides and incubated for 72 hours prior to lysis. Representative immunoblots of total cell lysates are shown. (**B**) BT549 cells transfected as in (A) were plated on 10μg/ml fibronectin for 4 hours and imaged by time-lapse phase microscopy for 12.5 minutes. Cell outlines of the first and last frames (pseudo-colored gray and black, respectively) of representative cells from a siCtl and siB3-1 movie are shown. (**C**) The average protrusive area was determined by measuring the area shown in black. Data represent the mean ± SEM of at least 12 cells over at least 4 videos (*, $p<0.005$). (**D**) The average time to maximal membrane extension was determined by kymography. Data represent the mean ± SEM of at least 12 kymographs over 3 separate videos (*, $p<0.005$). *Panels A-D provided by Dr. Randy Schrecengost.* (**E**) MCF-7 cells expressing BCAR3 under the control of a tetracycline-inducible (Tet-off) promoter were treated in the presence (lane 1) or absence (lane 2) of 1μg/ml doxycycline (Dox) for 72 hours. Total cell protein and Crk immune complexes were immunoblotted with the designated antibodies. *Panel E provided by Dr. Michael Guerrero.* (**F**) MCF-7 cells were treated with or without Dox as described in (E), then plated on 10μg/ml fibronectin overnight and subjected to time-lapse differential interference contrast (DIC) microscopy for 1 hour. Tracings generated as in (B) for representative cells from a +Dox and –Dox movie are shown. (**G**) The average protrusive area per cell was determined as in (C). Data represent the mean ± SEM of 31 cells per condition over 3 separate videos (*, $p<0.02$). (**H**) Cell motility was measured by tracing the movement of the nucleus over time. The average rate of migration was calculated by dividing the total distance traveled by time for each cell. Data represent the mean ± SEM of at least 72 cells per condition over 3 separate movies (*, $p<0.0001$).

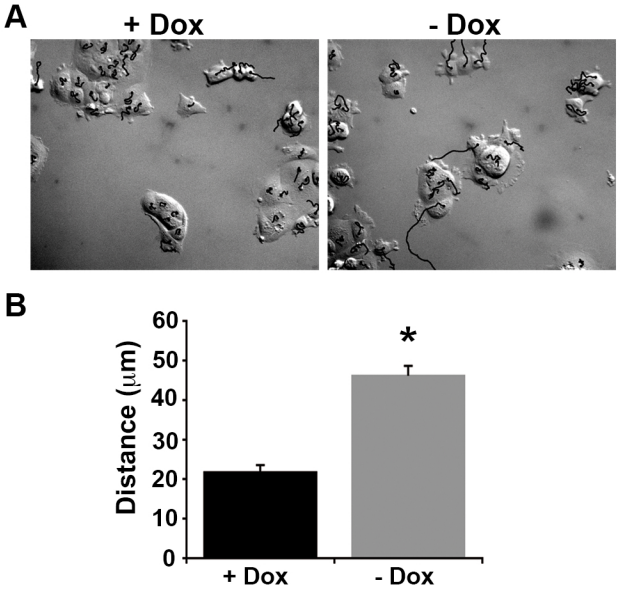
A
+ Dox
- Dox
B
Distance (μm)
60
50
40
30
20
10
0
*
+ Dox
- Dox

Figure 2.2. BCAR3 overexpression increases migration distance. (**A**) MCF-7 cells expressing endogenous (+Dox) or overexpressed (-Dox) BCAR3 were imaged by time-lapse microscopy. Migration distance was determined by tracing the movement of the cell nuclei using ImageJ. Representative tracings from a +Dox and –Dox movie are shown. (**B**) Quantification of migration distance (*, $p<0.05$).

studies by our group have shown that Cas tyrosine phosphorylation, which is required for Cas/Crk association, is increased upon BCAR3 overexpression [129]. Consistent with this finding, the amount of Cas present in association with Crk was found to be significantly elevated when BCAR3 was overexpressed (**Fig 2.1E**, bottom panels). Thus, in addition to increasing membrane protrusiveness and migration, BCAR3 overexpression induces elevated Cas/Crk coupling.

2.2.2 BCAR3 promotes membrane protrusiveness through activation of Rac1

Because Rac1 activity is required for membrane protrusions [136], we next investigated whether BCAR3 promotes membrane protrusiveness through its ability to modulate Rac1 activity [124]. To test this hypothesis, active GTP-bound Rac1 was measured in BT549 cells transfected with siCtl or siB3-1 oligonucleotides. While total Rac1 expression was equivalent in control and BCAR3-depleted cells, Rac1-GTP levels were significantly decreased in the absence of BCAR3 (**Fig 2.3A**). To determine whether this decrease in Rac1 activity was responsible for the loss of protrusiveness seen in the absence of BCAR3, constitutively active Rac1 (Myc-RacL61) was transiently expressed in control and BCAR3-depleted cells and actin-rich membrane protrusions were visualized by immunofluorescence microscopy. As expected, BCAR3 depletion reduced the percentage of cells exhibiting protrusions in the absence of RacL61 (**Fig 2.3C**). However, while expression of RacL61 in control cells did not have a significant effect on membrane protrusions (**Fig 2.3B**, left panel, compare cell marked with arrow to adjacent cell), RacL61 expression in BCAR3-depleted cells significantly increased the percentage of cells containing membrane protrusions (**Fig 2.3B**, right panel, compare cell marked with arrow to adjacent cells marked with arrowheads; **Fig 2.3C**). Interestingly, BCAR3-depleted cells that did not express RacL61 (**Fig 2.3B**, right panel,

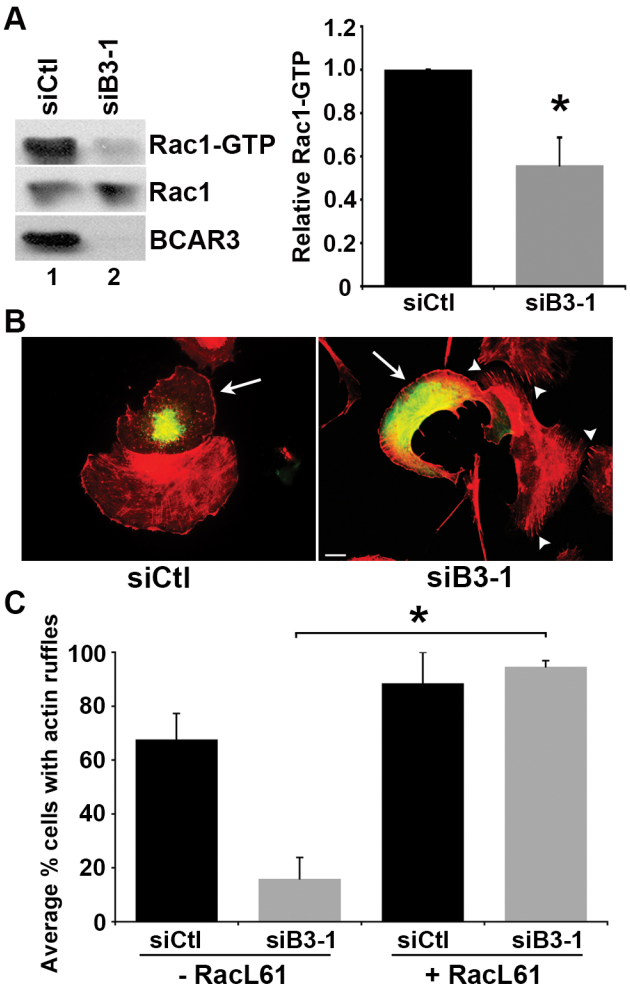
A
siCtl
siB3-1
Rac1-GTP
Rac1
BCAR3
1
2
Relative Rac1-GTP
1.2
1.0
0.8
0.6
0.4
0.2
0
*
siCtl
siB3-1
B
siCtl
siB3-1
C
Average % cells with actin ruffles
100
80
60
40
20
0
*
siCtl
siB3-1
siCtl
siB3-1
- RacL61
+ RacL61

Figure 2.3. BCAR3 promotes Rac1 activity. (**A**) BT549 cells transfected with siCtl (lane 1) or siB3-1 (lane 2) siRNA oligonucleotides were incubated for 72 hours, held in suspension for 90 minutes, then plated on 10μg/ml fibronectin for 1 hour. GTP-bound Rac1 was isolated from whole cell lysates by incubation with p21-activated kinase (PAK)-1-binding domain agarose. Bound proteins (top panel) and total Rac1 (middle panel) were detected by immunoblotting with a Rac1 antibody, and BCAR3 knockdown was confirmed with a BCAR3-specific antibody (bottom panel). Quantification of the relative GTP-Rac1 level is shown. Data represent the mean ± SEM of 3 independent experiments (*, $p<0.05$). *Panel A provided by Dr. Randy Schrecengost.* (**B**) BT549 cells were transfected with siCtl or siB3-1 oligonucleotides, incubated for 24 hours, followed by transfection with plasmids encoding Myc-RacL61 for an additional 48 hours. Cells were plated onto 10μg/ml fibronectin-coated coverslips for 1-3 hours and processed for immunofluorescence as described in the methods. Actin is stained with Texas red-conjugated phalloidin (red) and Myc (RacL61) with FITC (green). Arrows indicate Myc-RacL61 expressing cells. Arrowheads indicate actin-rich stress fibers. The images shown are representative of 6 separate experiments. Scale bar=15μm. (**C**) The percentage of cells exhibiting actin-rich ruffles was determined for non-transfected and RacL61-expressing cells. Data represent the mean ± SEM of at least 36 cells per condition over to 2 separate experiments (*, $p<0.05$). *Panel C provided by Dr. Randy Schrecengost.*

arrowheads) exhibited prominent actin-rich stress fibers that were not evident in control cells or BCAR3-depleted cells expressing constitutively active Rac1. Our group has reported this stabilization of stress fibers in the absence of BCAR3 previously [119]. Collectively, these data show that BCAR3 promotes membrane protrusions through a Rac1-dependent mechanism.

2.2.3 BCAR3 alters actin cytoskeletal and adhesion remodeling

The presence of prominent stress fibers in BCAR3-depleted cells [119] suggests that BCAR3 may influence actin cytoskeletal remodeling. To test this, BT549 cells were transfected with siCtl, siB3-1, or a BCAR3-specific siRNA smartpool of oligonucleotides (siB3-2) (**Fig 2.4C**). The cells were allowed to spread on fibronectin for 3 hours and then actin and adhesion structures were visualized by immunofluorescence microscopy. In control cells, actin was present in peripheral ruffles and diffusely throughout the cytoplasm (**Fig. 2.4A**, panel a). Vinculin was localized adjacent to actin-rich foci in what appeared to be nascent focal complexes (panels b and c) [137]. When BCAR3 was depleted from these cells, prominent actin-rich stress fibers were present throughout the cytoplasm (panels d and g). The majority of these structures appeared to be dorsal stress fibers that originate from single vinculin-containing focal adhesions (panels e, f, h and i). As is the case for ventral stress fibers that have adhesions at both ends, dorsal stress fibers are highly contractile and contribute to intracellular tension [51]. Interestingly, the length of the adhesions in BCAR3-depleted cells was significantly increased compared to control cells (**Fig 2.4B**), suggesting a defect in adhesion turnover. This was further investigated by total internal reflective fluorescence (TIRF)-based video microscopy using GFP-vinculin as a marker of adhesions (**Fig 2.5A and B**). Images representing the first, middle, and last frames of the time-lapse TIRF videos

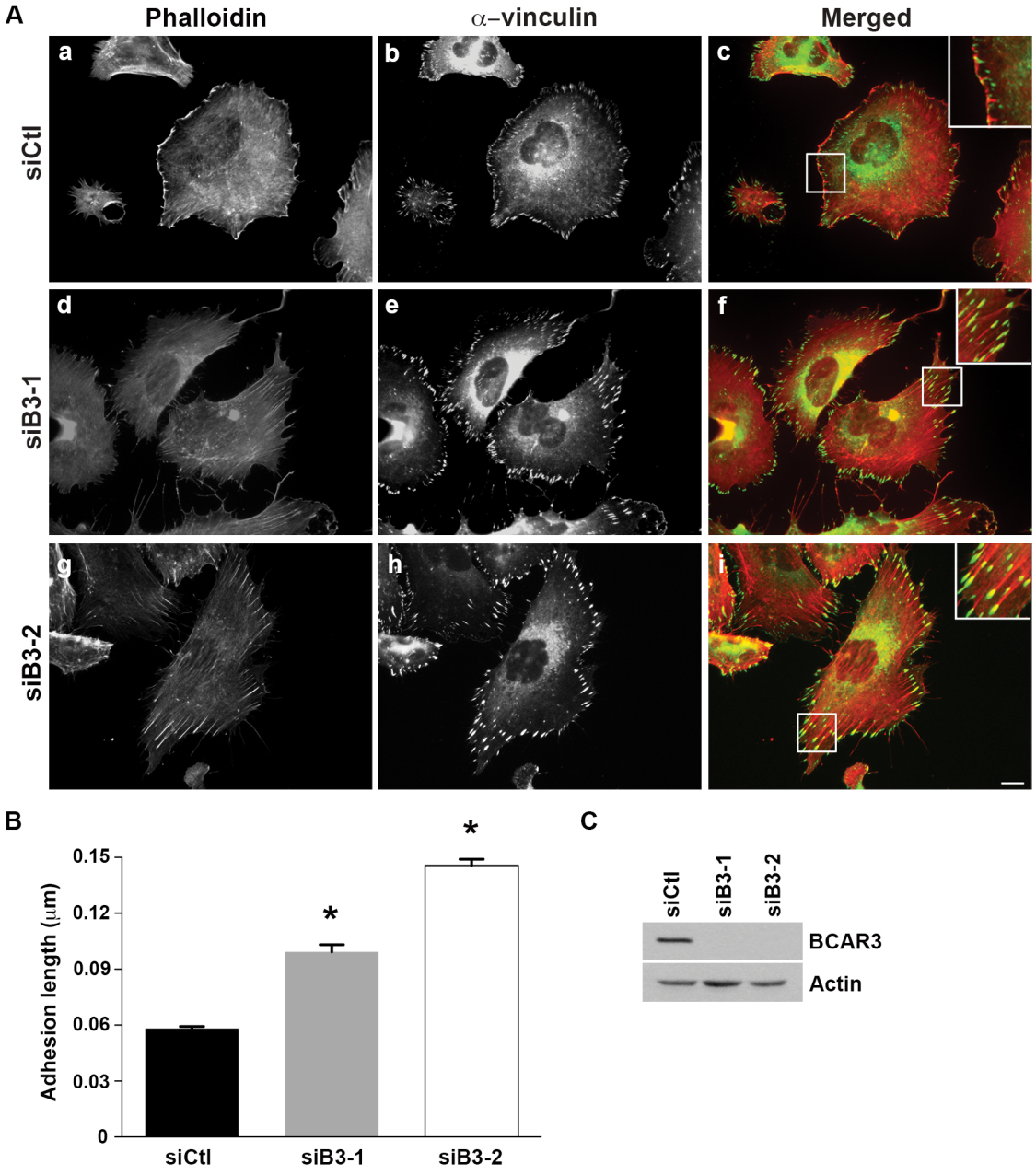
A
Phalloidin
α–vinculin
Merged
siCtl
siB3-1
siB3-2
a
b
c
d
e
f
g
h
i
B
Adhesion length (μm)
0.15
0.12
0.09
0.06
0.03
0
*
*
siCtl
siB3-1
siB3-2
C
siCtl
siB3-1
siB3-2
BCAR3
Actin

Figure 2.4. BCAR3 alters actin organization and adhesion size and distribution in invasive breast cancer cells. (**A**) BT549 cells were transfected with siCtl, siB3-1, or a smartpool consisting of 4 BCAR3-specific siRNA (siB3-2) oligonucleotides, incubated 72 hours, re-plated onto 10μg/ml fibronectin-coated glass coverslips for 3 hours, and then processed for immunofluorescence as described in the methods. Actin and vinculin-containing adhesions were visualized with phalloidin (red) and vinculin (green) antibodies, respectively. Merged images are shown in the right panels, with insets showing higher magnifications of cell peripheries. Scale bar=15μm. A similar adhesion phenotype was observed with paxillin (unpublished data). *Image panels a-f provided by Dr. Randy Schrecengost.* (**B**) Vinculin-containing adhesions in siCtl (black bar), siB3-1 (gray bar), and siB3-2 (white bar) treated cells were measured in ImageJ. Data represent the mean ± SEM of at least 136 adhesions from at least 6 cells for each condition (*, $p<0.0001$). Asterisks indicate values that are significantly different from the control condition. (**C**) BT549 cells were transfected as described in (A). Representative immunoblot is shown confirming knockdown of BCAR3 using 2 distinct siRNA oligonucleotides.

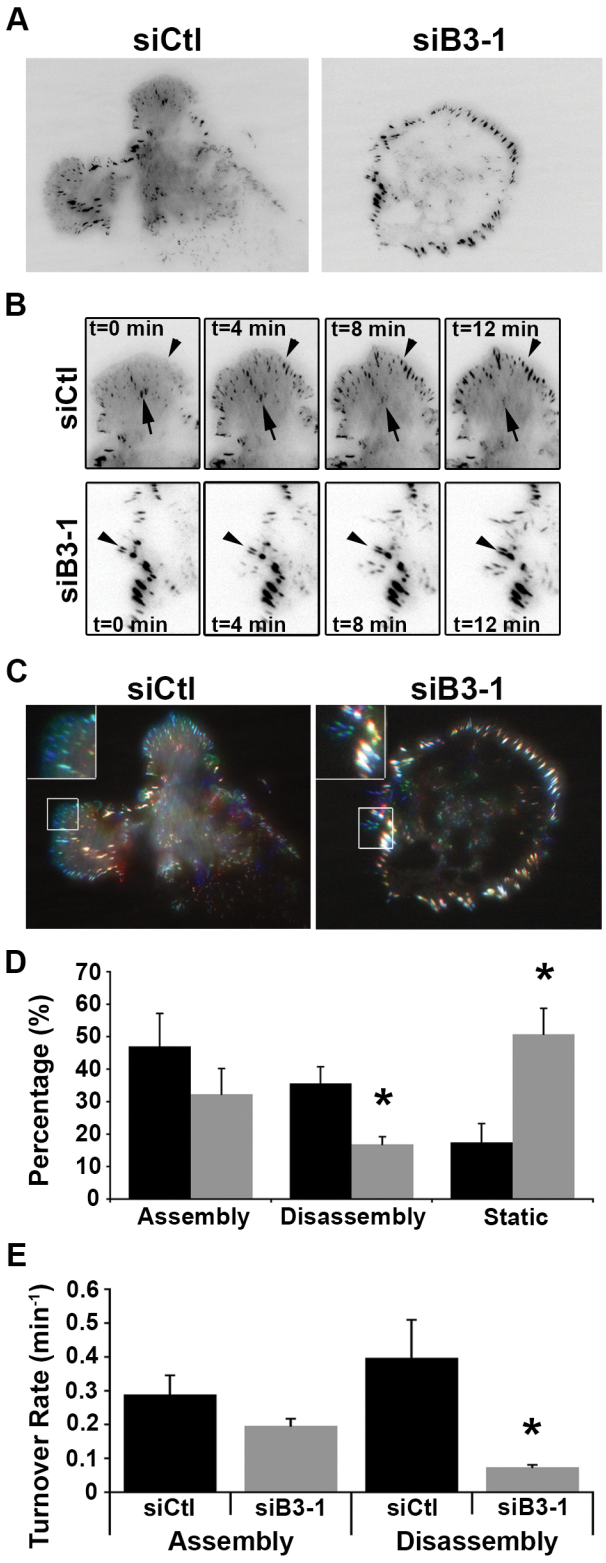
A
siCtl
siB3-1
B
siCtl
siB3-1
t=0 min
t=4 min
t=8 min
t=12 min
C
siCtl
siB3-1
D
Percentage (%)
70
60
50
40
30
20
10
0
*
*
Assembly
Disassembly
Static
E
Turnover Rate (min-1)
0.6
0.5
0.4
0.3
0.2
0.1
0
*
siCtl
siB3-1
siCtl
siB3-1
Assembly
Disassembly

Figure 2.5. BCAR3 regulates adhesion disassembly. (**A**) BT549 cells were transfected with siCtl or siB3-1 siRNA oligonucleotides, incubated for 24 hours, and then transfected with plasmids encoding GFP-vinculin for an additional 48 hours. Cells were plated on 2μg/ml fibronectin for 4 hours and then visualized by TIRF-based video microscopy to analyze adhesion dynamics. Representative images from a siCtl and siB3-1 movie are shown. (**B**) Time-lapse images from TIRF microscopy show assembly (arrowheads) and disassembly (arrows) of vinculin-containing adhesions over the specified time course for control (top row) and BCAR3-depleted (bottom row) cells. (**C**) Analysis of vinculin-containing adhesion turnover. The first, middle, and final frames from a representative siCtl and siB3-1 movie were pseudo-colored red, green, and blue, respectively, and then merged into a single image to visualize adhesion dynamics. At least 3 cells per condition were pseudo-colored. Insets show higher magnifications of peripheral adhesions. (**D**) Quantitative analysis of the adhesions that assembled, disassembled, or remained static over the time course shown in (B) for control (black bars) and BCAR3-depleted (gray bars) cells (*, $p<0.05$). (**E**) Quantitative analysis of the turnover rate of vinculin-containing adhesions. At least 18 adhesions from 3 separate control (black bars) and BCAR3-depleted (gray bars) cells were measured as described in the methods (*, $p<0.005$). Asterisks indicate values that are significantly different from control conditions. *Figure 2.5 provided by Dr. Randy Schrecengost.*

were pseudo-colored red, green, and blue, respectively, and merged into a single color image to more readily visualize the dynamics of adhesion assembly and disassembly (**Fig 2.5C**). In control cells, adhesion assembly (**Fig 2.5B**, top row, arrowheads; **Fig 2.5C**, green or blue adhesions) was most often observed at the periphery of the cell, while adhesion disassembly (**Fig 2.5B**, top row, arrows; **Fig 2.5C**, yellow or red adhesions) was observed in more centrally located regions of the cell. Adhesions in BCAR3-depleted cells were predominantly localized to the periphery of the cell and showed accumulation but little loss of GFP-vinculin over time (**Fig 2.5B**, bottom row, arrowheads; **Fig 2.5C**, white adhesions). To quantify adhesion assembly and disassembly rates, the pixel intensity of vinculin-containing structures was determined as a function of time. While the percentage of adhesions undergoing assembly was not statistically different between control and BCAR3-depleted cells, cells lacking BCAR3 contained a significantly reduced number of adhesions undergoing disassembly (**Fig 2.5D**). This resulted in a greater number of adhesions remaining "static" or stable. Moreover, the few adhesions that were seen to undergo disassembly in cells lacking BCAR3 had a significantly slower turnover rate (**Fig 2.5E**). Taken together, these data indicate that BCAR3 regulates adhesion dynamics, particularly disassembly, in invasive breast cancer cells.

2.2.4 Growth factor-induced cytoskeletal remodeling is regulated by BCAR3

Thus far, we have shown that BCAR3 controls cytoskeletal changes that arise in response to cell adhesion to fibronectin. We previously reported that BT549 cells depleted for BCAR3 also failed to undergo characteristic cytoskeletal remodeling following growth factor stimulation (i.e. severing of actin-rich stress fibers and acquisition of membrane protrusions) [119]. Given these findings, we sought to define the extent to

which BCAR3 regulated cytoskeletal dynamics in response to EGF stimulation. By using a second invasive breast cancer cell line (MDA-MB-231), we also sought to determine whether the impact of BCAR3 signaling on the actin cytoskeleton was consistent across multiple cell lines. MDA-MB-231 cells treated with control siRNA oligonucleotides exhibited robust actin cytoskeletal and adhesion remodeling in response to EGF, marked by a loss of stress fibers (**Fig 2.6A**, compare panels a and d; **Fig 2.6B**, black bars) and the redistribution of adhesions to sites of broad, actin-rich lamellipodia (**Fig 2.6A**, compare panels b and c with panels e and f). In contrast, cells treated with siB3-1 siRNAs exhibited an attenuated response characterized by stabilization of stress fibers (**Fig 2.6A**, panels g and j; **Fig 2.6B**, gray bars) and large adhesions (**Fig 2.6A**, panels h, i, k and l). Knockdown of BCAR3 in MDA-MB-231 cells using siB3-2 resulted in a similar, albeit somewhat less pronounced, defect in the cytoskeletal response to EGF (**Fig 2.6A**, panels m through r; **Fig 2.6B**, white bars). We attribute this difference to the fact that siB3-2 was less efficient at reducing BCAR3 expression in MDA-MB-231 cells than was siB3-1 (**Fig 2.6C**). These data indicate that BCAR3 regulates actin cytoskeletal remodeling and adhesion dynamics in response to EGF as well as fibronectin.

2.2.5 RhoA-mediated contractility predominates upon loss of BCAR3

RhoA-dependent stress fibers and focal adhesions create intracellular tension, which is a hallmark of highly contractile cells [138]. Thus, our findings that BCAR3-depleted cells exhibit prominent stress fibers and mature adhesions in response to adhesion and growth factor signaling supports a hypothesis whereby RhoA activity is increased in the absence of BCAR3. To test this hypothesis, active GTP-bound RhoA levels were measured in control and BCAR3-depleted BT549 cells transiently expressing

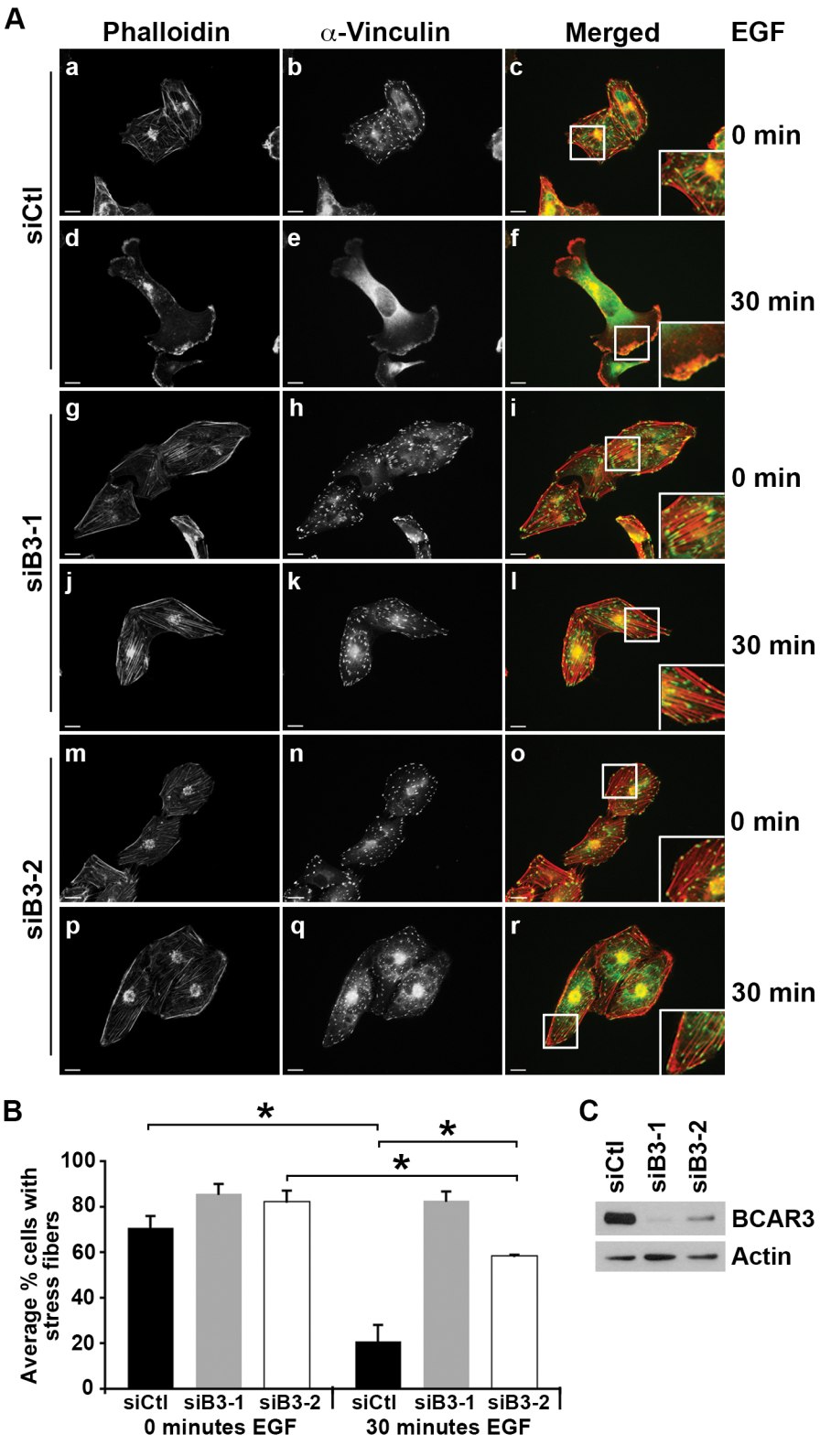
A
Phalloidin
α-Vinculin
Merged
EGF
siCtl
siB3-1
siB3-2
0 min
30 min
0 min
30 min
0 min
30 min
B
Average % cells with stress fibers
100
80
60
40
20
0
siCtl siB3-1 siB3-2
0 minutes EGF
siCtl siB3-1 siB3-2
30 minutes EGF
C
siCtl
siB3-1
siB3-2
BCAR3
Actin

Figure 2.6. BCAR3 regulates actin cytoskeletal and adhesion remodeling in response to growth factor. (**A**) MDA-MB-231 cells were transfected with siCtl, siB3-1, or siB3-2 oligonucleotides and incubated for 24 hours prior to plating onto 10μg/ml fibronectin-coated glass coverslips. Cells were serum-starved for 16-18 hours, stimulated with 100ng/ml EGF for 0 or 30 minutes, and then fixed and processed for immunofluorescence as described in the methods. Actin and vinculin-containing adhesions were visualized with phalloidin (red) and vinculin (green) antibodies, respectively. Merged images are shown in the right panels; insets show higher magnifications of actin and adhesion structures. Scale bars=15μm. (**B**) The percentage of siCtl (black bars), siB3-1 (gray bars), and siB3-2 (white bars) treated cells containing actin-rich stress fibers was determined. Data represent the mean ± SEM of at least 730 cells per condition from 3 separate experiments (*, $p<0.04$). (**C**) MDA-MB-231 cells were transfected as described in (A). Representative immunoblots are shown confirming knockdown of BCAR3 using 2 separate siRNA oligonucleotides.

GFP-tagged RhoA. GTP-bound GFP-RhoA levels were increased by approximately 2.6-fold in the absence of BCAR3 (**Fig 2.7A**). Downstream of RhoA, ROCK becomes activated and phosphorylates MLC. Consistent with elevated RhoA/ROCK activity, pMLC levels were increased 2.7-fold over control cells when BCAR3 was depleted (**Fig 2.7B**, compare lanes 1 and 3; see graph). As expected, MLC phosphorylation was dependent on ROCK activity, since pMLC levels were nearly undetectable in the presence of the ROCK inhibitor Y-27632, irrespective of BCAR3 expression (lanes 2 and 4).

ROCK signaling downstream of RhoA is also important for adhesion maturation. To investigate whether ROCK contributes functionally to the increased adhesion length present in cells depleted for BCAR3, vinculin-containing adhesions were examined under conditions in which ROCK activity was inhibited with Y-27632. As was shown in **Figure 2.4**, adhesion length was significantly greater in cells depleted for BCAR3 compared with control cells (**Fig 2.8A**, compare panels a and c; **Fig 2.8B**, compare bars 1 and 3). Inhibition of ROCK resulted in a reversal of this phenotype in BCAR3-depleted cells (**Fig 2.8A**, panel d; **Fig 2.8B**, compare bars 3 and 4), demonstrating that ROCK is required for the increase in adhesion length seen upon loss of BCAR3.

A second RhoA effector that has been implicated in adhesion maturation is mDia [81]. To determine whether mDia1 contributes to the adhesion response seen in BCAR3-depleted cells, BT549 cells were transfected with siCtl or siB3-1 along with mDia1-specific siRNAs (siDia1). In the presence of endogenous BCAR3, loss of mDia1 had no effect on adhesion size (**Fig 2.8B**, compare bars 1 and 5), although the adhesions appeared more centrally located (**Fig 2.8A**, compare panels a and e). In contrast, depletion of mDia1 in cells lacking BCAR3 diminished the elongated adhesion response seen in BCAR3-depleted cells, resulting in shorter adhesions (**Fig 2.8A**,

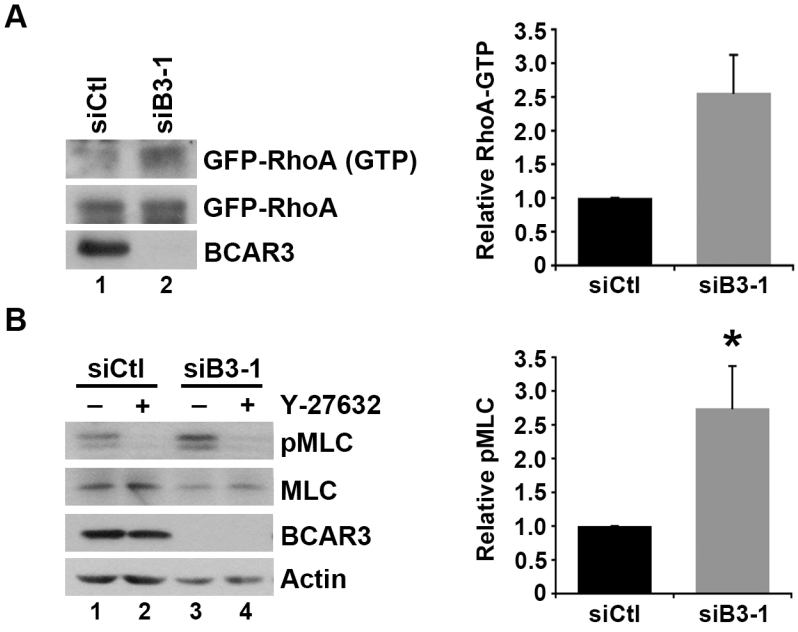
A
siCtl
siB3-1
GFP-RhoA (GTP)
GFP-RhoA
BCAR3
1
2
Relative RhoA-GTP
3.5
3.0
2.5
2.0
1.5
1.0
0.5
0
siCtl
siB3-1
B
siCtl
siB3-1
–
+
–
+
Y-27632
pMLC
MLC
BCAR3
Actin
1
2
3
4
Relative pMLC
*
3.5
3.0
2.5
2.0
1.5
1.0
0.5
0
siCtl
siB3-1

Figure 2.7. Loss of BCAR3 elevates RhoA activity and ROCK-mediated phosphorylation of MLC II. (**A**) BT549 cells were transfected with siCtl (lane 1) or siB3-1 (lane 2) siRNA oligonucleotides, incubated for 48 hours, followed by transfection with plasmids encoding GFP-tagged RhoA. Twenty-four hours later, cells were trypsinized, held in suspension for 90 minutes, and then plated on 10μg/ml fibronectin for 1 hour. GTP-bound GFP-RhoA was isolated from whole cell lysates by incubation with Rhotekin binding domain (RBD) agarose. Bound proteins (top panel) and total GFP-RhoA (middle panel) were detected by immunoblotting with a Rho antibody, and BCAR3 knockdown was confirmed with a BCAR3-specific antibody (bottom panel). Quantification of the relative RhoA-GTP level is shown. RhoA activity was increased by an average of 2.6-fold ± 0.6 (n=2). Error bars represent standard deviation. (**B**) BT549 cells transfected with siCtl or siB3-1 siRNA oligonucleotides were held in suspension for 90 minutes and then plated onto 10μg/ml fibronectin in the absence or presence of 20μM Y-27632. Cells were lysed in 2X boiling hot sample buffer, sheared with a 27-gauge needle, resolved by 12.5% SDS-PAGE, and immunoblotted with antibodies recognizing phospho-specific MLC (pThr18/pSer19) or total MLC (top panels). Total cell lysates were resolved by 8% SDS-PAGE and immunoblotted with antibodies recognizing BCAR3 and actin (bottom panels). Quantification of the relative pMLC level is shown. pMLC was increased by an average of 2.7-fold ± 0.6 (n=5; *, $p<0.05$) in cells lacking BCAR3. Error bars represent SEM.

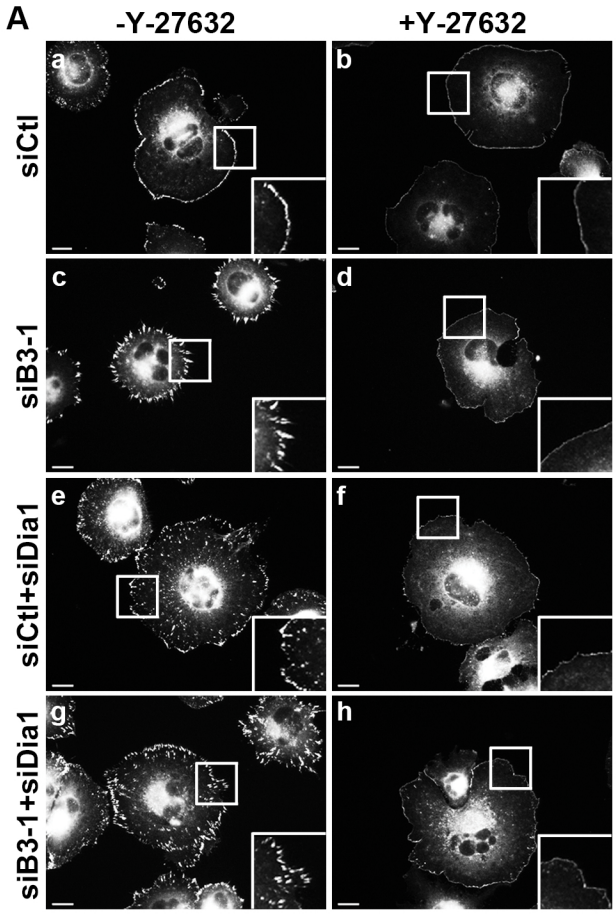
A
-Y-27632
+Y-27632
siCtl
siB3-1
siCtl+siDia1
siB3-1+siDia1
a
b
c
d
e
f
g
h

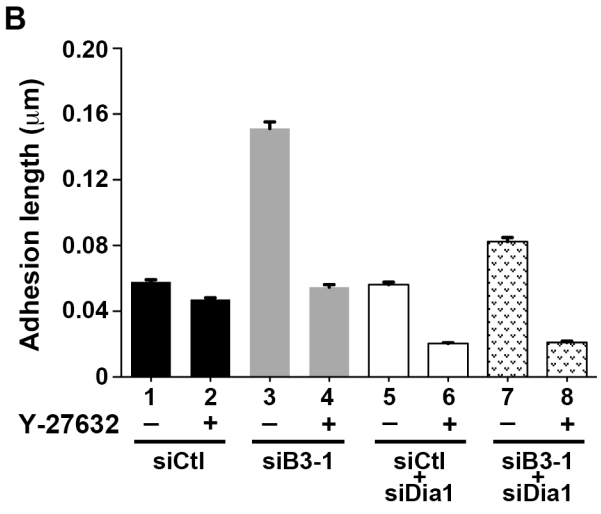
B
Adhesion length (μm)
0.20
0.16
0.12
0.08
0.04
0
1 2 3 4 5 6 7 8
Y-27632
– + – + – + – +
siCtl
siB3-1
siCtl + siDia1
siB3-1 + siDia1

Figure 2.8. RhoA effector signaling mediates adhesion length in BCAR3-depleted invasive breast cancer cells. (**A**) BT549 cells transfected with siCtl or siB3-1 ± mDia1-targeted (siDia1) siRNA oligonucleotides were held in suspension for 90 minutes, plated onto 10μg/ml fibronectin in the absence or presence of 20μM Y-27632, and then processed for immunofluorescence as described in the methods. Adhesions were visualized using a vinculin antibody; insets show higher magnifications of peripheral adhesions. Scale bars=15μm. Similar results were obtained with paxillin staining (unpublished data). (**B**) Quantification of adhesion length in siCtl (black bars), siB3-1 (gray bars), siCtl+siDia1 (white bars), and siB3-1+siDia1 (hashed bars) treated cells in the absence or presence of Y-27632. Data represent the mean ± SEM of at least 343 adhesions from at least 13 cells from 2 separate experiments. ANOVA analysis confirmed all conditions were significantly different from one another ($p<0.0001$) except the following comparisons: siCtl-Y vs. siCtl+siDia1-Y (bars 1 and 5), siCtl+Y vs. siB3-1+Y (bars 2 and 4), and siCtl+siDia1+Y vs. siB3-1+siDia1+Y (bars 6 and 8).

compare panels c and g; **Fig 2.8B**, compare bars 3 and 7). This shows that, like ROCK, mDia1 contributes to the increased adhesion size observed under conditions of BCAR3 depletion. Interestingly, simultaneous inhibition/loss of ROCK and mDia1 resulted in adhesions that were markedly smaller than those present in control cells (**Fig 2.8A**, compare panels a and f; **Fig 2.8B**, compare bars 1 and 6). Moreover, this phenotype was maintained under conditions of BCAR3 loss (compare bars 6 and 8), demonstrating that dual blockade of the ROCK and mDia arms of RhoA signaling completely abrogates the effect of BCAR3 depletion on focal adhesion length. Together, these data show that RhoA-dependent pathways predominate in invasive breast cancer cells in the absence of BCAR3.

2.3 Discussion

A balance between Rac1 and RhoA signaling is critical for cell motility. In tumor cells, the aberrant expression and/or activity of molecules that are responsible for regulating the activity of these GTPases can disrupt this balance and promote metastasis [139]. In this work, we demonstrate that BCAR3, an adaptor molecule that regulates cell motility and invasion, tips the balance in favor of Rac1 in invasive breast cancer cells, thus promoting Rac1-dependent events such as membrane protrusions and adhesion turnover (**Fig 2.9A**). The critical role played by BCAR3 in regulating this balance is underscored by the increase in RhoA activity and RhoA-dominant phenotypes (stable stress fibers, elevated pMLC, and large ROCK/mDia1-dependent focal adhesions) seen in these cells upon BCAR3 depletion (**Fig 2.9B**).

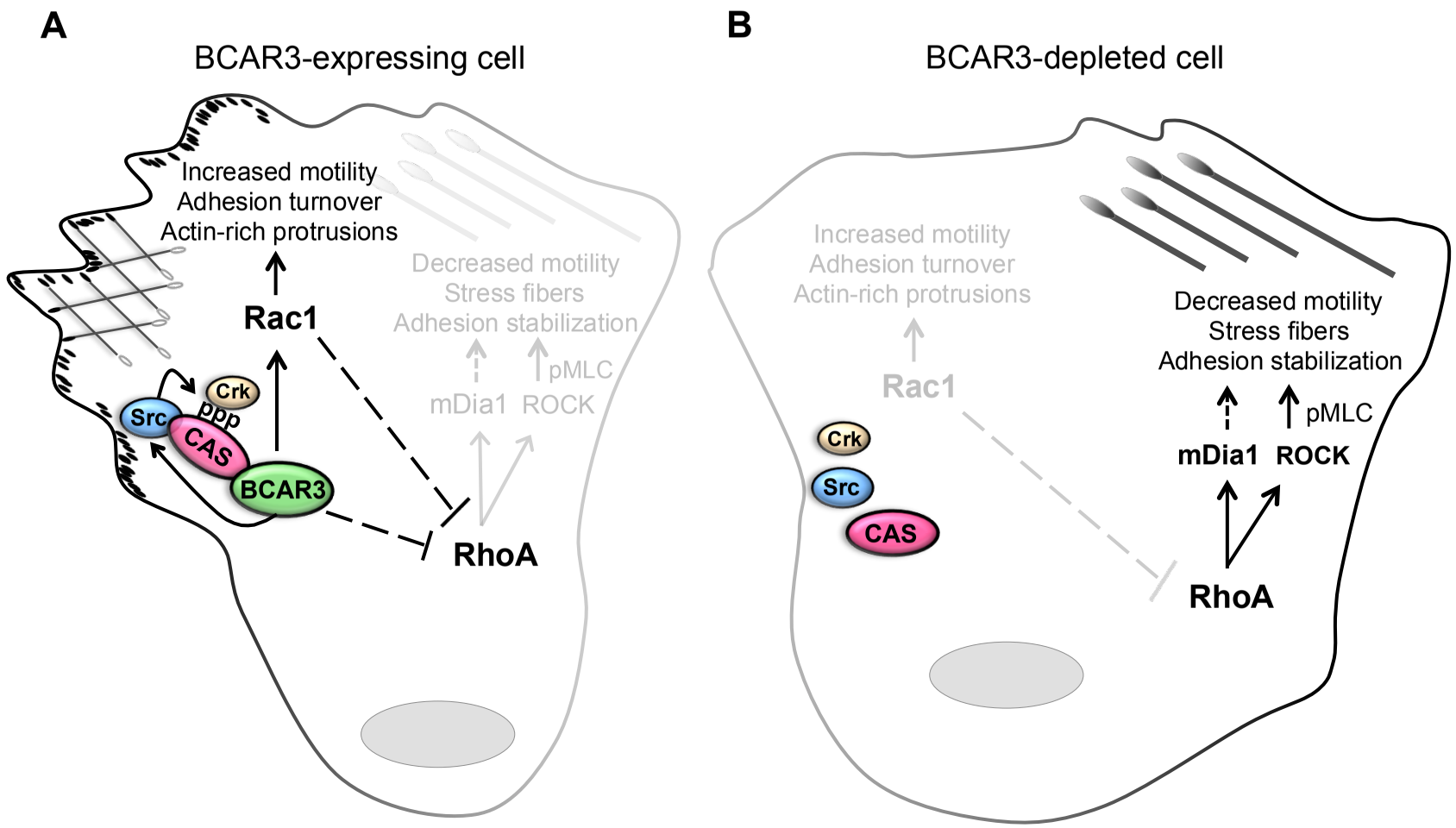
A
BCAR3-expressing cell
Increased motility
Adhesion turnover
Actin-rich protrusions
Rac1
Decreased motility
Stress fibers
Adhesion stabilization
pMLC
mDia1
ROCK
Crk
ppp
Src
CAS
BCAR3
RhoA
B
BCAR3-depleted cell
Increased motility
Adhesion turnover
Actin-rich protrusions
Rac1
Decreased motility
Stress fibers
Adhesion stabilization
pMLC
mDia1
ROCK
Crk
Src
CAS
RhoA

Figure 2.9. BCAR3 regulates the balance between Rac1 and RhoA signaling in invasive breast cancer cells. (**A**) When BCAR3 protein is expressed at high levels, as is the case in invasive breast cancer cell lines, it promotes Rac1 activity, membrane protrusiveness, adhesion turnover, and rapid cell motility. We suggest that BCAR3 may enhance Rac1 activity through Src/Cas/Crk coupling. It is also possible that BCAR3 may actively suppress RhoA activity/signaling, and in doing so, indirectly elevate Rac1 activity. (**B**) When BCAR3 is depleted from these cells, RhoA activity is elevated and RhoA-dependent phenotypes predominate, resulting in the presence of prominent stress fibers, elevated pMLC levels, and large ROCK/mDia1-dependent focal adhesions.

2.3.1 Regulation of Rac1 by BCAR3

Considering that the GEF-like C-terminal domain of BCAR3 adopts a "closed" conformation that is prohibitive for catalytic activity, it is unlikely that BCAR3 functions directly as a GEF [125]. Instead, it is possible that the Rac1 GEF DOCK180/ELMO becomes activated through BCAR3-dependent augmentation of Cas/Crk coupling [114, 116, 117, 140, 141] (**Fig 2.9A**). In support of this possibility, our group has shown that elevated BCAR3 protein expression in breast cancer cells promotes Src/Cas interactions, Src kinase activity, Src-mediated Cas tyrosine phosphorylation, Cas/Crk association, and Rac1 activity ([119, 129], and data herein). Additional data from Adam Lerner's group show that BCAR3/Cas interactions are required for Src to bind to, and phosphorylate, Cas as well as to promote optimal cell motility [142, 143]. Whether Cas is directly required for BCAR3-mediated Rac1 activation has been difficult to determine because BCAR3 expression becomes significantly reduced when Cas is depleted in BT549 or MDA-MB-231 cells (data not shown). Our group is currently working to understand the mechanism underlying this regulation.

Recently, PTPα has been shown to function as a molecular bridge that can serve as a link between adhesion signals and the BCAR3/Cas/Src signaling axis [130]. It is therefore interesting to note that PTPα-null cells share phenotypic and biochemical characteristics with BCAR3-depleted cells, including decreased adhesion-dependent Rac1 activity, Src/Cas interactions, Src kinase activity, Cas phosphorylation, Cas/Crk association, cell spreading, and motility/invasion [119, 129, 130]. Catherine Pallen's group suggests that PTPα/BCAR3 interactions are important for recruiting Cas to membrane-proximal regions of the cell [130], which could in turn augment Cas/Src interactions, Src activity, and ultimately Rac1 activation [129, 144]. This model emphasizes the importance of Src in mediating cytoskeletal responses to adhesion and

growth factor signals, and helps to explain how BCAR3 may be an important regulator in these processes. It is interesting to speculate that the nature of the initiating adhesion signal (e.g. engagement of specific integrins and/or level of activation) may influence the temporal and spatial activation of this pathway.

Although not mutually exclusive, a second possibility that may account for the BCAR3-dependent Rac1 activity observed in invasive breast cancer cells is that BCAR3 may actively suppress RhoA signaling, leading indirectly to Rac1 activation (**Fig 2.9A**). Indeed, there are numerous examples showing reciprocal regulation of Rac1 and RhoA signaling, such that when one GTPase is locally active, the other is suppressed [85]. This active suppression of RhoA by BCAR3 could arise from its ability to either positively regulate a Rho GAP and/or negatively regulate a Rho GEF. There are a number of candidate targets for this regulation. For example, the activity of p190RhoGAP is positively regulated by Src [104], which makes it a potentially attractive downstream target of BCAR3 signaling. There are additional candidate Rho GAPs (e.g. p250RhoGAP, DLC-1) and GEFs (e.g. p115RhoGEF, p190RhoGEF, LARG) downstream of integrins that are modulated by Src and other Src-family kinases (SFKs) [103, 145]. Future studies will determine whether any of these molecules contribute to the suppression of RhoA by BCAR3 and, in so doing, help to elucidate the mechanism by which BCAR3 influences the balance between Rac1 and RhoA signaling in invasive breast cancer cells. Finally, it is important to note that Rac1-RhoA reciprocity could not only account for Rac1 activation through suppression of RhoA, but the converse could also be true in that the high RhoA activity seen in BCAR3-depleted cells could result from diminished Rac1 activity (**Fig 2.9B**).

2.3.2 BCAR3 and breast cancer progression

BCAR3 protein expression is elevated in cell lines representative of TNBC compared to ER^+ cells [119, 120]. As discussed above, BCAR3 function is intimately linked to two proteins, Cas and Src. Like BCAR3, these molecules are established regulators of cell motility, antiestrogen resistance, and other aggressive breast cancer behaviors [15, 96, 99, 110, 113, 146]. Interestingly, Src kinase activity is also elevated in TNBC [147, 148]. Since BCAR3 has been shown to function through Cas to activate Src [129, 149], we suggest that its upregulation in TNBC may contribute to the elevated Src activity seen in these tumors.

In addition to Src, EGFR is frequently overexpressed in aggressive breast tumors and TNBC cell lines, as are a number of downstream components of EGF signaling pathways [8, 65, 150]. The data presented above showing that BCAR3 regulates the cytoskeletal response of invasive breast cancer cells to EGF thus provide a second point of convergence between BCAR3 and intracellular signaling pathways that control tumor cell motility and invasion. As is the case for the BCAR3/Src/Cas/Crk signaling axis, EGFR/BCAR3 signaling may contribute to actin remodeling through Rac1. However, a second potential mechanism involves cofilin, which becomes activated in response to EGF and causes stress fiber dissolution to produce a pool of free actin monomers available for polymerization [65]. Thus, it will be important to explore the possibility that BCAR3 may also contribute to actin remodeling through the EGF-mediated cofilin pathway. There is considerable evidence for a role of EGF in promoting breast cancer cell invasion, and we have shown that BCAR3 can regulate the migration/invasion of breast tumor cells toward EGF [119, 151]. Whether this is achieved through the actin remodeling activities of BCAR3 is yet to be determined.

Despite strong evidence for BCAR3 as a regulator of breast cancer cell motility and invasion, the role of BCAR3 in other cell types is not widely known. While BCAR3 mRNA is present in multiple cell types and tissues, its expression appears to be largely dispensable for development since BCAR3 knockout mice are born at the expected Mendelian frequency and have normal lifespans (The Human Protein Atlas, [118, 126]). In fact, the only spontaneous defect reported for these mice is in the lens of the eye [126]. Thus it is interesting that this molecule plays such an essential role in regulating cytoskeletal remodeling, adhesion turnover, and cell motility in invasive breast cancer cells. We hypothesize that BCAR3 expression may become upregulated in breast tumor cells in response to selective pressures present in the TME such as hypoxia or nutrient deprivation. The BCAR3 signaling pathway would then be in place to promote rapid and efficient invasion/migration of these tumor cells to distal sites in response to these environmental stresses. Importantly, our finding that these cells fail to respond properly to chemotactic (e.g. EGF) and mechanical (e.g. adhesion signals) stimuli in the absence of BCAR3 could have significant implications for treatment of breast cancers that express this protein, as it may be possible to target BCAR3 (or other molecules within the BCAR3/Cas/Src signaling network) in the tumors with limited collateral damage to other tissues. Future work is needed to determine the potential benefits of this type of an approach.

CHAPTER 3: Direct interaction between BCAR3 and Cas promotes adhesion disassembly in invasive breast cancer cells

3.1 Introduction

The assembly and subsequent disassembly (or turnover) of cellular adhesions governs adhesion dynamics [51]. As discussed in **Chapter 1**, adhesion turnover is required for persistent protrusion/motility and is initiated when there is a lack of tension to reinforce the adhesion. Adaptor molecules present in adhesions locally activate Rac1 and inhibit RhoA signaling, thereby reducing tension and promoting adhesion disassembly [75, 76]. We have previously demonstrated that the adaptor molecule BCAR3 promotes Rac1 activity and adhesion disassembly in invasive breast cancer cells (**Chapter 2**, [47]). However, the mechanism through which BCAR3 performs this action remains to be elucidated. Recently, a direct physical association between BCAR3 and Cas has been shown to be important for many of the biological activities of BCAR3 [132]. In this current work, we set out to determine the significance of direct BCAR3/Cas interaction in adhesion dynamics. We show for the first time that BCAR3 co-localizes with Cas in adhesions. While the incorporation of BCAR3 into adhesions does not require a direct interaction with Cas, we discovered that the rate at which BCAR3 dissociates from adhesions is significantly reduced when it is unable to directly bind to Cas. Interestingly, we demonstrate that direct association between BCAR3 and Cas is required for efficient BCAR3-mediated adhesion disassembly in invasive breast cancer cells, as evidenced by the slower dissociation rates of multiple adhesion proteins observed in the absence of BCAR3/Cas interaction. Together, we propose that BCAR3 locally increases Rac1 activity and promotes adhesion disassembly through the BCAR3/Cas complex.

3.2 Results

3.2.1 BCAR3 co-localizes with Cas in adhesions

It has previously been reported that BCAR3 can localize to vinculin-containing adhesions and this is dependent upon the SH2-domain of BCAR3 and its interaction with PTPα [130]. However, these studies were performed as overexpression systems in wildtype and PTPα-null mouse embryonic fibroblasts (MEFs). To determine the localization of BCAR3 in a more physiologically relevant setting, we generated a GFP-tagged BCAR3 construct in which BCAR3 expression is under the control of a low expression "speckled" promoter [152]. This technology resulted in the expression of very low levels of exogenous BCAR3 protein in invasive human breast cancer cells, so as not to disturb endogenous signaling. BT549 cells were transfected with speckled GFP-BCAR3 and allowed to spread on fibronectin for 4 hours. Cells were then fixed and stained with an endogenous Cas antibody prior to visualizing adhesions via TIRF microscopy. Under these conditions, BCAR3 co-localized with endogenous Cas in small, peripheral adhesion structures reminiscent of focal complexes (**Fig 3.1**, top panels) as well as in more mature focal adhesions situated further back from the leading edge within the lamellum (bottom panels). To our knowledge, this is the first time co-localization of these two adaptor proteins in adhesions has been shown.

3.2.2 Localization of BCAR3 to adhesions does not require direct interaction with Cas

Given that a direct association between BCAR3 and Cas is required for their reciprocal stability as well as BCAR3-mediated chemotaxis towards EGF [125, 132], we next asked whether the localization of BCAR3 to adhesions requires a direct interaction with Cas. This was addressed using a BCAR3 molecule containing two point mutations,

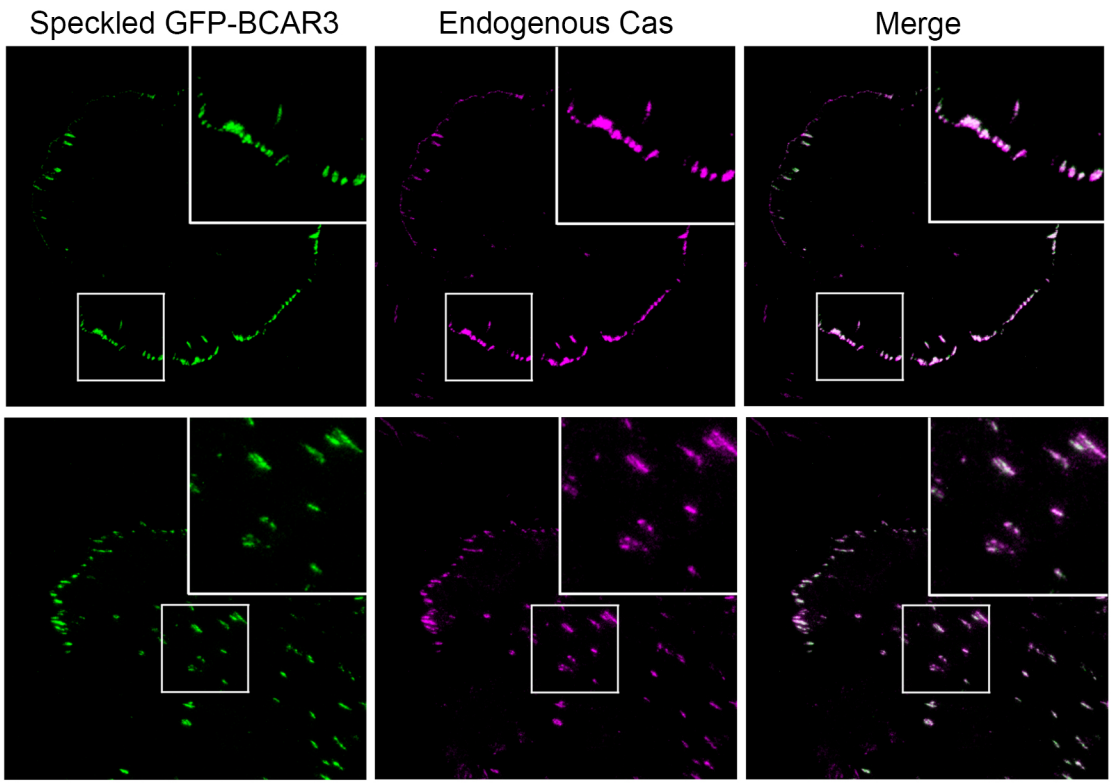
Speckled GFP-BCAR3
Endogenous Cas
Merge

Figure 3.1. BCAR3 co-localizes with endogenous Cas in adhesions. BT549 invasive breast cancer cells were transfected with a plasmid in which GFP-tagged BCAR3 expression is driven off of a speckle promoter. Cells were then incubated for 24 hours prior to plating on 10μg/ml fibronectin-coated coverslips. Cells were allowed to spread for 4 hours, then fixed and stained with polyclonal Cas antibodies as described in the methods to detect endogenous Cas. Adhesions were visualized via TIRF microscopy. Merged images are shown in the right panels. Insets show higher magnifications of cell peripheries.

L744E and R748E, which were recently shown to completely abolish the interaction between BCAR3 and Cas [132]. To verify that these point mutations abrogated Cas binding, Cas immune complexes were isolated from untransfected BT549 cells or BT549 cells transfected with wildtype (WT) GFP-BCAR3 or L744E/R748E GFP-BCAR3 (**Fig 3.2A**). As expected, endogenous BCAR3 (lanes 4-6) and WT GFP-BCAR3 (lane 5) were both present in Cas immune complexes. However, L744E/R748E GFP-BCAR3 was completely absent (lane 6). To test whether BCAR3 and Cas association is necessary for BCAR3 localization to adhesions, BT549 cells were transfected with either WT or L744E/R748E GFP-BCAR3 and allowed to spread on fibronectin for 4 hours. Cells were then fixed and stained with an endogenous Cas antibody prior to visualizing adhesions via TIRF microscopy. Surprisingly, L744E/R748E GFP-BCAR3 was present in adhesions despite the fact that it was unable to interact with Cas (**Fig 3.2B**, bottom panels). To further explore the need for Cas in localizing BCAR3 to adhesions, GFP-BCAR3 was expressed in Cas-/- MEFs. GFP-BCAR3 was seen to co-localize with vinculin in adhesions under these conditions despite the fact that Cas was not expressed (**Fig 3.3**). Together, these data demonstrate that BCAR3 localization to adhesions does not require direct association with Cas, and suggest that other proteins may be responsible for positioning and stabilizing BCAR3 in adhesions, at least when Cas is absent or unable to bind to BCAR3.

3.2.3 Direct interaction between BCAR3 and Cas is required for efficient dissociation of BCAR3 from adhesions

While localization of BCAR3 to adhesions does not require a direct interaction with Cas, we have shown that BCAR3 regulates adhesion dynamics, in particular

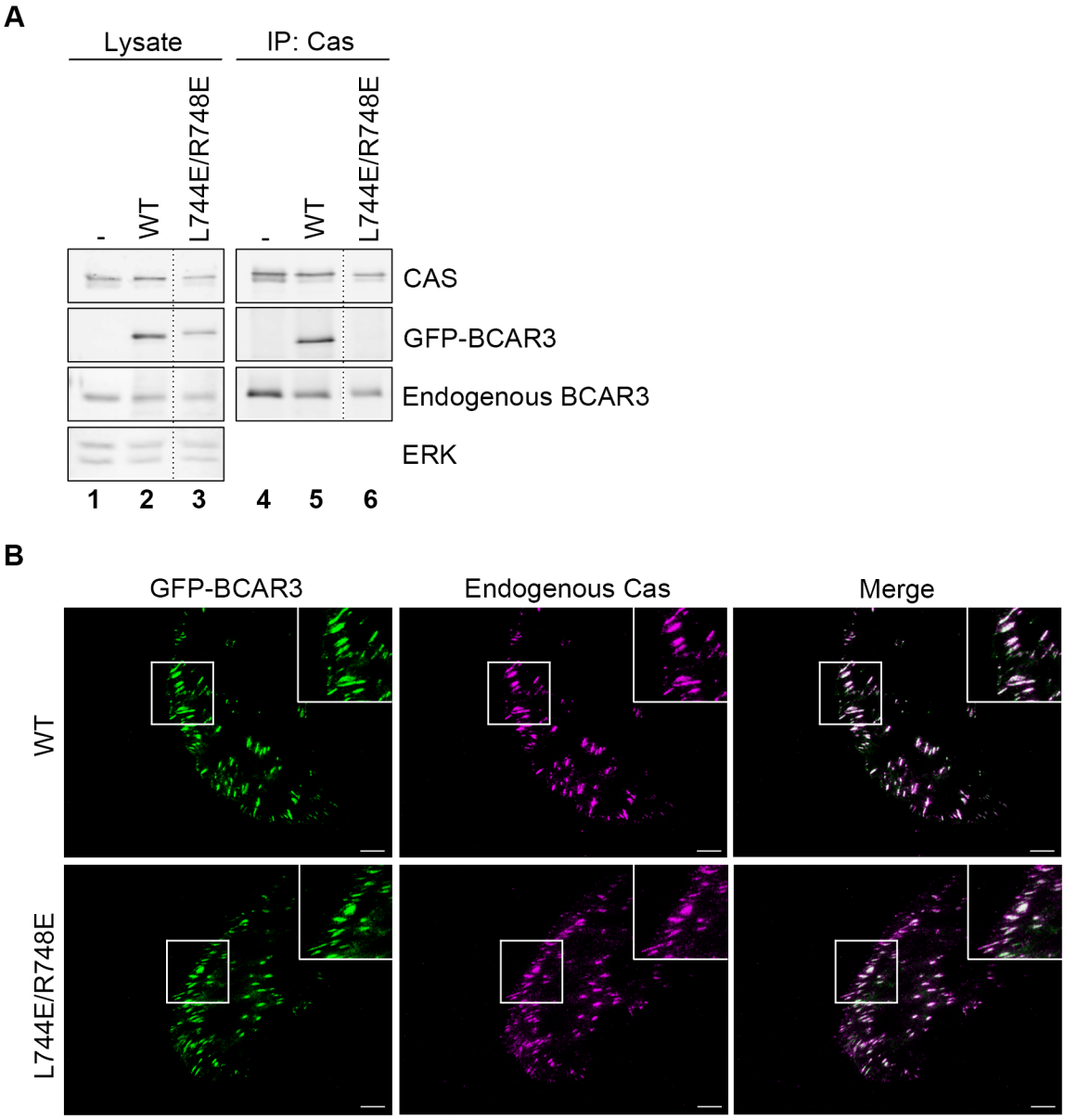
A
Lysate
IP: Cas
-
WT
L744E/R748E
-
WT
L744E/R748E
CAS
GFP-BCAR3
Endogenous BCAR3
ERK
1
2
3
4
5
6
B
GFP-BCAR3
Endogenous Cas
Merge
WT
L744E/R748E

Figure 3.2. Localization of BCAR3 to adhesions does not require direct interaction with Cas. (**A**) Untransfected BT549 cells or BT549 cells transfected with plasmids encoding WT GFP-BCAR3 or L744E/R748E GFP-BCAR3 were incubated for 24 hours prior to lysis in non-reducing buffer (50mM Tris-HCl, pH 7.5, 120mM NaCl, 1% Triton X-100, 2 mM EDTA, 5% glycerol, 1mM sodium orthovanadate, 1mM sodium fluoride, 1mg/ml aprotinin, 1mg/ml leupeptin, and 1 mM phenylmethylsulfonyl fluoride). Total cell protein and Cas immune complexes were separated on 8% SDS-PAGE and immunoblotted with BCAR3 and Cas antibodies. ERK antibody was used as a loading control. *Panel A provided by Allison Batties.* (**B**) BT549 cells were transfected with plasmids encoding WT GFP-BCAR3 or L744E/R748E GFP-BCAR3. Cells were then incubated for 24 hours prior to plating on 10µg/ml fibronectin-coated coverslips. Cells were allowed to spread for 4 hours, fixed and stained with polyclonal Cas antibodies to detect endogenous Cas. Adhesions were visualized via TIRF microscopy. Merged images are shown in the right panels. Insets show higher magnifications of cell peripheries.

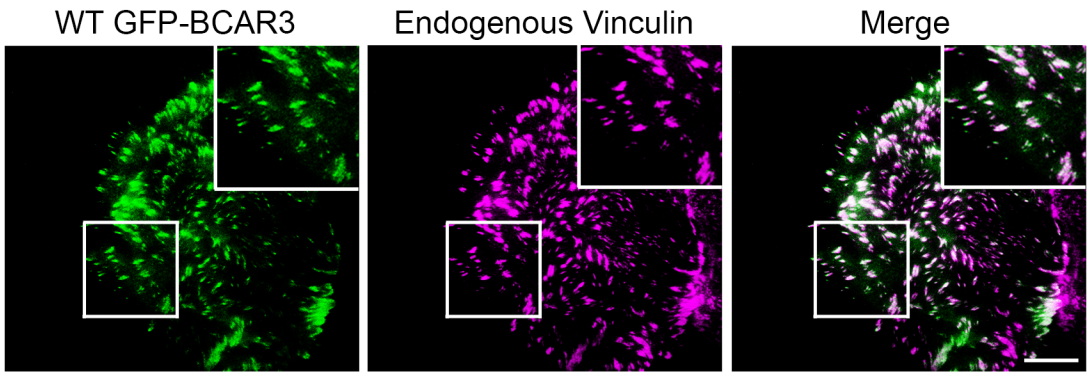
WT GFP-BCAR3
Endogenous Vinculin
Merge

Figure 3.3. BCAR3 localizes to vinculin-containing adhesions in Cas-/- MEFs. Cas-/- MEFs were transfected with plasmids encoding WT GFP-BCAR3. Cells were then incubated for 24 hours prior to plating on 10μg/ml fibronectin-coated coverslips. Cells were allowed to spread for 1 hour, then were fixed and stained with a vinculin antibody. Adhesions were visualized via TIRF microscopy. Merged image is shown in the right panel. Insets show higher magnifications of the cell periphery.

adhesion disassembly (**Chapter 2, Fig 2.5**, [47]). Therefore, we hypothesized that the ability of BCAR3 to function as a regulator of adhesion dynamics might require binding to Cas even though accumulation of BCAR3 into adhesions was not dependent on direct interaction with Cas. To test this, BT549 breast cancer cells were co-transfected with mCherry-tagged Cas plus either WT GFP-BCAR3 or L744E/R748E GFP-BCAR3. Twenty-four hours post-transfection, cells were allowed to spread for 30-40 minutes on fibronectin-coated glass bottomed dishes prior to live-imaging TIRF microscopy. There were no apparent spreading defects between WT versus L744E/R748E-expressing tumor cells, and both WT (**Fig 3.4A**) and mutant BCAR3 (**Fig 3.4E**) co-localized with Cas in dynamic adhesions that exhibited turnover (incorporation of BCAR3/Cas into adhesions is indicated by black arrowheads, while dissociation of BCAR3/Cas from adhesions is indicated by pink arrowheads). To quantify adhesion turnover, adhesions at peripheral, protruding edges were manually selected for analysis. Representative analyses for individual WT BCAR3-expressing and L744E/R748E BCAR3-expressing adhesions are shown (**Fig. 3.4B-D and F-H**, respectively). Complete fluorescence intensity time tracings for individual adhesions were plotted, normalized, and background intensity corrected by subtracting an average intensity value corresponding to a background region away from the cell (**Fig 3.4C and G**). The incorporation and dissociation of BCAR3 and Cas were linear when converted to semi-logarithmic plots (**Fig 3.4D and H**), and rate constants were determined from the slopes of these graphs. We found that BCAR3 and Cas incorporate into adhesions at nearly indistinguishable rates (**Fig 3.4I**, compare bars 1 and 3), and this was independent of BCAR3-Cas interactions because L744E/R748E BCAR3 entered adhesions at a rate similar to WT BCAR3 (**Fig 3.4I**, compare bars 1 and 2). The assembly kinetics of Cas were also not altered in L744E/R748E BCAR3- compared to WT BCAR3-expressing adhesions (**Fig**

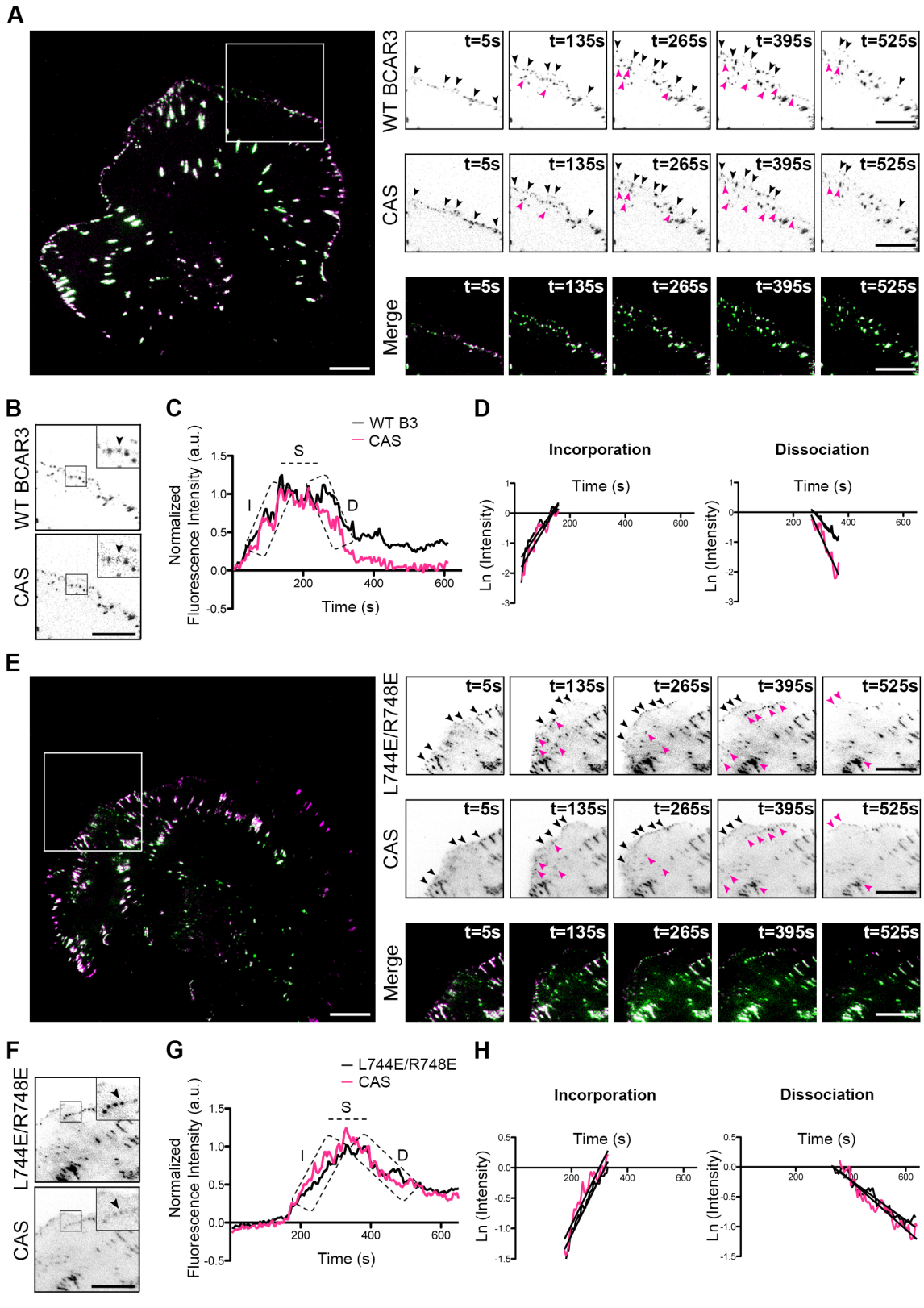
A
WT BCAR3
CAS
Merge
t=5s
t=135s
t=265s
t=395s
t=525s
B
WT BCAR3
CAS
C
WT B3
CAS
Normalized Fluorescence Intensity (a.u.)
S
I
D
Time (s)
D
Incorporation
Dissociation
Time (s)
Ln (Intensity)
E
L744E/R748E
CAS
Merge
F
L744E/R748E
CAS
G
L744E/R748E
CAS
Normalized Fluorescence Intensity (a.u.)
S
I
D
Time (s)
H
Incorporation
Dissociation
Time (s)
Ln (Intensity)

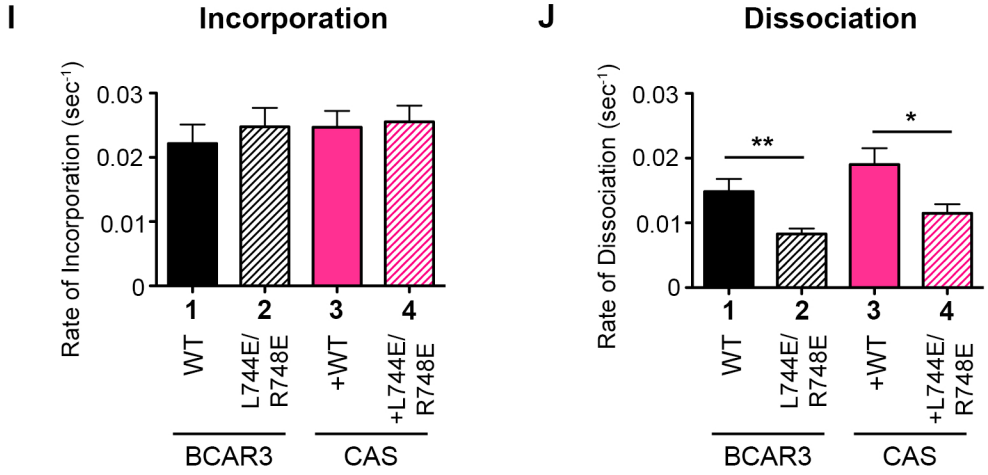
I
Incorporation
Rate of Incorporation (sec-1)
0.03
0.02
0.01
0
1
2
3
4
WT
L744E/ R748E
+WT
+L744E/ R748E
BCAR3
CAS
J
Dissociation
Rate of Dissociation (sec-1)
0.03
0.02
0.01
0
**
*
1
2
3
4
WT
L744E/ R748E
+WT
+L744E/ R748E
BCAR3
CAS

Figure 3.4. Direct interaction between BCAR3 and Cas is required for efficient dissociation of BCAR3 from adhesions. (**A**) BT549 invasive breast cancer cells were co-transfected with plasmids encoding WT GFP-BCAR3 and mCherry-Cas and then incubated for 24 hours. After the incubation, cells were trypsinized and then washed in serum-containing media to inactivate the trypsin. Subsequently, cells were spun at ~1200rpm for 5 minutes to remove all traces of trypsin, and then resuspended in CCM1 media pre-warmed to 37°C for imaging. Cells were plated on 2μg/ml fibronectin-coated glass-bottomed TIRF dishes and allowed to spread for 30-40 minutes prior to visualizing adhesion dynamics via live-imaging TIRF microscopy. The merged image of the first frame of a representative movie is shown (left). Representative time-lapse images from TIRF microscopy show incorporation (black arrowheads) and dissociation (pink arrowheads) of WT BCAR3 (top panels), Cas (middle panels), and WT BCAR3/Cas merged (bottom panels) over the specified time course. (**B-D**) Quantification of adhesion turnover. (**B**) Representative images of an individual adhesion co-expressing WT BCAR3 (top) and Cas (bottom) are shown. (**C**) Representative complete fluorescence intensity time tracings for the individual adhesions in (B) are shown. WT BCAR3 (B3, black line), Cas (pink line). Dashed boxes/line indicate incorporation (I), stability (S), and dissociation (D) as indicated. (**D**) The incorporation and dissociation of BCAR3 and Cas were linear when converted to semi-logarithmic plots. Representative plots of incorporation (left) and dissociation (right) with linear regression lines of best fit are shown. WT BCAR3 (black line), Cas (pink line). (**E**) BT549 invasive breast cancer cells were co-transfected with plasmids encoding mutant L744E/R748E GFP-BCAR3 and mCherry-Cas and visualized by live-imaging TIRF microscopy as described in (A). (**F-H**) Similar analysis of adhesion turnover was performed on BT549 cells co-expressing L44E/R748E BCAR3 and mCherry-Cas as described in (B-D). (**I**) Quantitative analysis

of the incorporation rates, as determined from the best fit lines shown in panels D and H (left graphs), of WT BCAR3 (bar 1), L744E/R748E BCAR3 (bar 2), Cas co-expressed with WT BCAR3 (bar 3), and Cas co-expressed with L744E/R748E BCAR3 (bar 4). (**J**) Quantitative analysis of the dissociation rates, as determined from the best fit lines shown in panels D and H (right graphs), of WT BCAR3 (bar 1), L744E/R748E BCAR3 (bar 2), Cas co-expressed with WT BCAR3 (bar 3), and Cas co-expressed with L744E/R748E BCAR3 (bar 4). Data in panels (I) and (J) represent the mean ± SEM of at least 35 adhesions from 3 separate WT BCAR3/Cas or 3 separate L744E/R748E BCAR3/Cas movies from 3 independent experiments. Conditions that are significantly different from one another are indicated with asterisks (*, $p<0.05$) (**, $p<0.01$).

3.4I, compare bars 3 and 4). Together, these data demonstrate that BCAR3 can efficiently incorporate into adhesions without being directly bound to Cas. It remains unclear, however, whether Cas can incorporate into adhesions without being directly bound to BCAR3 in BT549 cells because of the presence of residual endogenous BCAR3 under these conditions (**Fig 3.4I**, bar 4).

While there was no significant difference between the rates at which WT and L744E/R748E BCAR3 incorporate into adhesions, the rate of dissociation from adhesions was significantly slower when BCAR3 was unable to bind to Cas (**Fig 3.4J**, compare bars 1 and 2). This argues that a direct interaction between BCAR3 and Cas is necessary for efficient dissociation of BCAR3 from adhesions. Interestingly, Cas was also less efficient at dissociating from adhesions in the presence of L744E/R748E BCAR3 (**Fig 3.4J**, compare bars 3 and 4). Taken together, these data support a hypothesis whereby direct interaction between BCAR3 and Cas is one potential mechanism by which BCAR3 promotes efficient adhesion turnover (particularly disassembly) in invasive breast cancer cells.

3.2.4 BCAR3 promotes adhesion disassembly via its direct interaction with Cas

Although the dissociation of BCAR3 and Cas from adhesions was delayed under conditions when the two proteins were not in complex, it was not clear whether this delay was unique to these molecules or whether the adhesion complex as a whole disassembled at a slower rate in the presence of L744E/R748E BCAR3. To distinguish between these two possibilities, we examined the adhesion dynamics of two other well-established adhesion proteins, talin and α-actinin, when co-expressed with either WT or L744E/R748E BCAR3. BT549 cells were co-transfected with constructs encoding WT GFP-BCAR3 or L744E/R748E GFP-BCAR3 plus mCherry-tagged talin (**Fig 3.5**) or

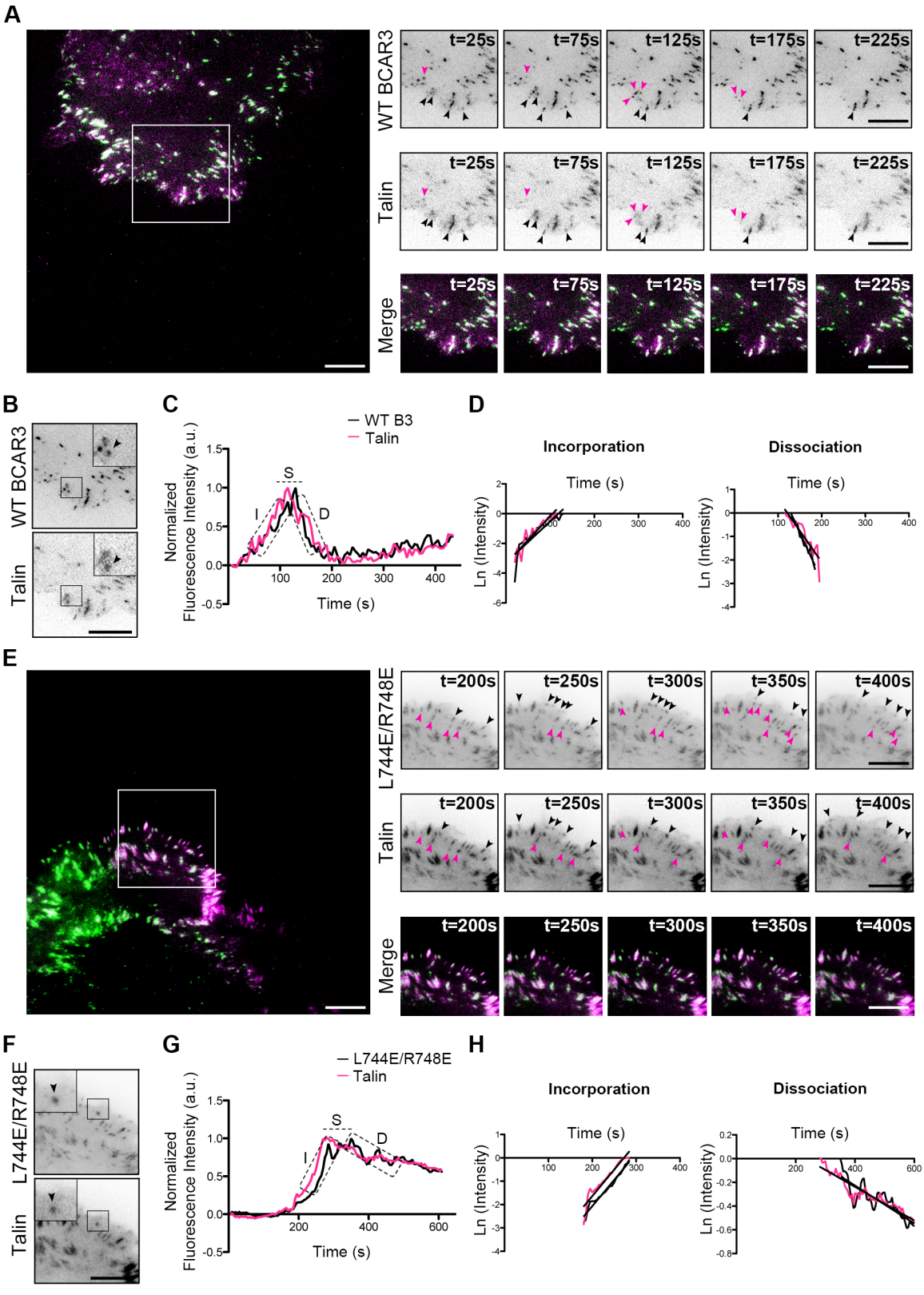
A
WT BCAR3
Talin
Merge
t=25s
t=75s
t=125s
t=175s
t=225s
B
WT BCAR3
Talin
C
WT B3
Talin
Normalized Fluorescence Intensity (a.u.)
Time (s)
I
S
D
D
Incorporation
Dissociation
Time (s)
Ln (Intensity)
E
L744E/R748E
Talin
Merge
t=200s
t=250s
t=300s
t=350s
t=400s
F
L744E/R748E
Talin
G
L744E/R748E
Talin
Normalized Fluorescence Intensity (a.u.)
Time (s)
H
Incorporation
Dissociation
Time (s)
Ln (Intensity)

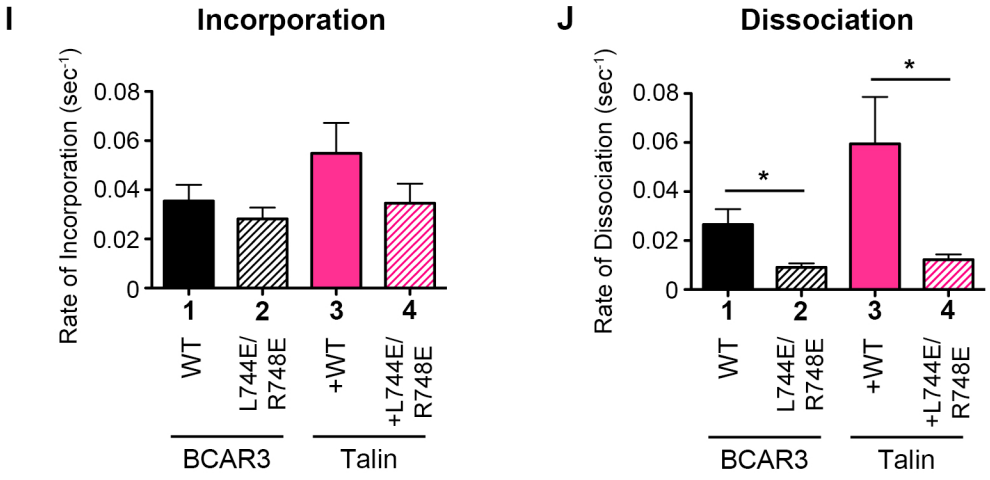
I
Incorporation
Rate of Incorporation (sec-1)
0.08
0.06
0.04
0.02
0
1
2
3
4
WT
L744E/ R748E
+WT
+L744E/ R748E
BCAR3
Talin
J
Dissociation
Rate of Dissociation (sec-1)
*
*

Figure 3.5. Direct interaction between BCAR3 and Cas is required for efficient dissociation of talin from adhesions. (**A**) BT549 invasive breast cancer cells were co-transfected with plasmids encoding WT GFP-BCAR3 and mCherry-Talin and incubated for 24 hours. Cells were processed for live-imaging TIRF microscopy as described in **Figure 3.4**. The merged image of the first frame of a representative movie is shown (left). Representative time-lapse images from TIRF microscopy show incorporation (black arrowheads) and dissociation (pink arrowheads) of WT BCAR3 (top panels), Talin (middle panels), and WT BCAR3/Talin merged (bottom panels) over the specified time course. (**B-H**) Quantification of adhesion turnover for WT BCAR3/Talin (**B-D**) and L744E/R748E BCAR3/Talin (**E-H**) was performed as described in **Figure 3.4**. (**I**) Quantitative analysis of the incorporation rates, as determined from the best fit lines shown in panels D and H (left graphs), of WT BCAR3 (bar 1), L744E/R748E BCAR3 (bar 2), Talin co-expressed with WT BCAR3 (bar 3), and Talin co-expressed with L744E/R748E BCAR3 (bar 4). (**J**) Quantitative analysis of the dissociation rates, as determined from the best fit lines shown in panels D and H (right graphs), of WT BCAR3 (bar 1), L744E/R748E BCAR3 (bar 2), Talin co-expressed with WT BCAR3 (bar 3), and Talin co-expressed with L744E/R748E BCAR3 (bar 4). Data in panels (I) and (J) represent the mean ± SEM of at least 14 adhesions from 5 separate WT BCAR3/Talin or 3 separate L744E/R748E BCAR3/Talin movies from 3 independent experiments. Conditions that are significantly different from one another are indicated with asterisks (*, $p<0.05$).

mCherry-tagged α-actinin (**Fig 3.6**). Twenty-four hours post-transfection, cells were allowed to spread for 30-40 minutes on fibronectin-coated glass bottomed dishes prior to live-imaging TIRF microscopy (**Figs 3.5 and 3.6, A and E**). Adhesion turnover was quantified as in **Figure 3.4**, and representative analyses for an individual WT or L744E/R748E BCAR3-expressing adhesion co-expressing either talin (**Fig 3.5B-D and F-H**, respectively) or α-actinin (**Fig 3.6B-D and F-H**, respectively) are shown. Once again, the incorporation of BCAR3 into adhesions was not dependent on its ability to directly bind to Cas, as both WT and L744E/R748E BCAR3 entered adhesions at similar rates (**Figs 3.5I and 3.6I**, compare bars 1 and 2). Interestingly, while the assembly kinetics of talin were not significantly altered in WT versus L744E/R748E BCAR3-expressing adhesions (**Fig 3.5I**, compare bars 3 and 4), the rate of incorporation of α-actinin was significantly faster in adhesions co-expressing WT BCAR3 versus L744E/R748E BCAR3 (**Fig 3.6I**, compare bars 3 and 4). Also, although not statistically significant, there appears to be a trend wherein α-actinin incorporates into adhesions more rapidly than BCAR3 (**Fig 3.6I**, compare bars 1 and 3). This is not surprising considering α-actinin has been shown to enter nascent adhesions in distinct clusters and at a faster rate than integrin [68]. Furthermore, we found that the dissociation rates of both talin and α-actinin were significantly slower in adhesions co-expressing L744E/R748E BCAR3 versus WT BCAR3 (**Figs 3.5J and 3.6J**, compare bars 3 and 4). Once again, this was coincident with a slower dissociation rate for L744E/R748E BCAR3 (**Figs 3.5J and 3.6J**, compare bars 1 and 2). Together, these data argue that a direct interaction between BCAR3 and Cas is required for efficient adhesion complex disassembly, as the dissociation kinetics of multiple adhesion proteins are impaired in L744E/R748E BCAR3-expressing adhesions.

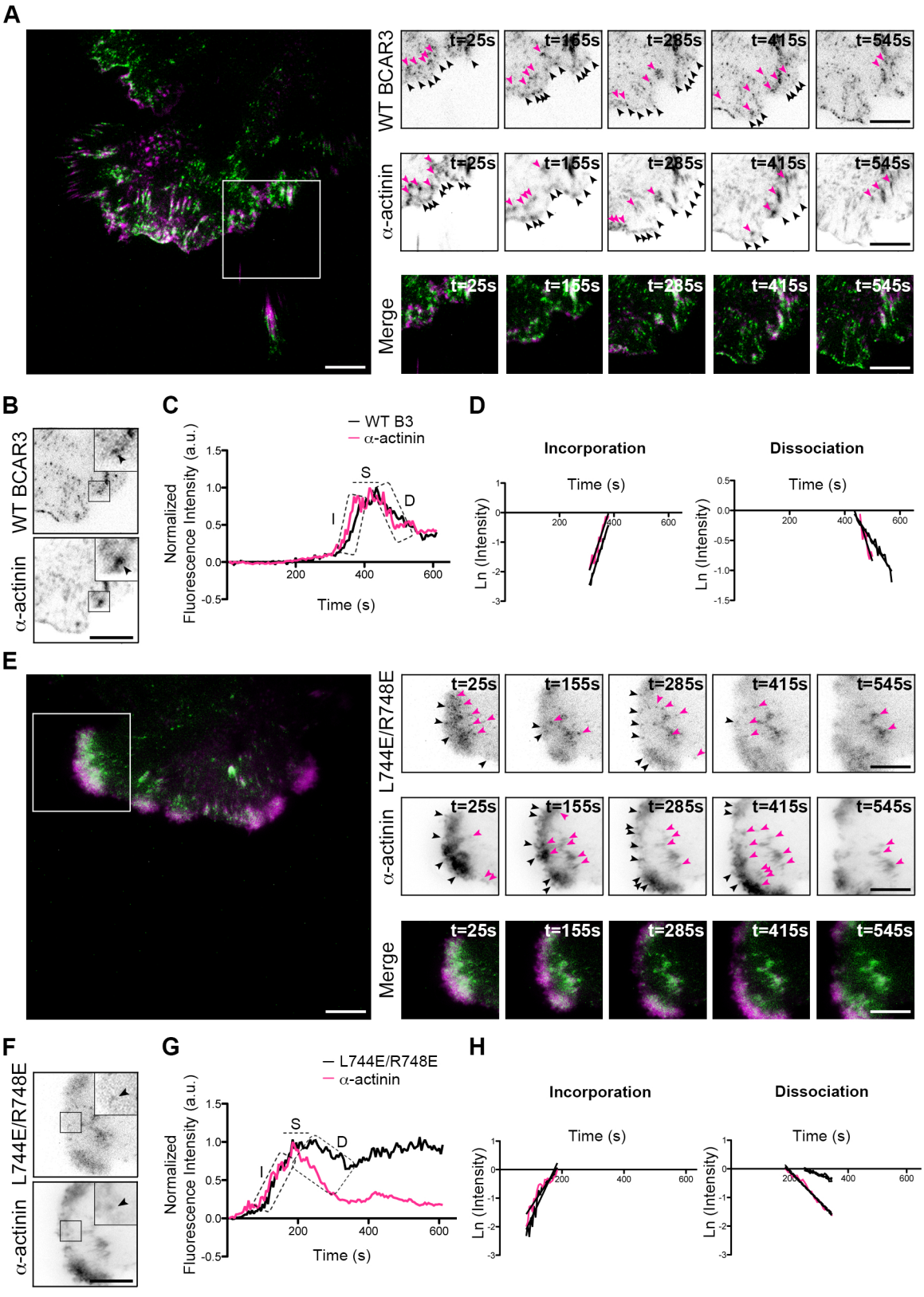
A
WT BCAR3
α-actinin
Merge
t=25s
t=155s
t=285s
t=415s
t=545s
B
WT BCAR3
α-actinin
C
WT B3
α-actinin
Normalized Fluorescence Intensity (a.u.)
Time (s)
S
D
I
D
Incorporation
Dissociation
Time (s)
Ln (Intensity)
E
L744E/R748E
α-actinin
Merge
F
L744E/R748E
α-actinin
G
L744E/R748E
α-actinin
Normalized Fluorescence Intensity (a.u.)
Time (s)
H
Incorporation
Dissociation
Time (s)
Ln (Intensity)

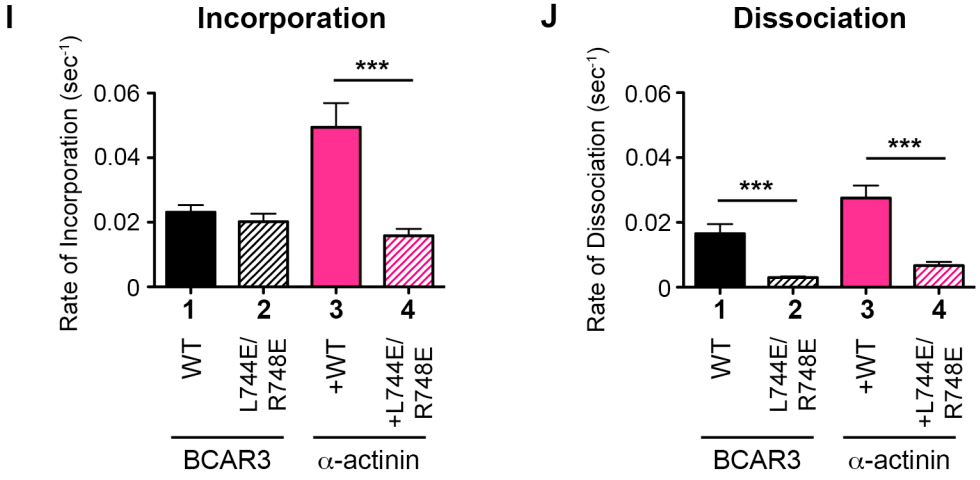
I
Incorporation
Rate of Incorporation (sec-1)
0.06
0.04
0.02
0
***
1
2
3
4
WT
L744E/ R748E
+WT
+L744E/ R748E
BCAR3
α-actinin
J
Dissociation
Rate of Dissociation (sec-1)
0.06
0.04
0.02
0
***
***
1
2
3
4
WT
L744E/ R748E
+WT
+L744E/ R748E
BCAR3
α-actinin

Figure 3.6. Direct interaction between BCAR3 and Cas is required for efficient incorporation and turnover of α-actinin in adhesions. (**A**) BT549 invasive breast cancer cells were co-transfected with plasmids encoding WT GFP-BCAR3 and mCherry-α-actinin and incubated for 24 hours. Cells were processed for live-imaging TIRF microscopy as described in **Figure 3.4**. The merged image of the first frame of a representative movie is shown (left). Representative time-lapse images from TIRF microscopy show incorporation (black arrowheads) and dissociation (pink arrowheads) of WT BCAR3 (top panels), α-actinin (middle panels), and WT BCAR3/α-actinin merged (bottom panels) over the specified time course. (**B-H**) Quantification of adhesion turnover for WT BCAR3/α-actinin (**B-D**) and L744E/R748E BCAR3/α-actinin (**E-H**) was performed as described in **Figure 3.4**. (**I**) Quantitative analysis of the incorporation rates, as determined from the best fit lines shown in panels D and H (left graphs), of WT BCAR3 (bar 1), L744E/R748E BCAR3 (bar 2), α-actinin co-expressed with WT BCAR3 (bar 3), and α-actinin co-expressed with L744E/R748E BCAR3 (bar 4). (**J**) Quantitative analysis of the dissociation rates, as determined from the best fit lines shown in panels D and H (right graphs), of WT BCAR3 (bar 1), L744E/R748E BCAR3 (bar 2), α-actinin co-expressed with WT BCAR3 (bar 3), and α-actinin co-expressed with L744E/R748E BCAR3 (bar 4). Data in panels (I) and (J) represent the mean ± SEM of at least 13 adhesions from 4 separate WT BCAR3/α-actinin or 2 separate L744E/R748E BCAR3/α-actinin movies from 3 independent experiments. Conditions that are significantly different from one another are indicated with asterisks (***, $p<0.001$).

3.3 Discussion

This study demonstrates for the first time that BCAR3 co-localizes with Cas in adhesions, but surprisingly, their direct interaction is not required to recruit or position BCAR3 in adhesions. This is evidenced by the fact that L744E/R748E BCAR3, which is unable to directly bind to Cas and is not present in Cas immune complexes, is able to incorporate into adhesions as efficiently as WT BCAR3 (**Fig 3.7**, inset box A). However, once incorporated into adhesions, direct BCAR3/Cas interaction becomes necessary to drive efficient adhesion disassembly. When BCAR3/Cas interactions are prevented, adhesions disassemble at significantly slower rates, as highlighted by the slower dissociation rates of multiple adhesion proteins including BCAR3, Cas, talin, and α-actinin.

3.3.1 BCAR3/Cas interactions are required for efficient BCAR3-mediated adhesion disassembly

We have previously shown that BCAR3 promotes adhesion disassembly in invasive breast cancer cells (**Chapter 2, Fig 2.5**, [47]). The data presented in the current report provide mechanistic insight into how BCAR3 may perform this action. Under conditions in which BCAR3/Cas complexes are able to be formed (i.e. WT BCAR3), we observed rapid disassembly of multiple adhesion proteins. Given that BCAR3 promotes Src-mediated Cas phosphorylation and subsequent Cas/Crk coupling [119, 129, 130], we propose that BCAR3/Cas complexes promote localized activation of Rac1 via the canonical Cas/Crk/Rac1 activation pathway, which in turn promote Rac1 signaling (and/or suppression of RhoA/tension) coincident with rapid adhesion turnover (**Fig 3.7**, inset box B). However, under conditions in which BCAR3/Cas complexes are blocked at the adhesion sites (i.e. L744E/R748E BCAR3, **Fig 3.7**, inset box C), we

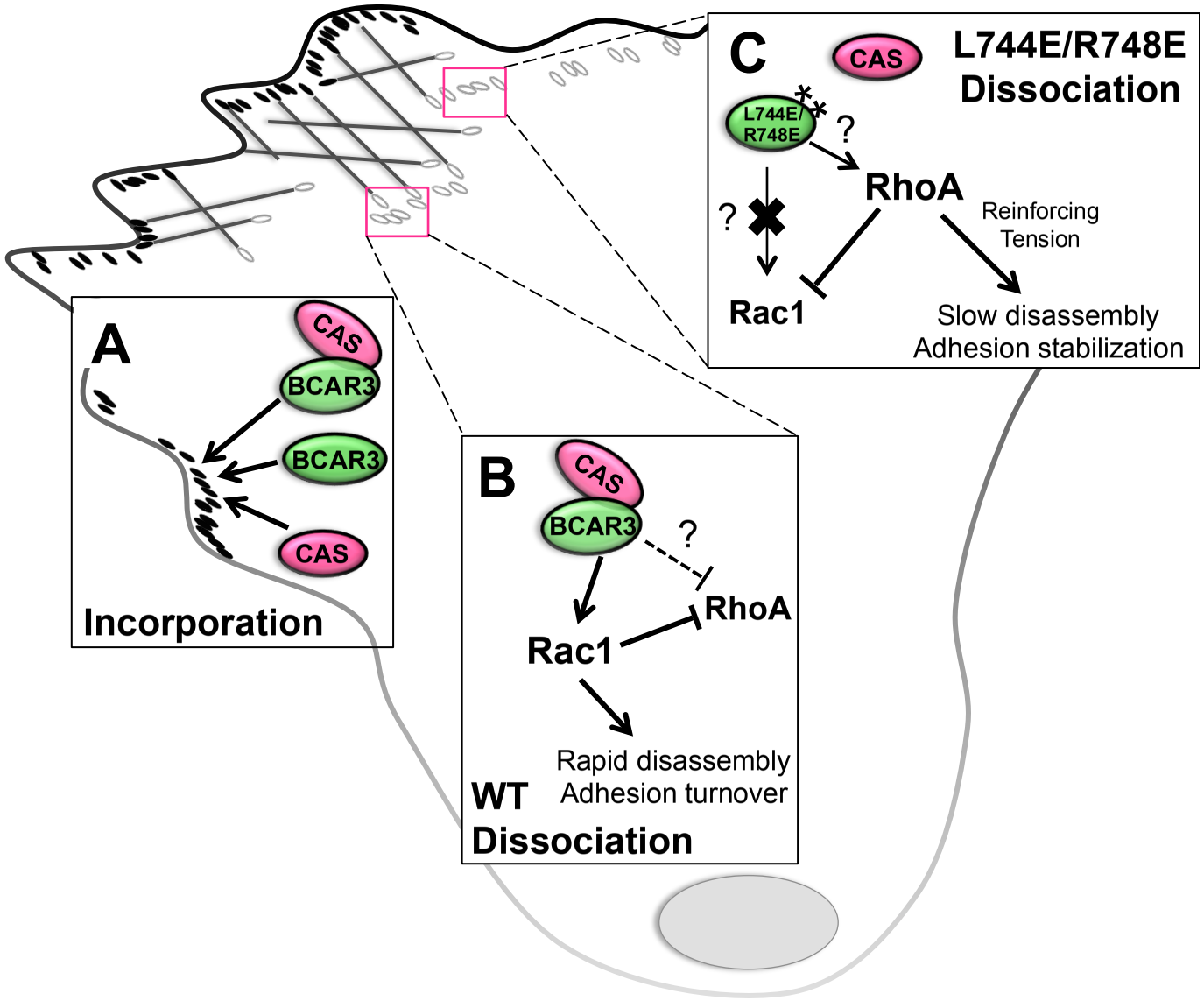
C
CAS
L744E/R748E
Dissociation
L744E/
R748E
**
?
RhoA
?
Reinforcing
Tension
Rac1
Slow disassembly
Adhesion stabilization
A
CAS
BCAR3
BCAR3
CAS
Incorporation
B
CAS
BCAR3
?
RhoA
Rac1
Rapid disassembly
Adhesion turnover
WT
Dissociation

Figure 3.7. BCAR3/Cas interactions control efficient BCAR3-mediated adhesion disassembly. (**A**) BCAR3 can efficiently incorporate into adhesions whether or not it is in direct complex with Cas. (**B**) Under conditions where BCAR3/Cas interactions are enabled (i.e. WT BCAR3), rapid disassembly of multiple adhesion proteins are observed. We propose BCAR3/Cas complexes promote localized activation of Rac1 and/or suppression of RhoA under these conditions (see **Chapter 2, Fig 2.9**), therefore enhancing adhesion turnover. (**C**) When BCAR3/Cas interactions are prevented (i.e. L744E/R748E BCAR3), we speculate that Rac1 activation is no longer promoted, and instead a localized rise in RhoA-mediated tension provides the reinforcement necessary to stabilize adhesions and slow the rate of disassembly.

speculate that Rac1 fails to be activated and instead, a local rise in RhoA-mediated tension provides the reinforcement necessary to stabilize adhesions and reduce the rate of adhesion disassembly. Interestingly, the adhesion turnover defect that occurs under conditions in which BCAR3 and Cas fail to interact phenocopies the effect of BCAR3 knockdown that we reported in an earlier study (**Chapter 2**, [47]). Coincident with a stabilization of nascent adhesions, BCAR3-depleted breast cancer cells exhibited a decrease in Rac1 activity and an increase in RhoA activity (**Chapter 2**, [47]). It remains to be determined whether L744E/R748E BCAR3 is less efficient at promoting Rac1 activity and/or more efficient at promoting RhoA activity than WT BCAR3.

It is important to note that we developed the above model based on what we observed previously under BCAR3 knockdown conditions (i.e. high Rho activity and low Rac activity, see **Chapter 2**). However, in this current study, we ectopically expressed a mutant BCAR3 molecule in the presence of wildtype BCAR3, which is very different from depleting the wildtype protein. Therefore, it is also possible that BCAR3 may act through another unknown substrate besides Cas. In this case, Cas may simply help to stabilize BCAR3 in adhesions so that it can bind to another adaptor or kinase molecule and promote signaling. In the absence of BCAR3/Cas interaction (i.e. L744E/R748E), the affinity of BCAR3 for this other molecule may be either weakened or prevented, ultimately leading to a condition that favors adhesion stabilization over disassembly. Furthermore, as discussed in **Chapter 1**, adhesions can be relatively large complexes with many protein-protein interactions, therefore it is also possible that by disturbing BCAR3/Cas interaction, the orientation and/or composition of the entire adhesion complex may be altered, which could have adverse effects on adhesion turnover.

3.3.2 BCAR3/Cas complexes may regulate the molecular switch between adhesion turnover and maturation in invasive breast cancer cells

It is important to reiterate that efficient adhesion turnover requires a delicate balance between Rac1 and RhoA. We suggest that the BCAR3/Cas complex may serve as an important rate-limiting step in the spatiotemporal control of Rac/Rho GTPase signaling in adhesions. As discussed in **Chapter 1**, as nascent adhesions assemble, they eventually reach a critical decision point near the back of the lamellipodium that dictates whether they disassemble or mature into focal complexes. Rac1 activation encourages turnover, while RhoA-mediated tension supports maturation. We speculate that, as BCAR3/Cas complexes are incorporated into assembling adhesions and/or form in nascent adhesions, they promote local Rac1 activity and inhibit RhoA, thereby encouraging adhesion turnover. In this way, BCAR3/Cas complexes could enhance breast tumor cell motility. However, if these complexes fail to form, RhoA signaling pathways would predominate and adhesions would undergo maturation. Interestingly, our results suggest that this can occur even if both proteins are present in the adhesions as long as they are prohibited from interacting with one another.

Under conditions where BCAR3 and Cas can interact (i.e. WT BCAR3), we observed rapid incorporation and dissociation of α-actinin in adhesions. This is consistent with recent reports showing that α-actinin enters and exits adhesions with its own unique periodicity [68]. However, in the presence of L744E/R748E BCAR3, where BCAR3 and Cas fail to associate, α-actinin was observed to incorporate and dissociate from adhesions at significantly slower rates compared to WT BCAR3-expressing adhesions. One possibility that may explain the incorporation defect is that the entry of α-actinin into adhesions may be directly dependent upon BCAR3/Cas interactions. We are currently investigating whether α-actinin binds to BCAR3. A second possibility is that

the elevated tension that is predicted to occur in the absence of BCAR3/Cas interactions may support an environment that is unfavorable for entry of α-actinin into adhesions. A similar argument can be made for dissociation, since the entire adhesion appears to turn over at a slower rate under conditions in which BCAR3 and Cas do not interact. Whether this is a result of localized elevation of Rho activity and tension remains to be determined.

3.3.3 When and where is BCAR3 present along the adhesion continuum?

While BCAR3 and Cas enter adhesions with similar rates, it remains to be determined exactly when and where BCAR3 is first present in adhesions. Given that the adhesions we quantified herein persisted for roughly 3-4 minutes and were roughly 1-3μm in length, we argue that BCAR3 is present in what are most likely relatively short-lived focal complexes that subsequently either turn over or mature. However, our work raises several compelling questions. For instance, is BCAR3 present in earlier nascent adhesions? Are BCAR3 and Cas recruited to adhesions together? Do they typically enter as a complex or is a complex formed only after they are individually situated in adhesions? Novel fluorescent fluctuation methods recently introduced by Bachir *et al.* show the hierarchical recruitment of specific proteins to nascent adhesions [68]. Although several of the proteins they examined, including α-actinin and talin, were recruited to integrin-containing complexes at the same time, they showed that their rates of incorporation and/or stoichiometries were different [68]. Similar fluorescent fluctuation analyses of BCAR3 and Cas in adhesions may reveal whether they are recruited as a complex or not. Our data demonstrate that BCAR3 can localize to adhesions without being directly bound to Cas. In fact, the complete absence of L744E/R748E BCAR3 in Cas immune complexes (**Fig 3.2A**) shows that BCAR3 can enter adhesions without

being associated with Cas whatsoever. This finding is surprising considering that a recent report showed that BCAR3/Cas interaction leads to the stability of each protein [132]. Furthermore, we demonstrate that disruption of BCAR3/Cas complex signaling influences the rate at which α-actinin can incorporate into adhesions. Considering α-actinin is one of the earliest markers of nascent adhesions, this suggests that BCAR3 and BCAR3/Cas complexes may be very early components of newly formed adhesions.

While Cas can bind directly to other adhesion proteins, such as FAK, Src and vinculin [107, 115], it is unclear how BCAR3 is recruited to adhesions independently of Cas binding. It is important to note that, under normal conditions, endogenous BCAR3 may very well be recruited to adhesions with Cas, at least in BT549 and MDA-MB-231 cells, due to the fact that all BCAR3 is found associated with Cas (Dr. Michael Guerrero, *personal communication*). However, under conditions in which BCAR3 cannot interact with Cas (e.g. L744E/R748E BCAR3 and Cas-/- MEFs), other mechanisms must be available to recruit BCAR3 to adhesion sites. Catherine Pallen's group has previously reported that BCAR3 can localize to vinculin-containing adhesions through a mechanism that involves an interaction between the SH2-domain of BCAR3 and phosphorylated tyrosine 789 on membrane-bound PTPα [130]. Considering that PTPα is the only other established binding partner of BCAR3 besides Cas, it may play an important role in positioning BCAR3 in integrin-associated complexes. In fact, this group showed that an SH2-domain mutant BCAR3 molecule that fails to bind to PTPα was unable to localize to adhesions. Similarly, they showed that BCAR3 failed to localize to adhesions in PTPα-null MEFs re-expressing an unphosphorylatable mutant (Y789F) form of PTPα. However, recent data from our lab demonstrate that a triple-mutant BCAR3 molecule, L744E/R748E/R171V, which disrupts SH2 interactions, PTPα binding, and Cas binding, is still able to localize to adhesions (data not shown). The discrepancy between these

studies may be explained by the use of different cell lines. Nonetheless, our data indicate that, while PTPα and Cas are able to bind to BCAR3, they are evidently not the only proteins involved in recruiting BCAR3 to adhesions. Our lab is currently investigating whether BCAR3 interacts with any other adhesion proteins such as paxillin, vinculin and β-1 integrin.

Future work is critical to determine exactly when BCAR3 is first present in adhesions with respect to Cas as well as other adhesion proteins, and whether tension is required for the incorporation of BCAR3 into adhesions, as certain proteins require tension to enter adhesions while others do not [51, 68]. It is important to note that, as adhesions assemble and mature, the rates of incorporation of different adhesion proteins and their relative stoichiometries change [68]. Therefore it will be interesting to determine whether the number of BCAR3/Cas complexes varies along the adhesion continuum. It is intriguing to speculate that BCAR3/Cas complexes may be enriched in nascent adhesions that turn over as a potential mechanism to keep RhoA-mediated tension at bay, while fewer BCAR3/Cas complexes will be present when elevated tension is needed as the adhesions mature. Future studies are necessary to further elucidate the role of BCAR3/Cas interactions in regulating adhesion dynamics.

We demonstrate here that BCAR3/Cas interactions drive efficient BCAR3-mediated adhesion turnover in invasive breast cancer cells. These data, along with the recent finding that BCAR3/Cas association is required for BCAR3-mediated cytoskeletal remodeling and proliferation in the presence of antiestrogens [132], highlight the importance of signaling through the BCAR3/Cas complex to the promotion of aggressive breast tumor cell behaviors. Together, these data further support a role for this protein complex in breast tumor progression, suggesting that inhibiting their physical association may be a promising therapeutic strategy for tumors that co-express these molecules.

CHAPTER 4: BCAR3 protein levels are upregulated in multiple subtypes of human breast cancer

4.1 Introduction

BCAR3 mRNA and protein are ubiquitously expressed across many normal tissue types including breast, brain, lung, liver, and colon; however, their functions in normal cell types are largely unknown (The Human Protein Atlas, USCS Cancer Genomics Browser, [118]). Interestingly, BCAR3 may play important, but unique, roles in breast tumor progression. This stems from extensive literature highlighting the seemingly contradictory data regarding BCAR3 mRNA and protein levels associated with breast cancer prognosis. On one hand, there is abundant evidence that elevated BCAR3 protein levels correlate with poor breast cancer prognosis. For example, BCAR3 protein levels are elevated in invasive TNBC cell lines compared to early-stage ER^+ breast cancer cell lines [119, 120]. Elevated BCAR3 protein levels in human breast cancer cells promote Src activity, Src-mediated phosphorylation of Cas, Cas signaling, and invasive tumor cell behaviors *in vitro* ([47, 119, 129], **Chapters 2 and 3**). Enhanced Src activity is frequently associated with aggressive breast tumor subtypes and poor prognosis, and overexpression of Cas protein in primary human tumors is associated with poor tamoxifen response, poor relapse-free survival, and poor overall survival [98-100, 110, 111, 153]. Furthermore, BCAR3 protein, when in direct complex with Cas, has recently been shown to drive antiestrogen resistance in human breast cancer cells [132]. While high BCAR3 protein levels may associate with invasiveness, a major caveat to these studies is that the work was performed in breast cancer cell lines as opposed to human tumors. In fact, to our knowledge, BCAR3 protein levels have never been directly assessed in primary human breast tumors, and it remains to be determined

whether elevated BCAR3 protein levels correlate with aggressive breast tumor subtypes and/or tumor invasiveness.

On the other hand, BCAR3 mRNA levels have been directly evaluated for their predictive potential in primary human breast tumors, and surprisingly, elevated BCAR3 mRNA expression is associated with a favorable breast cancer prognosis. First, a study from Lambert Dorssers' group assessing a panel of 242 primary tumor tissues from metastatic breast cancer patients receiving tamoxifen revealed that elevated BCAR3 mRNA levels correlated with progression-free survival and a favorable tamoxifen response [133]. Elevated levels of Cas and Src mRNA were also not found to be associated with tumor aggressiveness or tamoxifen response in this study [133]. Similarly, a study from Sieuwerts *et al.* also found that higher BCAR3 mRNA levels in tumor tissues from 285 recurrent breast cancer patients treated with tamoxifen were significantly associated with a favorable progression-free survival [134]. Lastly, a recent study by Guo *et al.* assessing BCAR3 mRNA levels in primary breast tumors from treated and non-treated patients showed that higher BCAR3 mRNA levels correlated with both distant metastasis-free survival and relapse-free survival [135]. Strikingly, this group also found that loss of heterozygosity at the BCAR3 gene locus correlated with lymph node invasion, suggesting that BCAR3 may play a role in suppressing breast tumor progression [135]. However, an important caveat to all of the aforementioned studies is that they did not examine BCAR3 protein levels in the tumors.

Given the inconsistent data between BCAR3 protein and mRNA levels in human breast cancer cell lines and tumors, respectively, it is critical to directly assess BCAR3 protein levels in human breast tumors to determine whether its expression correlates with incidence or outcome. In the current study, we evaluated BCAR3 protein levels across a panel of 74 whole human breast tumors and 8 normal breast tissue specimens

by immunohistochemistry (IHC). A significant advantage of using whole breast tumor sections to analyze BCAR3 protein expression is that, within a given tumor section, there may be regions of both DCIS and invasive carcinoma, and in some cases normal ducts adjacent to tumor. We found that normal mammary ductal epithelial cells express low to undetectable levels of BCAR3 protein. In contrast, BCAR3 protein levels were upregulated in localized regions of the tumor adjacent to normal mammary ductal epithelial cells. This upregulation was seen across multiple subtypes of human breast cancer, including ER^+, HER2-amplified and TNBC. While BCAR3 protein levels were elevated in both DCIS and invasive carcinoma, the highest BCAR3 protein levels were observed within regions of high-grade DCIS. Thus, our data show for the first time that BCAR3 protein levels are elevated in human breast tumors, particularly high-grade DCIS, compared to normal breast tissue. These initial findings further highlight the potential clinical relevance of BCAR3-mediated signaling in breast tumor progression.

4.2 Results

4.2.1 BCAR3 protein levels are upregulated in tumor cells compared to normal ductal epithelial cells

To accurately measure BCAR3 protein levels in human breast tissue, we first validated the specificity of a human BCAR3 antibody using paraffin-embedded breast cancer cells as controls for tissue IHC (**Fig 4.1**). More specifically, BT549 cells, which are invasive human breast cancer cells that express high levels of BCAR3 protein, were transfected with control (siCtl) or BCAR3-specific (siB3) siRNA oligonucleotides. Cells were then incubated in normal growth medium for 72 hours prior to centrifugation. Control and BCAR3-depleted BT549 cells were formalin-fixed, paraffin-embedded, sectioned, and stained with BCAR3 antibody. Robust BCAR3 protein expression was

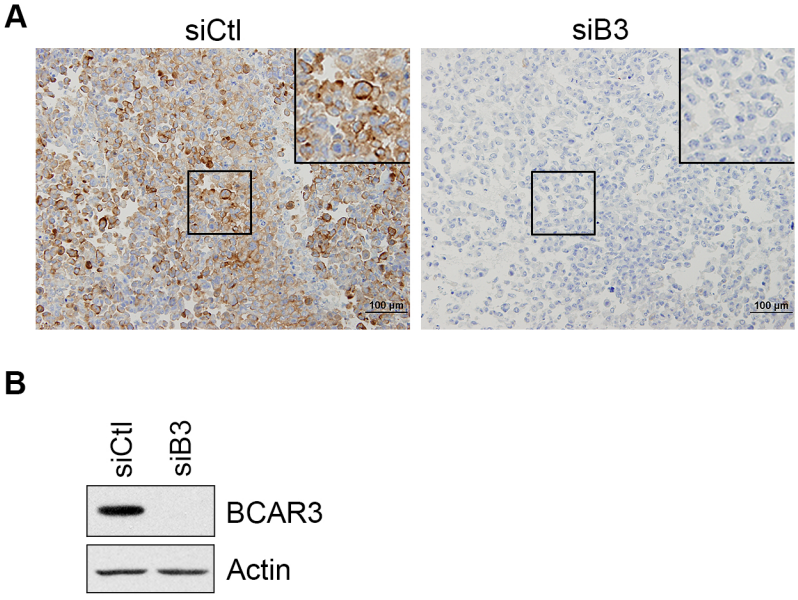
A
siCtl
siB3
100 µm
100 µm
B
siCtl
siB3
BCAR3
Actin

Figure 4.1. BCAR3 expression is readily detectable in human breast cancer cells via immunohistochemistry. (**A**) BT549 invasive human breast cancer cells were transfected with control (siCtl) or BCAR3-specific (siB3) siRNA oligonucleotides. Cells were incubated for 72 hours prior to collection by centrifugation. Control and BCAR3-depleted BT549 cells were formalin-fixed, paraffin-embedded, sectioned, and stained with a human BCAR3 antibody as described in the methods. Scale bar=100μm. (**B**) BT549 cells transfected as in (A) were incubated for 72 hours prior to lysis. Total cell protein was immunoblotted with the designated antibodies. Representative immunoblot confirming knockdown of BCAR3 with the BCAR3-specific siRNA oligonucleotide is shown.

detected in control cells via IHC (**Fig 4.1A**, left panel) and immunoblot (**Fig 4.1B**). As expected, BCAR3 staining was predominantly localized to the cytoplasm, with many cells exhibiting rich membranous staining. Conversely, BCAR3 protein was nearly undetectable in knockdown cells (**Fig 4.1A**, right panel; **Fig 4.1B**). These data demonstrate the specificity of the antibody.

We performed an analysis of 74 archival human breast tumors from women previously diagnosed with and treated for breast cancer at the University of Virginia (UVA) Health Systems. We also assessed BCAR3 protein levels in 8 normal breast tissue sections. Paraffin-embedded tissue blocks were hand-selected from the UVA breast tumor bank by a clinical breast pathologist, serially sectioned, and stained for hematoxylin & eosin (H&E) and BCAR3 using the validated human BCAR3 antibody described above. The staining intensity of BCAR3 protein was scored in a blinded fashion by a pathologist on a 0 (negative), 1^+ (low), 2^+ (moderate), 3^+ (strong) numerical scale. Each tumor section was assigned a staining intensity based on the highest BCAR3 expression observed in that tumor. Normal ductal epithelial cells expressed low to undetectable levels of BCAR3 protein (**Fig 4.2**, top panels). In contrast, BCAR3 protein levels were elevated in breast tumor cells, including tumor cells directly adjacent to normal ducts (**Fig 4.2**, middle and bottom panels). Furthermore, BCAR3 protein levels were elevated in regions of both DCIS (**Fig 4.3**) and invasive ductal carcinoma (**Fig 4.4**). Interestingly, in the case of DCIS, BCAR3 staining intensity varied from 0 to 3^+, not only across an entire tumor mass but also intraductally (**Fig 4.3**, magnified insets a and b). In the case of invasive ductal carcinoma, elevated BCAR3 protein levels were sometimes observed at what appeared to be the invasive edge of a tumor (**Fig 4.4**, magnified inset). Taken together, these data show that BCAR3 is heterogeneously

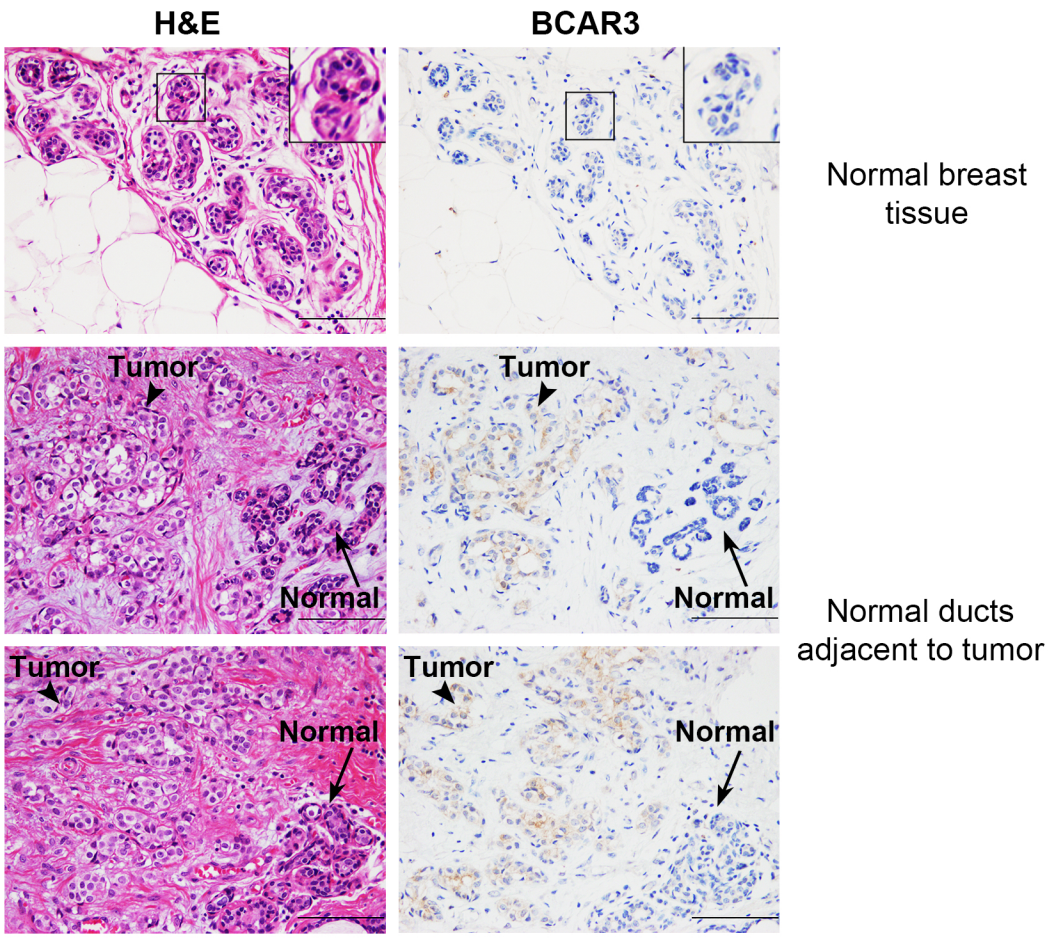
H&E
BCAR3
Normal breast tissue
Tumor
Normal
Tumor
Normal
Normal ducts adjacent to tumor
Tumor
Normal
Tumor
Normal

Figure 4.2. BCAR3 protein levels are upregulated in breast tumor cells compared to normal ductal epithelial cells. Paraffin-embedded breast tissue blocks were serially sectioned and stained for H&E (left panels) and BCAR3 (right panels) as described in the methods using the validated human BCAR3 antibody shown in **Fig 4.1**. Representative serial images of normal breast tissue (top panels) are shown. Magnified insets show ductal epithelial cells. Representative serial images of tumor cells adjacent to normal ducts (middle and bottom panels) are shown. Arrows point to normal ducts, arrowheads point to regions of tumor. Scale bar=100μm.

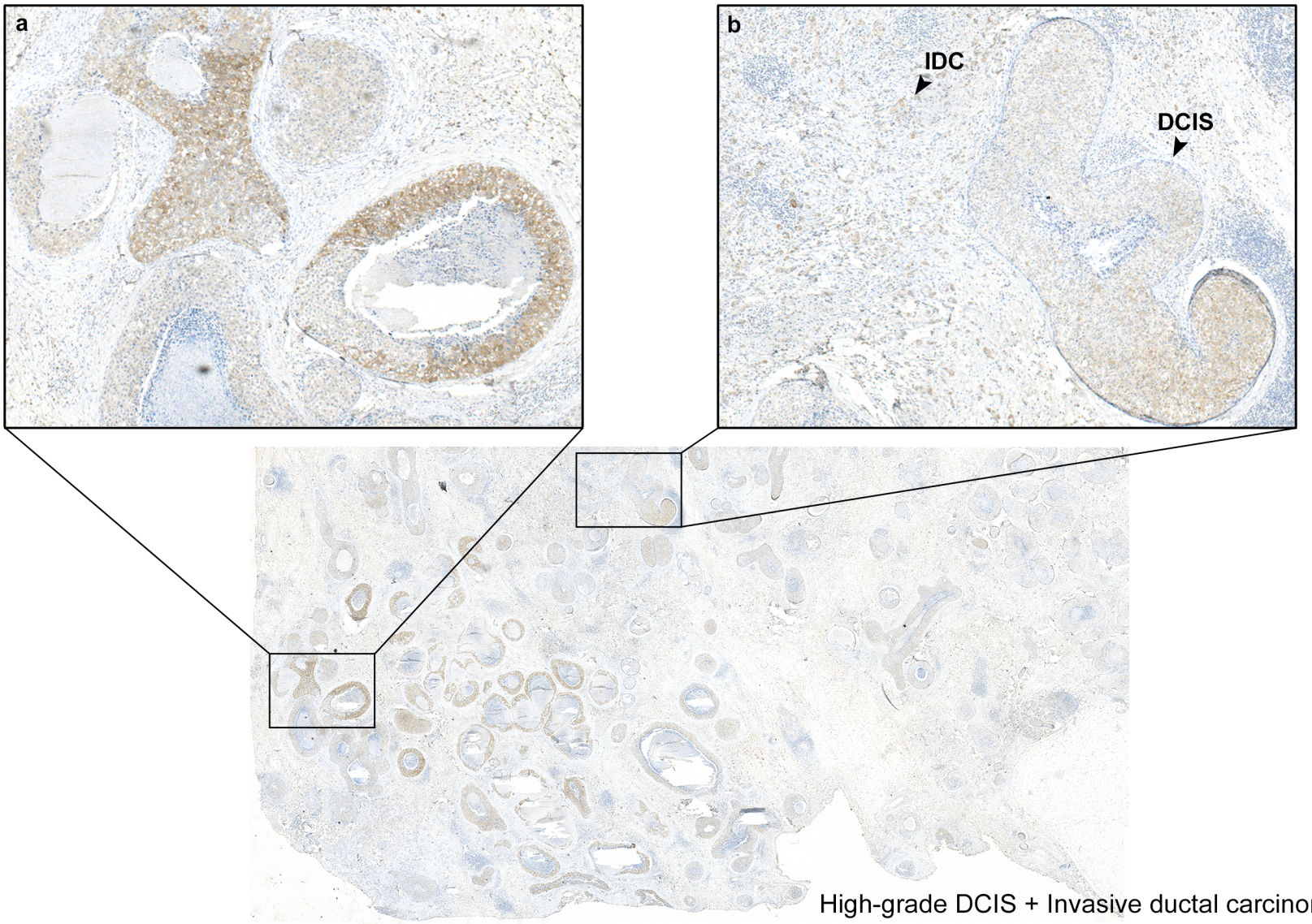
a
b
IDC
DCIS
High-grade DCIS + Invasive ductal carcinoma

Figure 4.3. BCAR3 protein levels are upregulated in DCIS. Human breast tumor sections were stained for BCAR3 as described in the methods. A representative tumor exhibiting regions of high-grade DCIS and invasive ductal carcinoma (IDC) is shown from a patient diagnosed with Grade 3 ER^- $HER2^+$ breast cancer. Image of tumor section was captured through a Zeiss Imager.Z2 microscope using Stereo Investigator Software (MBF Bioscience, MicroBrightField, Inc.) at 20X. Magnified insets (**a**) and (**b**) highlight the heterogeneity of BCAR3 protein expression within ducts. In magnified inset (b), arrowheads point to regions of DCIS and IDC within the tumor.

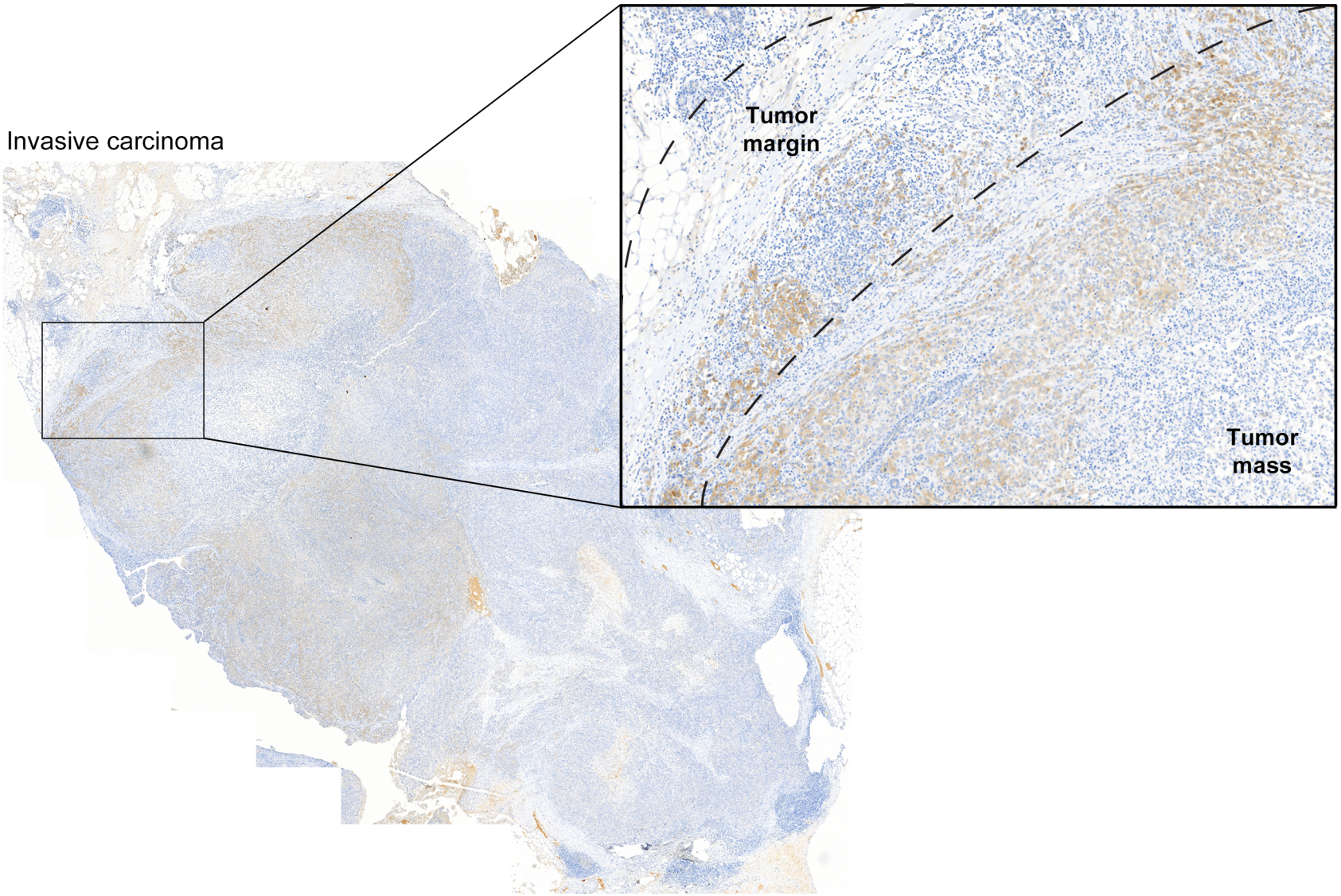
Invasive carcinoma
Tumor
margin
Tumor
mass

Figure 4.4. BCAR3 protein levels are upregulated in invasive ductal carcinoma (IDC). Human breast tumor sections were stained for BCAR3 as described in the methods. A representative tumor exhibiting IDC is shown from a patient diagnosed with triple-negative breast cancer. The whole section highlights the heterogeneity and "patchiness" of BCAR3 protein expression throughout the tumor. Image of tumor section was captured through a Zeiss Imager.Z2 microscope using Stereo Investigator Software (MBF Bioscience, MicroBrightField, Inc.) at 20X. Magnified inset shows elevated BCAR3 protein levels at an invasive edge of the tumor.

expressed at elevated levels in both DCIS and invasive ductal carcinoma compared to normal ductal epithelial cells.

4.2.2 BCAR3 is expressed across multiple subtypes of human breast cancer

BCAR3 protein levels are generally undetectable in cell lines representing early-stage ER^+ breast cancer and elevated in TNBC cell lines [47, 119, 120]. Therefore, we hypothesized that the human breast tumors would exhibit a similar pattern of BCAR3 expression. To address this, BCAR3 protein expression was measured across a panel of 74 breast tumors that were representative of five different subtypes of breast cancer, including (1) low-grade ER^+ $HER2^-$, (2) high-grade ER^+ $HER2^-$, (3) ER^+ HER2-amplified ($HER2^+$), (4) ER^- $HER2^+$, and (5) triple-negative (TN; ER^- PR^- $HER2^-$). A single section per tumor was evaluated and designated as 'positive' if it contained any BCAR3-positive regions, or 'negative' if there was no detectable BCAR3. Surprisingly, we found that BCAR3 was detected in the majority of tumors for all five subtypes, including low-grade ER^+ breast cancer (**Fig 4.5**). Interestingly, despite the small sample size, nearly all of the ER^+ $HER2^+$ tumors stained positive for BCAR3, while only half of the triple-negative tumors expressed BCAR3. Together, these data demonstrate that BCAR3 is expressed across multiple subtypes of breast cancer, and that the lack of BCAR3 expression in ER^+ breast cancer cell lines cultured *in vitro* is not an accurate reflection of the BCAR3 protein levels expressed in human breast tumors.

4.2.3 BCAR3 protein is expressed at the highest levels within regions of high-grade DCIS

Considering that all of the breast tumor subtypes that were analyzed showed BCAR3 protein expression, and that expression of this protein was highly variable within

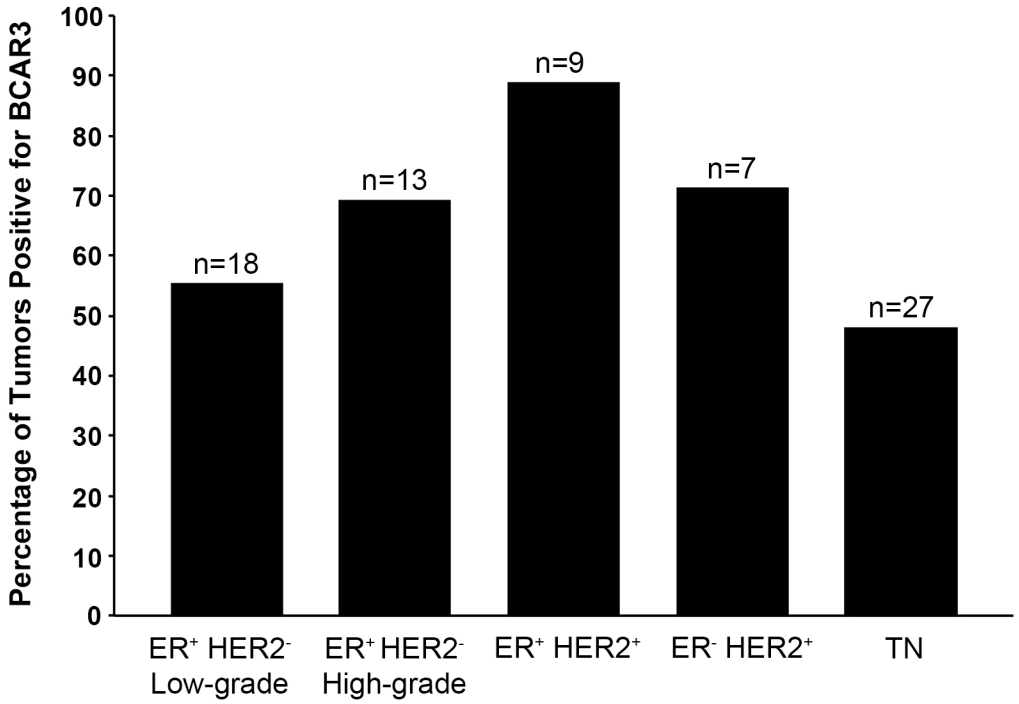
Percentage of Tumors Positive for BCAR3
100
90
80
70
60
50
40
30
20
10
0
n=18
n=13
n=9
n=7
n=27
ER+ HER2- Low-grade
ER+ HER2- High-grade
ER+ HER2+
ER- HER2+
TN

Figure 4.5. BCAR3 protein is expressed across multiple subtypes of human breast cancer. BCAR3 protein expression was evaluated by IHC across a panel of 74 breast tumors as described in the methods. Tumors represented five different subtypes of breast cancer, including (1) low-grade ER^+ $HER2^-$ (n=18), (2) high-grade ER^+ $HER2^-$ (n=13), (3) ER^+ $HER2^+$ (n=9), (4) ER^- $HER2^+$ (n=7), and (5) TN (triple-negative; ER^- PR^- $HER2^-$, n=27). Irrespective of staining intensity, a single section per tumor was designated as 'positive' if it contained any BCAR3-positive regions, or 'negative' if there was no detectable BCAR3. Data represent the percentage of tumors positive for BCAR3.

a given tumor, we sought to determine whether there was a quantitative difference between BCAR3 protein levels across tumor subtypes. BCAR3 staining intensity was evaluated across subtypes using a single section per tumor. Each tumor was assigned a staining score (i.e. 1^+, 2^+ or 3^+) that represented the highest level of staining seen in the tumor (**Fig 4.6A**). It appears from this limited sample number that the highest BCAR3 staining was observed in high-grade tumors, but that there was no bias toward any specific tumor subtype. We did notice, however, that the highest BCAR3 expression appeared to be present in high-grade DCIS. Consequently, we further categorized BCAR3 expression in regions of DCIS separated on the basis of tumor grade [154]. Irrespective of tumor subtype, we found that about 80% of tumors exhibiting regions of low-grade DCIS stained negative for BCAR3 and the remaining 20% expressed low levels of BCAR3 (**Fig 4.6B and 4.6C**, panels a and b). Conversely, nearly 70% of tumors exhibiting regions of high-grade DCIS expressed BCAR3, and of those, about one-third displayed moderate to very high BCAR3 protein levels (**Fig 4.6B and 4.6C**, panels c through h). Therefore, while high BCAR3 protein expression was not associated with a specific tumor subtype, it appeared to track with higher tumor grade, particularly within regions of DCIS.

4.2.4 BCAR3 protein levels are not altered in response to varying matrix rigidity

Increased ECM remodeling, including collagen deposition and crosslinking, has been shown to accompany breast tumor progression *in vivo* and the adoption of more aggressive breast tumor cell behaviors (e.g. invasion and metastasis) [155, 156]. Ultimately, this remodeling results in increased ECM stiffening, tissue rigidity, and integrin-based adhesion signaling [155]. Thus it was interesting that, in addition to being highly expressed within regions of high-grade DCIS, BCAR3 was also prevalent in tumor

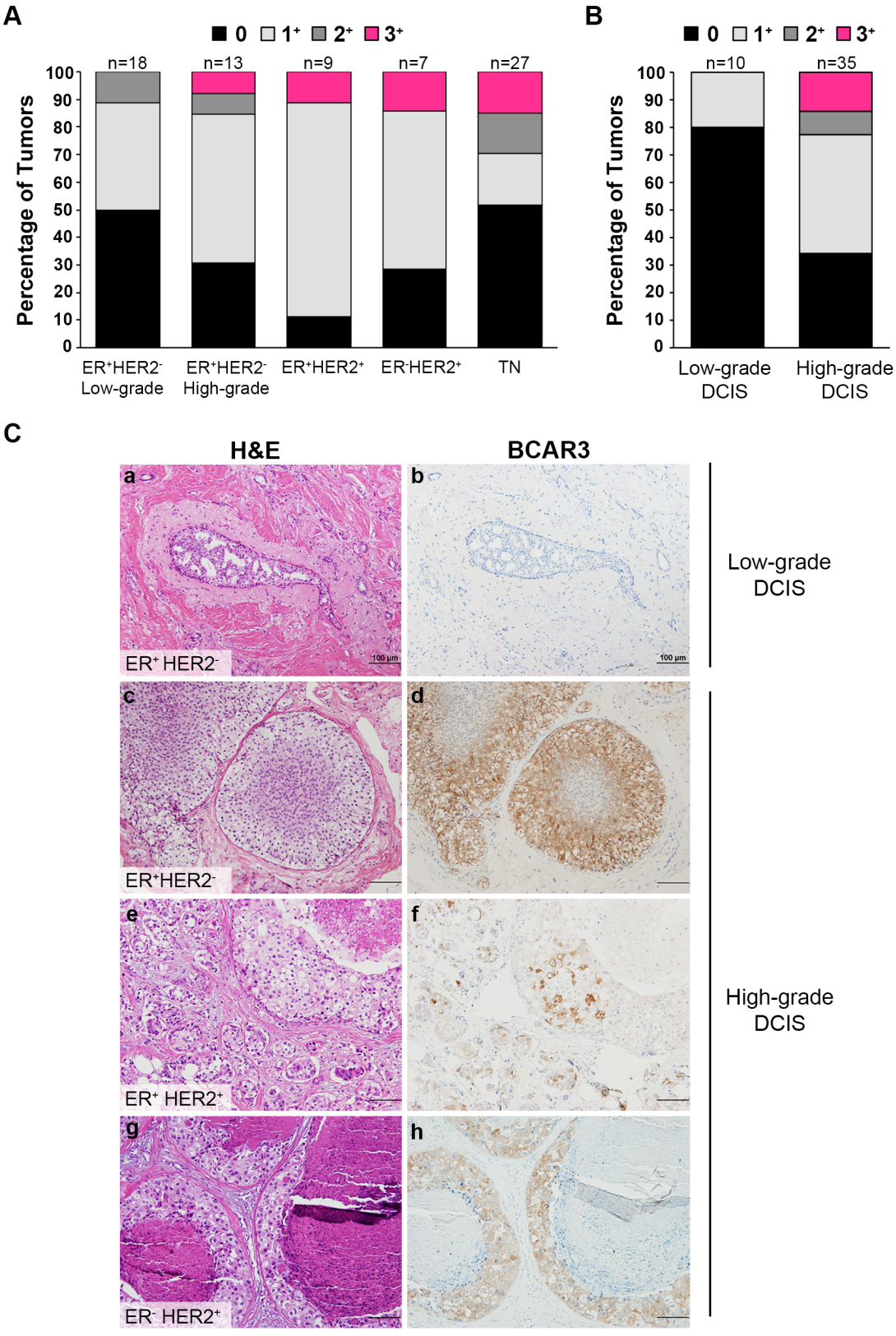
A
0 1+ 2+ 3+
n=18
n=13
n=9
n=7
n=27
Percentage of Tumors
100
90
80
70
60
50
40
30
20
10
0
ER+HER2- Low-grade
ER+HER2- High-grade
ER+HER2+
ER-HER2+
TN
B
0 1+ 2+ 3+
n=10
n=35
Percentage of Tumors
Low-grade DCIS
High-grade DCIS
C
H&E
BCAR3
a
b
c
d
e
f
g
h
ER+ HER2-
ER+HER2-
ER+ HER2+
ER- HER2+
100 µm
Low-grade DCIS
High-grade DCIS

Figure 4.6. Highest BCAR3 protein levels are observed within regions of high-grade DCIS. (**A**) BCAR3 staining intensity was evaluated across the five different subtypes of breast cancer described in **Figure 4.5**. Data represent the percentage of tumors that exhibit 0, 1^+, 2^+ or 3^+ staining intensity for BCAR3. A single section per tumor was assigned a staining score (i.e. 1^+, 2^+ or 3^+) that represented the highest level of staining seen in the tumor. (**B**) Irrespective of tumor subtype, BCAR3 staining intensity was evaluated in regions of low-grade (n=10) versus high-grade (n=35) DCIS. Histopathological features such as nuclear grade and cell necrosis were used to define high-grade DCIS [154]. Data represent the percentage of tumors that exhibit 0, 1^+, 2^+ or 3^+ staining intensity for BCAR3 in regions of DCIS. (**C**) Serial sections of tumors exhibiting regions of low-grade and high-grade DCIS were stained for H&E (left panels) and BCAR3 (right panels) as described in the methods. Representative serial images of low-grade and high-grade DCIS from patients whose tumors were of the indicated molecular subtype based on ER and HER2 expression are shown. Scale bar=100μm.

cells adjacent to regions that appeared to have higher collagen content marked by the bright pink eosin staining (**Fig 4.7**, panels a,c,e,g). Furthermore, some of the regions that contained high BCAR3 expression also exhibited a robust desmoplastic host response indicated by the grayish-pink stroma on the H&E stain (**Fig 4.7**, panel c, arrowhead).

Based on these findings, we hypothesized that BCAR3 protein levels are upregulated in response to increased matrix rigidity. This was tested by culturing BT549 breast cancer cells or non-tumorigenic MCF-10A mammary epithelial cells on collagen-coated polyacrylamide substrates of either 300 and 4800 Pascals (Pa), which mimic the lower rigidity of lung tissue or the higher rigidity of smooth muscle, respectively [157]. After 96 hours, BT549 cells and MCF-10A cells were more spread on the higher rigidity matrix compared to the lower rigidity matrix (**Fig 4.8A**). Additionally, there appeared to be a higher density of cells on the 4800 Pa substrates compared to the 300 Pa substrates, at least for the BT549 cells. Together, these data are consistent with the finding that BT549 cells and MCF-10A cells proliferate faster on higher rigidity substrates, and this increased proliferation is associated with the ability of cells to spread on the matrix [158]. Surprisingly, despite these notable morphological changes, BCAR3 protein levels were not altered in response to varying matrix rigidity (**Fig 4.8B**). Together, these data argue that the heterogeneous BCAR3 protein expression observed in human breast tumors is not likely to be due exclusively to increased ECM matrix stiffness.

4.3 Discussion

Considering the contradictory reports regarding BCAR3 protein and mRNA levels in human breast cancer cell lines and tumors, respectively, it was critical to directly

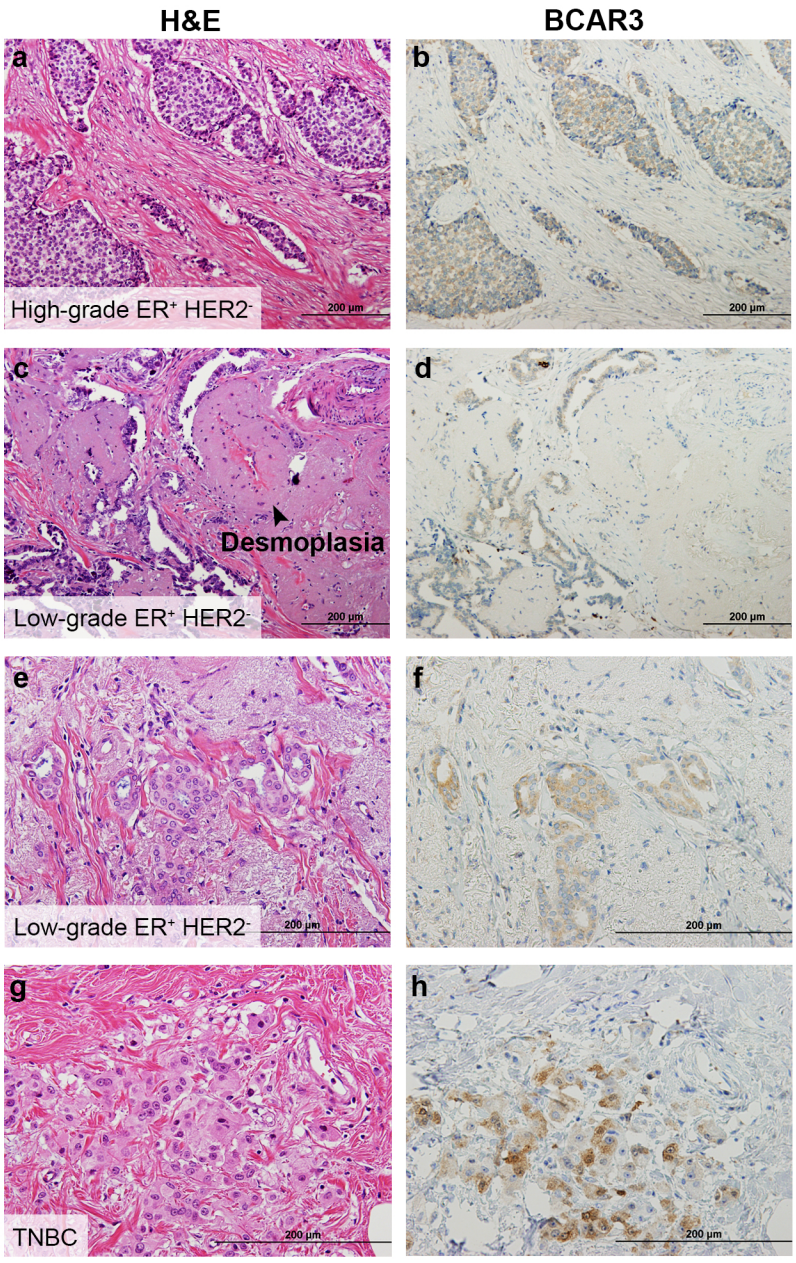
H&E
BCAR3
a
b
High-grade ER+ HER2-
200 µm
200 µm
c
d
Desmoplasia
Low-grade ER+ HER2-
200 µm
200 µm
e
f
Low-grade ER+ HER2-
200 µm
200 µm
g
h
TNBC
200 µm
200 µm

Figure 4.7. Ductal epithelial cells adjacent to regions of high collagen content and desmoplasia express high levels of BCAR3. Representative serial sections of tumors of the indicated molecular subtype were stained for H&E (left panels) and BCAR3 (right panels) as described in the methods. Collagen fibers and desmoplasia appear on H&E sections as bright pink and grayish-pink stroma, respectively. Arrowhead points to region of desmoplasia. Scale bar=200μm.

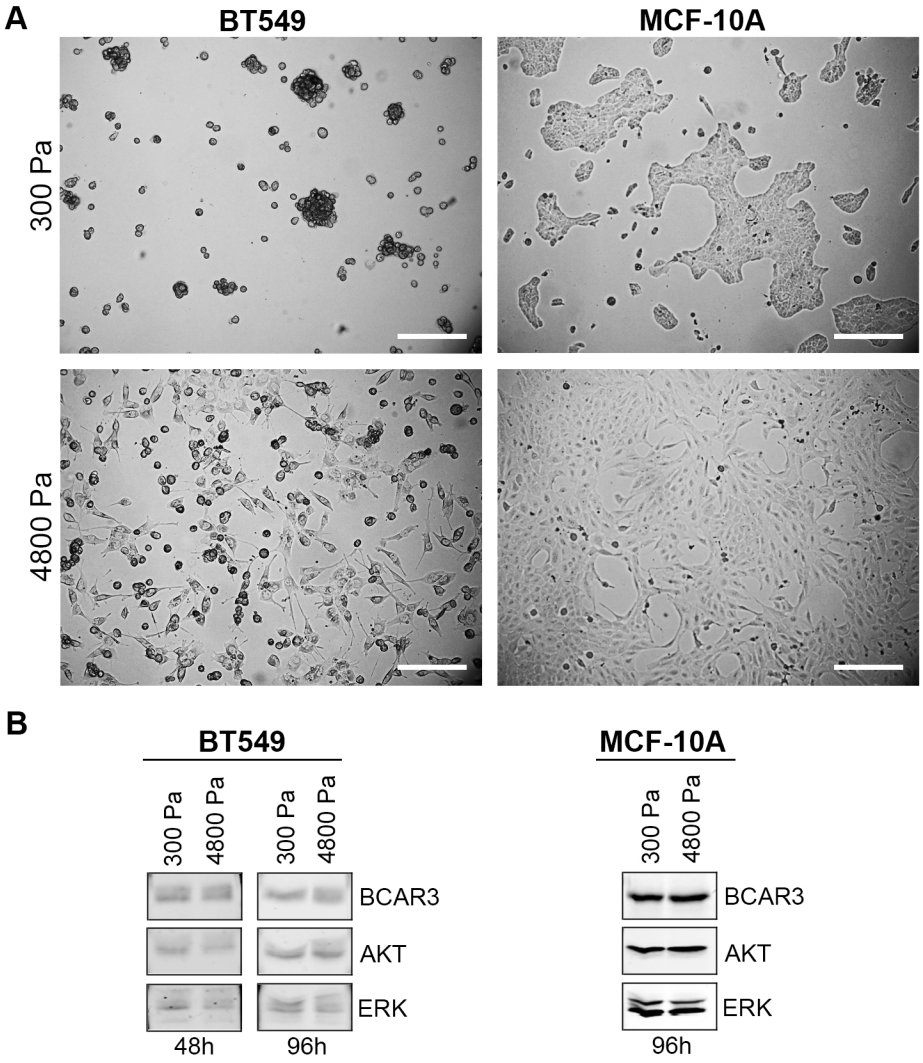
A
BT549
MCF-10A
300 Pa
4800 Pa
B
BT549
MCF-10A
300 Pa
4800 Pa
300 Pa
4800 Pa
BCAR3
AKT
ERK
48h
96h
300 Pa
4800 Pa
BCAR3
AKT
ERK
96h

Figure 4.8. BCAR3 protein levels in invasive breast cancer and non-tumorigenic mammary epithelial cells are unaltered in response to differing matrix rigidities. (**A**) BT549 invasive human breast cancer cells (left) and MCF-10A non-tumorigenic mammary epithelial cells (right) were plated for 96 hours on collagen-coated polyacrylamide substrates of 300 and 4800 Pascals as described in the methods. Scale bar=200μm. (**B**) The designated cells were cultured for 48 or 96 hours as in (A) and lysed as described in the methods. Total cell protein was immunoblotted with the designated antibodies.

examine BCAR3 protein levels in human tumors in order to gain further insight into its function in tumor progression. We have shown for the first time that BCAR3 protein levels are elevated in tumor tissue compared to normal breast tissue. Interestingly, BCAR3 protein is upregulated in both DCIS and invasive ductal carcinoma, with the highest expression observed in high-grade DCIS samples. Furthermore, we discovered that BCAR3 is expressed across multiple subtypes of human breast cancer. While BCAR3 protein levels do not seem to correlate with any particular subtype, our studies reveal the immense heterogeneity of BCAR3 expression within each tumor subtype.

It is important to note that, in our current study, BCAR3 expression was measured by IHC staining and not immunoblotting. The advantage of this approach is that it revealed the marked heterogeneity of BCAR3 expression in the tumor samples. However, because a low stringency test was applied to the binning of BCAR3 expression, this analysis potentially over-represents BCAR3 expression in human breast cancers. It would be beneficial in future studies to set thresholds; for example, a given tumor could be designated as 'positive' if greater than 50% of the tumor section showed positive staining for BCAR3 or as '3^{+}' if greater than 50% of the tumor exhibited 3^{+} staining. Nonetheless, it is unclear to what extent BCAR3 needs to be upregulated in tumors in order to be considered clinically and/or biologically significant.

4.3.1 BCAR3 protein levels correlate with high-grade DCIS

Given the role of BCAR3 in promoting breast tumor cell motility and invasiveness, and its elevated expression in invasive breast cancer cell lines ([47, 119, 120], **Chapters 2 and 3**), we hypothesized that the highest levels of BCAR3 protein would be associated with advanced-stage invasive breast cancer. Instead, the highest BCAR3 staining was found within regions of high-grade DCIS irrespective of tumor

subtype. While this finding is unexpected, it does indicate that BCAR3 protein may play an earlier role in breast tumor development than originally thought. High-grade DCIS is characterized by robust proliferation; the tumor cells can proliferate at such a rapid rate within ducts that the cells often outgrow their oxygen supply. This results in a very hypoxic environment that may promote local invasion and tumor cell escape [159]. Furthermore, in many cases of high-grade DCIS, tumor cells within the center of highly proliferative ducts undergo necrosis, which then calcify over time [159]. Interestingly, BCAR3-expressing tumor cells were observed directly adjacent to these necrotic regions (which stain bright pink on H&E stains) within ducts (for example, see **Fig 4.6C**, panels g and h).

Given our finding that BCAR3 expression correlates with high-grade DCIS, we suggest that BCAR3 may play an important, yet undiscovered, role in breast tumor cell proliferation. There is some evidence to support a role for BCAR3 in tumor cell proliferation. First, Adam Lerner's group has shown that BCAR3 expression contributes to activation of the cyclin D1 promoter in ER^+ breast cancer cells [120, 124]. Cyclin D1 is frequently overexpressed in high-grade ER^+ human breast tumors, and it correlates with antiestrogen resistance, poor relapse-free survival and poor overall survival [160-162]. Several of the high-grade DCIS samples that were analyzed in our current study and showed high BCAR3 expression were ER^+ breast tumors (e.g. see **Fig 4.6C**, panels d and f). Furthermore, work from our group has revealed that the staining pattern of BCAR3-expressing tumor cells in PyMT-driven mouse mammary gland tumors mimics that of cyclin D1-expressing tumor cells, further suggesting a potential correlation between BCAR3 and cyclin D1 expression (Allison Batties, *personal communication*, [10]). We are currently co-staining the tumors to determine if BCAR3 and cyclin D1 are indeed co-overexpressed in these mouse tumors. Second, a recent study showed that

BCAR3/Cas complexes activate ERK1/2 signaling *in vitro*, and this activation was required for BCAR3/Cas-induced tumor cell proliferation in the presence of antiestrogens [132]. Taken together, we suggest that high BCAR3 protein levels may enhance pro-proliferative signaling pathways within tumor cells, which may lead to, or perpetuate, DCIS. Future work will be necessary to determine whether high BCAR3 protein levels promote or just simply correlate with high-grade DCIS.

The fact that BCAR3 protein levels are elevated in pre-invasive DCIS lesions leads to a second hypothesis whereby upregulation of BCAR3 in premalignant tumor cells may promote local invasion through the basement membrane and into the surrounding stroma. While metastasis is a rare event in patients diagnosed with DCIS, as high as 50% of patients are estimated to develop invasive ductal carcinoma (IDC) if they do not undergo appropriate or adequate treatment regimens [163, 164]. Moreover, disseminated tumor cells have been detected in bone marrow samples from DCIS breast cancer patients, providing further evidence that tumor cells in premalignant DCIS lesions have the capacity to invade and metastasize [163, 165]. The fact that BCAR3 functions to promote motility and invasion ([47, 119], Chapters 2 and 3) is consistent with such a model.

4.3.2 Heterogeneity of BCAR3 protein expression in human breast cancer

In contrast to data from breast cancer cell lines, elevated BCAR3 protein levels do not appear to be restricted to specific tumor subtypes, hormone receptor status, or invasiveness in the cohort of human breast tumors we examined. In addition to being found across multiple breast tumor subtypes, BCAR3 expression was found to be extremely heterogeneous within a particular tumor. Although BCAR3 protein expression did not appear to track with matrix rigidity, at least in the two cell lines that were tested *in*

vitro, it may correlate with certain molecular signatures underlying breast tumor progression. A very recent study by Pape-Zambito *et al.* analyzing tumors from 36 patients concurrently diagnosed with both DCIS and IDC revealed extreme heterogeneity of DCIS lesions within individual breast cancer patients [164]. More specifically, they showed that varying levels of several "high-risk DCIS biomarkers" were expressed in locally distinct regions of DCIS lesions from a single patient. These markers included HER2, the proliferative marker Ki67, and p16, a protein typically involved in stress-induced cellular senescence but its deregulation in DCIS is associated with subsequent tumor progression [164, 166]. These data underscore the existence of distinct cell populations within DCIS lesions that may differentially contribute to the development of IDC [164]. The finding that BCAR3 protein levels were highly variable across DCIS lesions within individual patients who showed evidence of both DCIS and IDC (e.g. see **Fig 4.3**) suggests that BCAR3 may be a similar high-risk DCIS biomarker. Whether high BCAR3 protein levels correlate with other molecular markers of high-risk DCIS remains to be elucidated.

4.3.3 Is BCAR3 a good therapeutic target for breast cancer?

When evaluating whether BCAR3 would be a suitable target for the treatment of breast cancer, it will be critical to take into account findings from studies assessing both BCAR3 protein and mRNA expression with respect to clinical resistance and outcome. It will first be necessary to determine whether elevated BCAR3 protein levels in primary tumor tissues correlate with clinical outcomes, e.g. distant metastasis-free survival, relapse-free survival and/or overall survival. Given our finding that BCAR3 protein levels are elevated in breast tumors compared to normal breast tissue warrants a thorough investigation into whether this upregulation carries any prognostic value. Our *in vitro*

studies using human breast cancer cell lines highlight the roles of BCAR3 in promoting Src activity and, potentially, tumor invasiveness ([47, 129], **Chapters 2 and 3**). However, surprisingly, high BCAR3 expression was not skewed toward IDC in our panel of human breast tumors. In fact, BCAR3 expression was even detected in low-grade ER^+ breast tumors, suggesting that BCAR3 protein levels may track with some other feature(s) of breast tumor progression as opposed to invasiveness. We are currently collaborating with Bristol-Myers Squibb to determine whether high BCAR3 protein levels in primary human breast tumors correlate with sensitivity to the small molecule Src inhibitor, Dasatinib. Furthermore, a recent study has even reported that BCAR3 protein may play a role in preventing breast tumor progression by antagonizing the pro-metastatic TGFβ/Smad-mediated signaling pathway in invasive human breast cancer cells [135]. However, as stated, these data stem from studies performed in breast cancer cell lines and underscore the need to directly evaluate BCAR3 protein expression in human breast tumors in parallel with associated clinical data to determine whether elevated BCAR3 protein levels correlate with favorable or unfavorable disease outcomes.

While it remains to be determined whether BCAR3 protein levels correlate with clinical resistance and/or survival, elevated BCAR3 mRNA levels in primary human tumor tissue have been reported to correlate with improved tamoxifen response and better survival outcomes [133-135]. Based on these data, it is possible that targeting or silencing BCAR3 expression in patients may inadvertently promote therapeutic resistance. Clearly, further studies are necessary to determine whether elevated BCAR3 protein levels in primary tumor tissue correlate with tamoxifen response and/or survival in order to reconcile the contradictory findings between BCAR3 mRNA and protein expression in human tumors.

If future studies reveal that elevated BCAR3 protein levels associate with poor prognosis in breast cancer patients, its potential as a therapeutic target remains complex. On the one hand, BCAR3 protein appears to be relatively dispensable in normal cell types, as evidenced by BCAR3 knockout mice that develop normally and have no overt phenotypic abnormalities [126]. The fact that BCAR3 protein levels are upregulated in breast tumor cells compared to normal ductal epithelial cells suggests that it may be possible to target BCAR3 in tumor cells while causing limited collateral damage to normal ductal epithelial cells. On the other hand, our studies herein reveal the heterogeneity of BCAR3 protein expression in human breast cancer. As discussed in **Chapter 1**, this heterogeneity may serve to be a therapeutic challenge. Until we gain a better understanding of the mechanism through which BCAR3 protein levels are upregulated to varying degrees in different regions of breast tumors, it will be difficult to evaluate its prognostic and therapeutic potential.

Overall, our data demonstrate for the first time that BCAR3 protein levels are upregulated across multiple subtypes of human breast cancer. These initial findings help to lay the groundwork for future studies that will determine whether elevated BCAR3 protein levels correlate with clinical outcomes, and whether they can serve as a useful biomarker to identify tumors that exhibit aggressive subtypes of DCIS and/or high Src activity.

CHAPTER 5: Perspectives

The heterogeneity of tumors within and between patients proves to be a major therapeutic obstacle for the treatment of cancer. As we move further into the era of personalized medicine, it is critical that we gain a better understanding of the molecular drivers and cell signaling pathways that underlie disease progression. By elucidating key mechanisms of tumor cell proliferation, survival, motility and invasion, we will be better equipped to develop drugs and tailor therapeutic regimens for individualized patient care.

The work presented herein highlights the role of an adaptor molecule, BCAR3, in promoting invasive breast cancer cell motility. We demonstrate that BCAR3 localizes to adhesions, enhances Rac1 activity and drives several critical facets of cell motility, including membrane protrusion and adhesion turnover. BCAR3-mediated adhesion turnover is contingent on its ability to directly interact with its well-established binding partner, Cas. The requirement for BCAR3 in driving this pro-migratory phenotype is underscored by the fact that, when BCAR3 is selectively depleted from breast cancer cells, they fail to migrate/invade efficiently and respond properly to growth factor stimuli. Instead, RhoA signaling predominates under these conditions, resulting in increased tension, adhesion stabilization and decreased motility. Interestingly, disruption of BCAR3/Cas interactions has no effect on BCAR3 or Cas localization to adhesions but mimics the loss of BCAR3 in that the rate of adhesion disassembly is significantly reduced. We suggest that BCAR3, when in direct association with Cas in invasive breast cancer cells, influences the molecular switch between Rac1 and RhoA signaling in adhesions. We propose that the BCAR3/Cas complex drives local Rac1 activity, thus promoting breast tumor cell motility/invasion. Conversely, under conditions when this

complex is not favored, either due to experimental manipulation or to a change in signaling, Rac/Rho reciprocity is tipped in favor of RhoA signaling. This leads to the slower adhesion turnover and reduced motility observed under these conditions.

5.1 Do BCAR3/Cas complexes exist in 3D adhesions and what function do they serve in 3D cell motility/invasion?

While our data build a strong case for BCAR3/Cas complexes as key regulators of localized Rac/Rho signaling in invasive breast cancer cell lines, several important questions remain. First, data reported in this thesis demonstrate the importance of BCAR3/Cas signaling in two-dimensional (2D) adhesion dynamics and motility. In fact much of our mechanistic understanding of adhesion turnover and maturation has been revealed in cells plated on 2D planar substrates. However, the *in vivo* tumor microenvironment is a three-dimensional (3D) system in which a complex ECM surrounds tumor cells. This brings into question the relevancy of 2D findings when considering the complexity of the 3D microenvironment. More specifically, do BCAR3 and Cas co-localize in adhesions in 3D? Do BCAR3/Cas complexes influence Rac/Rho activity in 3D as they do in 2D? What roles do BCAR3/Cas complexes serve *in vivo?* Does BCAR3-mediated signaling promote tumor progression and metastasis *in vivo*? These questions will be explored in further detail below.

5.1.1 Adhesion and motility in 3D

Advances in multiphoton microscopy and intravital imaging have allowed for direct visualization of cell motility in primary tumors [45]. These studies have revealed the complexities of the 3D tumor microenvironment and how cells adjust and move differently with respect to their surroundings. Specifically, breast cancer cells in

mammary tumors have been shown to migrate at very high velocities in an amoeboid-like fashion along collagen fibers [45]. This is in stark contrast to the slow, fibroblast-like (or mesenchymal) movement of breast cancer cells on 2D substrates. One reason that may account for these differences in motility and rate is the extent to which tumor cells make contact with their surrounding ECM in 2D versus 3D systems. Condeelis and colleagues hypothesized that tumor cells would only make transient contacts (i.e. focal complexes) when "crawling" along collagen fibers *in vivo*, as opposed to the stable, mature focal adhesions that are seen on plastic [45]. Indeed, the seminal study described above has set the tone for the past decade of research that has aimed to study cell adhesion in 3D.

The size, location and morphology of adhesions in 3D have been largely debatable, including whether or not they actually exist [167]. Earlier work from Denis Wertz' group evaluated the localization of several GFP-tagged focal adhesion proteins (e.g. talin, α-actinin, paxillin, Cas, FAK) in HT-1080 fibrosarcoma cells fully embedded into a collagen I-based 3D matrix [168]. They discovered that these proteins were diffusely localized throughout the cytoplasm of migrating cells rather than being contained within distinct structures. The interpretation of these data was that focal adhesion-like structures are either undetectable or do not exist in 3D. However, they went on to demonstrate that selective depletion of core adhesion proteins affected 3D cell motility by controlling protrusion dynamics and cell speed [168].

In contrast, Kubow and Horwitz have argued that ectopic overexpression of fluorescently tagged proteins causes diffuse, background fluorescence that impedes visualization of 3D cell-matrix adhesions [169]. Instead, using a "speckled" (i.e. low expression) GFP-paxillin construct, Kubow and Horwitz observed distinct paxillin-containing focal adhesion-like structures in protrusions of U2OS osteosarcoma cells

migrating in 3D collagen gels [169]. Interestingly, paxillin has also been demonstrated to be a key regulator of integrin-based adhesion dynamics in MDA-MB-231 breast cancer cells in a 3D cell derived matrix (CDM) model [97]. CDM models are distinct from 3D collagen gels in that they are mechanically more stiff and, in addition to collagen, they are comprised of fibronectin and growth factors deposited by fibroblasts [170].

Recently, the Horwitz lab has shown that adhesion maturation in 3D requires myosin II activity, much like it does in 2D [171]. This study also demonstrated that the size and length of any given adhesion in 3D is contingent on the local matrix architecture surrounding that particular adhesion [171]. Specifically, local collagen fiber orientation and diameter guides adhesion maturation and restricts adhesion length [171]. This finding is very compelling and may explain why varying shapes of adhesions have been reported using different 3D matrix models [167]. Although the field of 3D adhesion biology is still in its infancy, and many aspects of 3D adhesion structure and function remain unclear, it is becoming evident that dynamic focal adhesion-like structures do exist in cells in 3D. However, visualizing adhesions in 3D is highly reliant on the types of 3D models and imaging techniques used [170].

5.1.2 Future studies: Visualizing BCAR3 and Cas in 3D adhesions

Our lab is uniquely positioned to determine whether BCAR3 and Cas are present in 3D adhesions using collagen-based 3D gels. Interestingly, members of our group have recently demonstrated that BCAR3, through its direct interaction with Cas, is required for invasion of MDA-MB-231 breast cancer cells in 3D (Allison Batties, *personal communication*). Thus it would be interesting to use similar methods to those described by Kubow and Horwitz [169] to visualize 3D adhesions in these breast cancer cells. This would be accomplished by seeding MDA-MB-231 breast cancer cells expressing EGFP-

BCAR3 and mCherry-Cas under the control of speckled promoters in collagen-based gels. Adhesions, together with collagen fibers, could then be visualized in spread cells using laser scanning confocal microscopy. Using this approach, we could determine whether BCAR3 and Cas co-localize in 3D adhesions as they do in 2D.

In addition to assessing co-localization of BCAR3 and Cas, it would be important to test whether BCAR3 and Cas directly interact in 3D adhesions using fluorescence resonance energy transfer (FRET)-based biosensor technology. FRET is an effective technique to determine whether two proteins directly interact and it can be used in 2D, 3D and *in vivo*. Traditional FRET involves tagging two proteins of interest with distinct fluorophores. One protein functions as the "donor" molecule, and the other as the "acceptor." When the donor is directly bound to the acceptor, excitation of the donor results in a transfer of energy to the acceptor (i.e. the donor is "quenched" and the acceptor is excited). Acceptor excitation is indicated by an increase in fluorescence intensity.

Recently, Deakin *et al.* used a popular variation of FRET known as acceptor photobleaching FRET (or apFRET) to assess protein-protein interactions in 3D cell-matrix adhesions. In apFRET, the acceptor molecule is photobleached. In this case, a positive FRET signal, and therefore a direct molecular interaction, would be indicated by an increase in the fluorescence intensity of the donor molecule (i.e. the donor gets "unquenched" as the acceptor is photobleached) [172]. This variation of FRET is advantageous because there are fewer issues with acceptor bleed-through and it allows for very accurate FRET efficiency measurements to be made strictly within 3D adhesion contacts versus in surrounding cytosolic regions [172-174]. Using a similar approach to Deakin *et al.*, MDA-MB-231 invasive breast cancer cells expressing a "donor" yellow fluorescent protein (YFP)-tagged BCAR3 construct and an "acceptor" red fluorescent

protein (RFP)-tagged Cas construct could be imaged after seeding in 3D collagen gels. Images can be captured in both channels (i.e. YFP and RFP) before and after photobleaching the acceptor (i.e. the RFP channel, or in this case, Cas). Direct BCAR3/Cas interaction in 3D adhesions would be indicated by an increase in the fluorescence intensity of YFP-BCAR3 following photobleaching of Cas relative to before photobleaching.

Lastly, if we discover that BCAR3/Cas complexes exist in 3D adhesions, we would be in a strong position to analyze the influence of direct BCAR3/Cas association on 3D adhesion dynamics. In this case, MDA-MB-231 cells would be co-transfected with speckled constructs encoding WT GFP-BCAR3 or L744E/R748E GFP-BCAR3 plus speckled mCherry-Cas, and the rates of adhesion assembly and disassembly in migrating cells in 3D collagen gels would be measured by capturing time-lapse Z-stacks via laser scanning confocal microscopy similar to the technique pioneered by Kubow and Horwitz [169].

Finally, it would also be possible to measure the dynamics of BCAR3 and Cas in 3D adhesions by fluorescence recovery after photobleaching (or FRAP). FRAP-based imaging involves photobleaching a fluorescently tagged protein of interest in a precise region and then following the recovery of its fluorescence signal over time. FRAP can measure the diffusion rates of proteins into and out of adhesions as well as immobile fractions in both 2D and 3D systems [175]. For these studies, we would again use the MDA-MB-231 cells co-expressing WT GFP-BCAR3 or L744E/R748E GFP-BCAR3 and mCherry-Cas under the control of a speckle promoter seeded in 3D collagen gels. GFP-tagged WT or mutant BCAR3 protein would then be photobleached in an adhesion co-expressing Cas, and the repopulation kinetics of BCAR3 in adhesions would be determined as a function of its ability to bind to Cas. To circumvent the potential

problem of having endogenous BCAR3 in adhesions, a similar study could be performed in a stable BCAR3-depleted MDA-MB-231 cell line that has been engineered to express a wobble (shRNA-resistant) form of WT or mutant L744E/R748E GFP-BCAR3 plus mCherry-Cas.

5.1.3 Future studies: BCAR3/Cas complexes and regulation of Rac/Rho signaling in 3D

Based on the data presented herein, we propose that BCAR3 controls the spatiotemporal balance between Rac1 and RhoA activity in invasive breast cancer cells grown on 2D substrates. Whether this requires direct interaction between BCAR3 and Cas remains to be determined. We are currently investigating whether mutant L744E/R748E BCAR3 is able to promote Rac1 activity in 2D.

As discussed above, members of our group recently demonstrated that BCAR3, via its direct interaction with Cas, controls invasive breast cancer cell invasion in 3D (Allison Batties, *personal communication*). An interesting question raised by this finding is whether BCAR3 carries out this action by regulating the relative activity levels of Rac and Rho during 3D invasion. Determining whether BCAR3 controls Rac/Rho activity during 3D invasion could be tested with Raichu-Rac1 or Raichu-RhoA FRET-based reporters. These Raichu (or "Ras superfamily and interacting protein chimeric unit") probes are very useful reporters of the spatiotemporal control of Rac1 and RhoA activity in 3D and *in vivo* [176, 177]. For instance, in the case of Raichu-Rac, the probe consists of Rac1 as the cyan fluorescent protein (CFP) sensor and p21-activated kinase-Cdc42/Rac interactive binding domain (PAK-CRIB) as the YFP ligand. In the presence of a Rac-GEF, GDP exchange for GTP will activate Rac1, resulting in intra-molecular binding of GTP-Rac1 to the PAK-CRIB domain on the probe, therefore causing FRET from CFP to YFP [176]. In our case, control or BCAR3-depleted MDA-MB-231 cells

expressing the Raichu-Rac1 or RhoA probes could be seeded in 3D collagen gels and the spatial activation of Rac1 or RhoA in the presence or absence of BCAR3 would be measured by fluorescence lifetime imaging microscopy (FLIM)-FRET, similar to methods used by Timpson *et al.* and Johnsson *et al.* [176, 177]. FLIM-FRET measures the reduction in the excited state lifetime of a donor molecule when it is in complex with its acceptor molecule [175]. If BCAR3 promotes Rac1 activation in invasive breast cancer cells during 3D invasion (e.g. by promoting local recruitment of a specific Rac1-GEF), then we would expect to observe increased Rac FRET in BCAR3-expressing cells compared to BCAR3-depleted cells. Similarly, if RhoA activity is increased under conditions where BCAR3 is silenced (as is the case in 2D, see **Chapter 2, Fig 2.7**), then we would expect to observe increased Rho FRET in BCAR3-depleted cells compared to BCAR3-expressing cells invading in 3D.

We may also be able to analyze the importance of BCAR3/Cas interactions in regulating Rac/Rho activity levels and subcellular localization during 3D invasion in the stable BCAR3-depleted MDA-MB-231 cells expressing wobble shRNA-resistant WT and mutant L744E/R748E BCAR3 proteins. By similarly applying the Raichu Rac and Rho biosensors described above, we could determine whether localization and activity of Rac1 and RhoA during 3D invasion is altered in cells where BCAR3/Cas interactions are prevented. If BCAR3/Cas association is required for Rac1 activity and/or RhoA suppression (as we argue in 2D), then we would expect to observe decreased Rac FRET and increased Rho FRET in MDA-MB-231 cells expressing wobble L744E/R748E BCAR3 in 3D collagen gels.

Finally, it is important to note that much of our work argues that BCAR3/Cas complexes regulate Rac/Rho activity. However, it is also possible that the opposite could be true, in that Rac/Rho signaling may regulate BCAR3/Cas complexes. In fact, it

has been demonstrated that Rac/Rho signaling can regulate the interaction between paxillin and vinculin in 2D and 3D adhesions [172]. This presents a compelling paradox: Is direct BCAR3/Cas interaction a cause or effect of Rac/Rho signaling? To test whether Rac1 activity promotes BCAR3/Cas association, we could use mutant forms of Rac1 and the apFRET approach described by Deakin *et al.* [172]. Specifically, we could express YFP-BCAR3 and RFP-Cas, plus either a constitutively active Myc-tagged Rac1 (i.e. Myc-RacL61 as used in **Chapter 2, Fig 2.3**) or a dominant negative Myc-tagged Rac1 (e.g. Myc-N17Rac1) in MDA-MB-231 cells. Under each of these conditions, we would measure FRET efficiency between BCAR3 and Cas. If Rac1 promotes or stabilizes BCAR3/Cas association, we would expect to observe high FRET efficiency between BCAR3 and Cas in cells that express Myc-RacL61 versus Myc-N17Rac1. Similar types of experiments can be performed using constitutively active or dominant negative forms of RhoA, in addition to, various pharmacological inhibitors of Rac/Rho activity or their downstream effectors (e.g. Y-27632) [172].

5.1.4 Future studies: BCAR3/Cas signaling in invadopodia

Invadopodia are specialized adhesive structures that are distinct from focal adhesions given their ability to locally degrade ECM by secreting MMPs [60, 178]. Invadopodia play a critical role in directed tumor cell motility, invasion and metastasis. They have been directly visualized in both 2D and 3D culture models (reviewed in [44]), as well as in mouse mammary tumors *in vivo* [179]. Invadopodia are actin-rich and contain cortactin, cofilin, N-WASP, the adaptor protein Tks5, as well as many other adhesion proteins [178, 180]. Interestingly, Rho-family GTPases drive the formation and maturation of invadopodia. Specifically, Cdc42 and RhoA play essential roles in invadopodial assembly and maturation, respectively, while RhoC activity promotes their

invasive and ECM-degrading capabilities [180]. Also, it has recently been demonstrated that Rac1 signaling is required for the disassembly of invadopodia [181]. Considering that BCAR3, together with Cas, influences the balance between Rac/Rho signaling in 2D adhesion/motility models of invasive breast cancer cells, it would be interesting to determine whether BCAR3-mediated signaling affects the dynamics of invadopodia in 3D.

To directly test whether BCAR3 affects the formation and function of invadopodia, we would assess the ability of control or BCAR3-depleted MDA-MB-231 cells to form invadopodia and degrade ECM using fluorescent gelatin-based matrices, similar to methods described by John Condeelis' group [179]. If we discover that BCAR3 is a positive regulator of invadopodia formation/function, we would further ask whether this function of BCAR3 requires a direct association with Cas using cells expressing wobble shRNA-resistant WT or mutant L744E/R748E BCAR3.

Finally, it would also be interesting to examine the live dynamics of invadopodia in MDA-MB-231 cells in 3D matrices [182]. Using an approach described by Magalhaes *et al.*, we would transfect control and BCAR3-depleted MDA-MB-231 cells with a plasmid encoding RFP-cortactin (a well-established marker of invadopodia), seed cells in 3D gel-based matrices, and image the protrusion/retraction cycles of invadopodia by capturing time-lapse Z-stacks. Data from these experiments would provide insight into whether BCAR3 mediates invadopodia protrusion and/or disassembly.

5.1.5 Future studies: In vivo mouse models of breast cancer

The findings presented in this thesis underscore an important role for BCAR3 in promoting breast tumor cell adhesion, motility, and invasion in 2D. While the 3D experiments proposed above will potentially provide new insights into how BCAR3 may

influence cell motility/invasion *in vivo*, these 3D models still oversimplify the tumor microenvironment. More sophisticated 3D *in vitro* models, such as organotypic cultures, can more accurately recapitulate the tumor microenvironment. In addition to collagen, these cultures include stromal cells like fibroblasts that can modify collagen fiber orientation and other ECM components. Therefore, 3D organotypic cultures may be useful to assess the importance of BCAR3 in a more complex microenvironment [170].

In vivo, cells are subject to a much softer, yet confined 3D microenvironment and the processes controlling adhesion and motility are far more complex [183]. In fact, intravital imaging experiments have revealed that distinct microenvironments within a single mammary tumor differentially influence the ability of tumor cells to invade and intravasate [46, 184]. Intravital studies have also demonstrated that tumor cells need to maneuver through both unconfined and confined microenvironments when disseminating. For instance, tumor cells need to squeeze in between endothelial cells lining the bloodstream during intravasation. This is a highly confined environment and it has recently been suggested that tumor cells may use different mechanisms of motility when moving through such areas [183, 185, 186]. Taken together, it is absolutely critical that we investigate whether BCAR3 regulates invasion and metastasis *in vivo* using an orthotopic mouse model of breast cancer metastasis.

To test whether BCAR3 regulates metastasis *in vivo*, we would first generate metastatic MDA-MB-231 breast cancer cells expressing lentiviral constructs encoding luciferase, a selectable marker (i.e. puromycin), and control (non-targeting) or BCAR3-specific shRNAs. Stable cell lines would then be orthotopically injected into the mammary fat pads of nude mice. Because the tumor cells express luciferase, we could directly monitor primary tumor progression and lung metastasis *in vivo* by bioluminescence imaging [187].

5.2 Is BCAR3 a developmentally regulated gene that is aberrantly re-expressed during breast tumor progression?

A major goal of the research presented in this thesis was to assess BCAR3 protein levels in human breast cancers because a thorough analysis had yet to be performed. We accomplished this task by analyzing BCAR3 protein expression across a panel of 74 human breast tumors, representing 5 different molecular subtypes of breast cancer, as well as 8 normal breast tissue samples. Perhaps one of the most significant discoveries made from this analysis was that BCAR3 expression is often upregulated to varying degrees in the tumor cells within a given mass, irrespective of subtype, compared to normal ductal epithelial cells that are fully differentiated. This finding raises some very interesting questions. Why are BCAR3 protein levels upregulated during breast tumor development and progression? Is BCAR3 an example of a developmentally regulated gene that is on during development, off in mature, differentiated tissues, and then re-expressed during neoplastic transformation? What role does BCAR3 play during mammary gland development? These questions will be explored in further detail below.

5.2.1 BCAR3: A regulatory switch for motility and invasion

A number of groups, including our own, have reported that BCAR3 protein expression is elevated in invasive breast cancer cell lines relative to less invasive, early-stage breast cancer cell lines [119, 120]. Also MCF-7 cells express lower BCAR3 mRNA levels compared to SK-BR-3 metastatic breast cancer cells (The Human Protein Atlas). We hypothesize that this may be due to epigenetic regulation of the *BCAR3* gene. While there are currently no data regarding epigenetic regulation of this gene,

aberrant epigenetic regulation of genes is a common feature of tumor development and progression [188]. It is interesting to speculate that the *BCAR3* gene is silenced in early-stage breast cancer cells, and that this silencing is relieved as cells undergo epithelial-mesenchymal transition (EMT), leading to aberrant overexpression of BCAR3 in invasive breast cancer cells.

Interestingly, our analysis of BCAR3 protein expression in normal and neoplastic breast tissue showed that normal mammary ductal epithelial cells express nearly undetectable levels of BCAR3 protein (**Chapter 4**). This is consistent with many other differentiated cell types that do not appear to express BCAR3 protein in human tissue, such as adipocytes, glial cells and smooth muscle cells (The Human Protein Atlas). We suggest that BCAR3 expression may be under similar epigenetic control in these highly differentiated cell types. If this is the case, the heterogeneity of BCAR3 protein expression observed within individual breast tumors may be a reflection of clonal epigenetic alterations within primary breast tumors; we would further suggest based on our *in vitro* data that it is this population of tumor cells that gain the ability to migrate/invade.

Data presented in this thesis argue strongly for a role of BCAR3 in cell adhesion and motility. In particular, we have shown that Invasive breast cancer cell lines are highly reliant on BCAR3 protein expression for their migration and invasion *in vitro*. However, early-stage breast cancer cell lines are still able to migrate despite the fact that they express low to undetectable levels of BCAR3 protein. One possible explanation for this is that cells can exhibit different types of motility. Differentiated epithelial cells often exhibit “collective” motility, while cells that have undergone EMT can exhibit amoeboid or mesenchymal motility [44, 45]. It is interesting to speculate that invasive breast cancer

cells that express high levels of BCAR3 may use this molecule to promote a more mesenchymal-like motility.

The possibility that BCAR3 may control the form and efficiency of cell migration and invasion is a particularly interesting possibility in light of the heterogeneity of BCAR3 expression that was observed in human breast cancers. One can imagine in this scenario that the tumor microenvironment itself could be the driving force underlying breast cancer cell dependency on BCAR3-mediated motility. It is possible that the changes in the microenvironment that accompany breast tumor progression could trigger BCAR3 upregulation in breast cancer cells. In fact, John Condeelis' group recently demonstrated that different cues within the tumor microenvironment control breast tumor cell phenotype and elicit different modes of breast tumor cell motility *in vivo* [46]. More specifically, they used an MDA-MB-231 orthotopic xenograft mouse model of breast cancer and multiphoton microscopy to show that breast cancer cells within different regions of the tumor microenvironment display either fast or slow locomotive ability. Interestingly, only slow-locomoting breast cancer cells exhibit invadopodia-like protrusions toward blood vessels and have the capacity to metastasize [46]. Perhaps this slow-locomotive motility is similar to mesenchymal motility. Given the role of BCAR3 in promoting membrane protrusiveness and potentially invadopodia, it would be interesting to determine whether this population of slow-locomoting breast cancer cells is dependent upon BCAR3-mediated adhesion and motility. To directly test whether BCAR3 regulates tumor cell motility and invasive potential *in vivo*, we could transfect metastatic MDA-MB-231 breast cancer cells with lentiviral constructs encoding control (non-targeting) or BCAR3-specific shRNAs. These stable cell lines could then be orthotopically injected into the mammary fat pads of SCID mice. By applying similar imaging techniques to those performed by Gligorijevic *et al.*, we could determine

whether BCAR3 expression is required for invadopodia formation in the population of slow-locomoting tumor cells described above [46].

Finally, other stressors within the tumor microenvironment, like hypoxia and nutrient deprivation, may also contribute to breast cancer cells upregulating BCAR3 protein levels. Recall that we observed the highest levels of BCAR3 protein in tumor cells within regions of high-grade DCIS (**Chapter 4, Fig 4.6**). High-grade DCIS is associated with a very hypoxic microenvironment, as highly proliferative tumor cells rapidly outgrow their oxygen supply within the confines of ducts. Under these conditions, breast cancer cells may upregulate BCAR3 as a means to locally invade and escape ducts. Upon breach of the basement membrane, we hypothesize that elevated BCAR3 protein levels would promote invasive breast cancer cell chemotaxis and motility toward EGF secreted by macrophages within the TME, leading tumor cells directly to blood vessels for intravasation [49, 53].

Interestingly, Gilkes *et al.* have recently shown that, under hypoxic conditions, hypoxia-inducible factors (or HIFs) promote transcription of RhoA and ROCK in MDA-MB-231 breast cancer cells [189]. Furthermore, HIF-mediated activation of Rho/ROCK signaling was shown to enhance contractility and breast cancer cell migration. Whether BCAR3 expression regulates HIFs or tumor cell responses to hypoxia remains to be determined.

5.2.2 BCAR3 as a potential regulator of the EMT

EMTs are critical in normal tissue differentiation, wound repair and tumor development and progression. EMT is a process where epithelial cells lose their epithelial characteristics and adopt features of mesenchymal cells [190]. Loss of E-cadherin expression is one of the most notable features of EMT. After EMT, cells exhibit

a highly motile and invasive phenotype [191]. Whether tumor cells actually undergo EMTs has been rather controversial; however, recent studies have yielded direct evidence of tumor cell EMT at the invasive margins of human tumors (reviewed in [192]). Considering EMTs are accompanied by changes in cell adhesion, motility and invasiveness, it is interesting to speculate that BCAR3 may play an important role in controlling EMT during breast tumor progression.

Growth factors, such as EGF and VEGF, can stimulate key drivers of EMT, such as the transcription factors SNAIL1/2 and Twist, which repress E-cadherin expression [192]. Interestingly, we demonstrate herein that BCAR3 promotes a pro-migratory phenotype and controls the cytoskeletal and adhesion responses of invasive breast cancer cells to EGF (**Chapter 2**). Moreover, high BCAR3 protein levels in breast cancer cell lines correlate with low levels of E-cadherin expression and elevated levels of the mesenchymal marker, vimentin [120]. In addition to the transcription factors that regulate E-cadherin expression, many molecular drivers of EMT are proteins involved in promoting tumor cell invasion and metastasis, which include the Rac and Rho GTPases. We provide extensive evidence that BCAR3 signaling regulates the balance between Rac and Rho in invasive breast cancer cells, which further argues a potential role for BCAR3 in regulating EMT during breast tumor progression.

5.2.3 BCAR3 and mammary gland development

A global BCAR3 knockout mouse has been generated and it shows no major developmental or phenotypic abnormalities at birth [126]. The only reported defect exhibited by these mice is a lens ulceration that is observed approximately 1 month after birth [126]. However, a thorough investigation into the role of BCAR3 in mammary gland development has never been explored. Our lab has been the first to evaluate BCAR3

protein expression in developing 3D mammary acini and mouse mammary glands. Interestingly, studies by members of our group revealed that BCAR3 protein levels are downregulated as human mammary MCF-10A acini develop/differentiate in 3D (Allison Batties, *personal communication*). Furthermore, BCAR3 protein levels were elevated in pre-pubertal, developing mouse mammary glands, but low in post-pubertal, mature mammary glands (Allison Batties, *personal communication*). Finally, mouse mammary tumors were shown to express varying levels of BCAR3 protein, with the highest expression in localized regions of early lesions (Allison Batties, *personal communication*). Work reported in this thesis shows that BCAR3 is also expressed in human breast tumors exhibiting both DCIS and IDC (**Chapter 4**). We propose from these combined data that BCAR3 may be a developmentally regulated protein that plays an important role in undifferentiated cells during mammary gland development, but then subsequently gets downregulated as tissues differentiate.

The paradigm wherein genes/proteins that are involved in the growth and differentiation of normal tissues become deregulated in cancer is not unique to BCAR3. The homeobox genes, including HOX and MSX genes, serve as some of the best examples of this type of regulation. HOX and MSX genes play important roles during embryogenesis and function in fate determination and EMT, respectively [193]. However, they are aberrantly overexpressed in many solid tumors and this is associated with the maintenance of tumor cells in a highly proliferative, undifferentiated state [193].

We plan to further investigate the potential role of BCAR3 in mammary gland development by continuing to evaluate BCAR3 protein levels in developing mouse mammary glands by IHC. It is important to extend our analysis to include mammary gland tissue from pregnant and lactating mice, because during these periods the

mammary gland undergoes extensive tissue remodeling. It will be interesting to determine whether BCAR3 protein is expressed during these highly proliferative phases.

5.3 Is BCAR3 a viable biomarker and/or therapeutic target for breast cancer?

Our *in vitro* work underscores the importance of BCAR3 expression to cell invasiveness and motility in triple-negative breast cancer cells. Therefore, we originally thought that targeting BCAR3 would be a promising therapeutic strategy for patients diagnosed with TNBC. Surprisingly, however, results from our human tumor analysis revealed the immense heterogeneity of BCAR3 expression across multiple subtypes of human breast cancer, not just TNBC. In fact, even ER^+ breast tumors exhibited elevated BCAR3 protein levels. Another unexpected discovery was that BCAR3 protein levels did not appear to correlate with tumor invasiveness; instead the highest levels of BCAR3 protein were expressed within regions of high-grade DCIS. Taking into account these new findings, it is important to reevaluate the therapeutic potential of BCAR3.

5.3.1 BCAR3 as a therapeutic target

Our data demonstrating that breast cancer cells are highly reliant on BCAR3 protein for cell adhesion, motility and invasion provide the rationale to explore its potential as a target for breast cancer. As discussed in Chapter 4, however, the therapeutic implications of targeting BCAR3 in human breast cancers remains complex. This stems from inconsistent findings between BCAR3 protein and mRNA expression in mediating antiestrogen resistance in breast cancer cell lines and tumor tissue, respectively. On the one hand, elevated BCAR3 mRNA levels in primary human tumor tissue have been reported to correlate with improved tamoxifen response and better survival outcomes [133-135]. Based on these data, it is possible that targeting or

silencing BCAR3 expression in patients may inadvertently promote tamoxifen resistance. On the other hand, elevated BCAR3 protein levels in ER^+ breast cancer cells drive resistance by promoting ERK-dependent proliferation in the presence of antiestrogens [132]. Based on these data, we propose that targeting BCAR3 protein in tumors may be beneficial. However, it remains to be elucidated as to whether the elevated BCAR3 protein levels observed in ER^+ human breast tumors correlate with resistance to hormonal therapy and/or poor survival outcomes. We could test this possibility directly by evaluating BCAR3 protein levels by IHC in ER^+ breast tumor samples from patients who failed hormonal therapy. If elevated, this suggests that BCAR3 protein expression may correlate with resistance to hormonal therapy in ER^+ breast tumors as it does in ER^+ breast tumor cell lines. Clearly, further studies using tumor samples with associated recurrence and survival data are necessary to determine whether elevated BCAR3 protein levels correlate with favorable or unfavorable treatment outcomes.

If we discover that elevated BCAR3 protein levels correlate with clinical resistance and/or poor survival, this prompts the question of how best to target an intracellular adaptor protein with no inherent catalytic activity. One particularly compelling possibility is to target the interaction between BCAR3 and Cas. We demonstrate in this thesis that BCAR3-mediated adhesion dynamics in invasive breast cancer cells is contingent on its ability to bind to Cas. Also, Elena Pasquale's group has shown that BCAR3-driven antiestrogen resistance in ER^+ breast cancer cells requires a direct association between BCAR3 and Cas [132]. Together, these data argue that disrupting BCAR3/Cas complex signaling may be an attractive therapeutic strategy for breast tumors that co-express these adaptor proteins.

Therapeutic targeting of protein-protein interactions (or PPIs) was originally deemed challenging because it was thought that the binding interfaces between proteins

did not have unique features that would be “druggable” [194]. However, advances in structural and computational biology-based methods have revealed the complexities of protein-protein interfaces, and in so doing, have led to the discovery and design of peptide inhibitors that prevent, weaken or modulate PPIs. Peptide inhibitors can bind with very high affinity and high specificity to binding interfaces, thereby disrupting a signaling complex. However, not all PPIs are good targets for peptide inhibitors; therefore it is critical to perform a rigorous analysis of the binding interface in order to determine whether a PPI is a worthwhile target [195].

Interestingly, the binding interface between BCAR3 and Cas has been extensively modeled and studied [125, 132]. In fact, it was through this work that the Cas-binding mutant of BCAR3, L744E/R748E, was predicted and then tested for interaction with Cas. Structural analysis revealed a very distinctive and tight binding pocket between a fold in the C-terminal domain of BCAR3 and the focal adhesion-targeting domain within the C terminus of Cas [125]. This binding pocket may prove to be an attractive target for a peptide inhibitor. While the design and development of peptide inhibitors that target signaling through the BCAR3/Cas complex will undoubtedly be challenging, recent and future advancements in high-throughput screening and computational biology may make this type of an approach possible [194].

Unfortunately, the intratumoral heterogeneity of BCAR3 protein expression that we have observed within individual tumors, as well as the heterogeneity of BCAR3 protein levels from tumor to tumor, may prove to be a major therapeutic obstacle. In this regard, it may be difficult to predict which patients will benefit from BCAR3-targeted therapy, since this may depend on the extent to which their tumors exhibit upregulation of BCAR3 protein. Currently we do not fully understand why BCAR3 protein levels are elevated in tumor cells in particular areas within primary tumors but not in others.

Furthermore, it is also possible that BCAR3 has other unknown functions in breast tumor cells independent of adhesion, motility and invasion (e.g. regulation of survival and/or proliferation pathways), and therefore targeting BCAR3 may have broader consequences. Clearly it is necessary to gain a better understanding of the role of BCAR3 protein in breast tumor development and progression prior to targeting it directly.

5.3.2 BCAR3 as a biomarker

Studies by our group and others have shown that BCAR3 is a potent promoter of Src kinase activity [129, 130]. While it is very difficult to assess Src activity levels in human tumors via IHC (i.e. stain tumors using a Src pY419 antibody), we demonstrate in this thesis the feasibility of evaluating BCAR3 protein levels in human breast tumors. We propose that BCAR3 may serve as a useful biomarker of Src activity in human breast tumors. To test this, our group is planning to evaluate tumor samples and associated clinical data from patients on a clinical trial who were treated with the Src inhibitor, dasatinib, to determine whether high BCAR3 protein levels correlate with dasatinib sensitivity and/or clinical outcome. If BCAR3 proves to be a good predictor of elevated Src activity, then it would be possible to stain primary tumor biopsies from patients for BCAR3 in the clinic to determine whether a particular patient would be a good candidate for Src-targeted therapies such as dasatinib.

Similarly, the data presented herein argue that BCAR3 may be a potential biomarker of high-grade DCIS (refer to **Chapter 4, Section 4.3**). Future work will obviously be necessary to determine whether this holds true and whether an evaluation of BCAR3 protein levels in tumor biopsies may help to stratify patients into low- versus high-risk DCIS groups.

In conclusion, the data and perspectives presented in this thesis provide further insight into our understanding of BCAR3-driven cell signaling pathways that underlie breast tumor development and progression. Our findings provide a stepping-stone for future studies aimed at uncovering the unique roles of BCAR3 in tumor cell motility and invasion *in vivo*, mammary gland development, and the progression of human breast cancer.

CHAPTER 6: Materials and Methods*

This chapter contains excerpts from Wilson et al., PLOS One, 2013

6.1 Antibodies and reagents

The following monoclonal antibodies were used: β-Actin and vinculin (Sigma-Aldrich, St. Louis, MO); Rac1, mDia1 and Crk (BD Biosciences, San Jose, CA); Rho (Millipore, Billerica, MA); Myc (9E10) (Lymphocyte Culture Center, UVA). The following polyclonal antibodies were used: BCAR3 for immunoblotting (Bethyl Laboratories, Inc., Montgomery, TX); BCAR3 for IHC (HPA014858, Sigma-Aldrich); pThr18/pSer19 MLC II and total MLC II (Cell Signaling Technology, Inc., Danvers, MA); ERK and AKT (Cell Signaling Technology, Inc.); FITC-conjugated goat anti-mouse and Texas red-conjugated goat anti-rabbit (Jackson ImmunoResearch Laboratories, Inc., West Grove, PA); CasB [196]. Texas red-conjugated phalloidin (Molecular Probes, Eugene, OR), fibronectin (Sigma-Aldrich), EGF (Sigma), and ROCK inhibitor, Y-27632 (Calbiochem, Billerica, MA) were also used.

6.2 Plasmids and cloning strategies

BCAR3 cDNA was cloned into the EcoRI and XbaI (New England BioLabs, Inc.) sites of pEGFP-C1 (Clontech Laboratories, Inc., Mountain View, CA) to generate pEGFP-BCAR3 (WT GFP-BCAR3). Dr. A.R. Horwitz generously provided pmCherry-C1 empty vector, plasmids encoding Myc-RacL61, GFP-RhoA, GFP-vinculin, mCherry-talin, and mCherry-α-actinin, and a construct containing a speckled (truncated CMV) promoter (UVA).

6.2.1 L744E/R748E GFP-BCAR3 cloning

Site-directed mutagenesis of pEGFP-BCAR3 was performed using the QuickChange II Site-Directed Mutagenesis kit (Agilent Technologies, Santa Clara, CA). Mutagenesis of Leucine 744 to Glutamic Acid (L744E) and Arginine 748 to Glutamic Acid (R748E) in BCAR3 cDNA was performed with the following primers: forward (5'-C ATG CTG AAC CAT GAG GCA ACA GCG GAA TTC ATG GCC GAG GCT GC-3') and reverse (5'-GC AGC CTG GGC CAT GAA TTC CGC TGT TGC CTC ATG GTT CAG CAT G-3') (mutated bases are underlined). Mutagenesis was confirmed via sequencing.

6.2.2 mCherry-Cas cloning

pRK5-Cas vector was digested with XbaI and BamHI (New England BioLabs, Inc.). Double-digested Cas insert was gel-purified using the PureLink™ Quick Gel Extraction kit (Invitrogen, Grand Island, NY). Empty vector pmCherry-C1 was double digested sequentially with XbaI then BamHI. Double digested pmCherry-C1 was treated with calf intestinal alkaline phosphatase (CIP, New England BioLabs, Inc.), and then purified by a phenol-chloroform extraction followed by ethanol precipitation. pmCherry-C1 vector was ligated to Cas insert using T4 DNA ligase (New England BioLabs, Inc.). mCherry-Cas was confirmed via digestion, sequencing and immunofluorescence.

6.3 Cell culture

BT549 and MDA-MB-231 cells (American Type Tissue Culture, Manassas, VA) and tetracycline-regulated MCF-7 cells stably expressing Myc-BCAR3 were cultured as previously described [119, 129]. Cas-null (Cas-/-) MEFs were maintained in DMEM with high glucose (Invitrogen), supplemented with 10% fetal bovine serum (FBS) and 1% sodium pyruvate. MCF-10A cells were maintained in DMEM/F12 (Invitrogen),

supplemented with 5% horse serum (Invitrogen), 20ng/ml EGF (Peprotech, Rocky Hill, NJ), 0.5mg/ml hydrocortisone (Sigma-Aldrich), 100ng/ml cholera toxin (Sigma-Aldrich), 10μg/ml insulin (Sigma-Aldrich), and 1% penicillin/streptomycin.

6.4 Small-interfering RNA and plasmid transfection

Cells were transfected with 20μM of the following small-interfering RNA (siRNA) oligonucleotides using Lipofectamine RNAiMAX reagent (Invitrogen) following the manufacturer's protocol: non-targeting control (siCtl; Ambion, Grand Island, NY), BCAR3 SH2-domain-targeting (siB3-1), BCAR3-targeting ON-TARGETplus SMARTpool (siB3-2), and mDia1-targeting ON-TARGETplus SMARTpool (siDia1) (Dharmacon, Lafayette, CO). The siB3-1 and siB3-2 oligonucleotides were described previously [119, 129]. Plasmid transfection of Myc-RacL61 or GFP-vinculin was performed using Fugene HD Transfection Reagent (Roche, Indianapolis, IN) following manufacturer's specifications. Plasmid transfection of WT GFP-RhoA was performed using Lipofectamine 2000 (Invitrogen) following manufacturer's specifications. Co-transfection of either WT GFP-BCAR3 or L744E/R748E GFP-BCAR3 along with mCherry Cas, mCherry-talin or mCherry-α-actinin was performed using Lipofectamine 2000 using only 0.1-0.25μg DNA. Co-transfections were performed in antibiotic-free, phenol red-free OPTI-MEM reduced serum medium (Invitrogen) for 3-4 hours at 37°C. After the incubation, cells were replenished with normal growth medium and incubated for 24 hours prior to imaging.

6.5 Immunoprecipitation, immunoblotting, and immunofluorescence

Cells were lysed in ice-cold radioimmune precipitation assay (RIPA) buffer supplemented with protease inhibitors and protein concentrations determined as previously described [119]. Immunoprecipitations and immunoblotting were performed

as previously described [119]. Cells fixed on fibronectin-coated glass coverslips were processed, visualized through a Nikon Eclipse TE2000-E microscope, and photographed as previously described [119].

6.6 Live-cell imaging

Cells were plated onto acid-washed fibronectin-coated glass bottom TIRF dishes (MatTek Corporation, Ashland, MA) (BT549) or 35mm Delta T dishes (Bioptechs, Inc., Butler, PA) (MCF-7) and cultured at 37°C, pH 7.4 in CCM1 media (Hyclone). For BT549 cells, phase images were captured every 5 seconds for 12.5 minutes on a light microscope (Diaphot, Nikon) with a video camera (KY-F55B, Victor Company of Japan). Images were then processed using MetaMorph Software (Molecular Devices, Sunnyvale, CA). For MCF-7 cells, phase images were captured every 30 seconds for 1 hour using an inverted microscope with a 20X differential interference contrast (DIC) objective, heated stage (Bioptechs, Inc.), and an ORCA camera. Images were then processed using Openlab software.

6.6.1 Protrusion dynamics

To quantify protrusive behavior, total cell area at the first and final frame of a time-lapse movie was traced and pseudo-colored gray (first frame) or black (last frame). The average protrusive area was determined by measuring the area shown in black using ImageJ software. The average time (in minutes) to maximal membrane extension was determined by creating kymographs of cells from the time-lapse videos using ImageJ. The average distance traveled was determined in ImageJ by tracing nucleus movement of each cell over the course of the time-lapse sequence. The average rate of migration was calculated by dividing the total distance traveled by each cell by time.

6.6.2 Adhesion dynamics

BT549 cells transfected with control or BCAR3-specific siRNAs and plasmids encoding GFP-vinculin were plated on 2μg/ml fibronectin-coated glass bottom TIRF dishes and allowed to spread prior to live imaging. BT549 cells co-transfected with WT GFP-BCAR3 or L744E/R748E GFP-BCAR3 plus either mCherry-Cas, mCherry-talin or mCherry-α-actinin were plated on 2μg/ml fibronectin-coated glass bottom TIRF dishes and allowed to spread for 30-40 minutes prior to live imaging. Images were captured using an inverted TIRF microscope (1X70; Olympus) with a 60X objective (±1.5X magnification), a cool charged-couple device camera (Retiga Exi; Qimaging), and heated objective/stage (Bioptechs). Images were captured every 5 seconds for 10-12 minutes using MetaMorph software. To quantify adhesion turnover, adhesions at peripheral, protruding edges were manually selected for analysis. Complete fluorescence intensity time tracings for individual adhesions were (1) normalized, (2) corrected for background intensity by subtracting an average intensity value corresponding to a background region away from the cell, and then (3) plotted. Both the increase (incorporation/assembly) and decrease (dissociation/disassembly) in fluorescence intensity were linear as a function of time on semi-logarithmic plots, and rate constants were determined from the slopes of these graphs. For vinculin-containing adhesions, rate constant measurements were obtained for 3-5 individual adhesions on 8-10 cells. For adhesions co-expressing WT BCAR3 or L744E/R748E BCAR3 plus either mCherry-Cas, mCherry-talin or mCherry-α-actinin, rate constant measurements were obtained for at least 13 individual adhesions on 2-5 cells.

6.7 GTP-bound GTPase pull-down assays

To measure GTP-Rac1, BT549 cells were transfected with siCtl or siB3-1 siRNA oligonucleotides, incubated for 72 hours, trypsinized, held in suspension for 90 minutes, and then plated on 10µg/ml fibronectin for 1 hour. Cells were rinsed twice with ice-cold PBS and lysed in ice-cold RIPA buffer. GTP-bound Rac1 was isolated from whole cell lysates by incubation with PAK-1-binding domain agarose (Millipore) following manufacturer's instructions. To measure GTP-RhoA, BT549 cells were transfected with siCtl or siB3-1 siRNA oligonucleotides, incubated for 48 hours, and then transfected with plasmids encoding GFP-RhoA. Twenty-four hours post-transfection, cells were trypsinized, held in suspension for 90 minutes, and then plated on 10µg/ml fibronectin for 1 hour. Cells were then rinsed twice with ice-cold PBS and lysed in ice-cold magnesium lysis buffer and incubated with Rhotekin binding domain (RBD) agarose (Millipore) following manufacturer's instructions.

6.8 Immunohistochemistry

An archival tumor analysis of 74 whole human breast tumors from women previously diagnosed with and treated for breast cancer at the University of Virginia (UVA) Health Systems was performed. Eight normal breast tissue sections were also evaluated for BCAR3 protein expression. Paraffin-embedded tissue blocks were hand-selected from the UVA breast tumor bank by a clinical breast pathologist. Four-micron histologic sections were cut and placed on charged glass slides (Superfrost Plus, Fisher Scientific, Pittsburgh, PA). Slides were then deparaffinized and antigen retrieval was performed in a PT Link instrument (Dako, Glostrup, Denmark) in low pH antigen retrieval solution at 97°C for 20 minutes. Immunohistochemistry was performed on a robotic platform (Autostainer, Dako). Endogenous peroxidases were blocked using Peroxidase and

Alkaline Phosphatase Blocking Reagent (Dako). Polyclonal rabbit antibody to BCAR3 (Sigma Aldrich) was diluted 1:200 and applied at ambient temperature for 30 minutes. Antibody binding was visualized by incubation with Envision^{TM} Dual Link (Dako) followed by incubation with 3,3'-diaminobenzidine tetrahydrochloride (DAB+). All slides were counterstained with hematoxylin. Slides were subsequently dehydrated, cleared and mounted for assessment. The staining intensity of BCAR3 protein was scored in a blinded fashion by a pathologist on a 0 (negative), 1^+ (low), 2^+ (moderate), 3^+ (strong) numerical scale. Histopathological features such as nuclear grade and cell necrosis were used to define high-grade DCIS [154].

6.9 Collagen-coated polyacrylamide substrates

Flexible polyacrylamide substrates were generated on glass coverslips and adapted for cell culture using the method of Pelham and Wang [197] and as described in Tilghman *et al*. [158]. Briefly, polyacrylamide gels contained 3% acrylamide and 0.05% bisacrylamide (300 Pa) or 7.5% acrylamide and 0.05% bisacrylamide (4800 Pa). The gels were polymerized on acid-washed, silanated, and glutaraldehyde-treated 22mm square glass coverslips. Each rigidity gel was placed in a well of a 6-well plate and activated using the crosslinker Sulfo-SANPAH (Pierce) followed by coating with collagen I (100µg/ml, Thermo Fisher Scientific, Inc.) for 4 hours at room temperature or overnight at 4°C. Gels were incubated in the appropriate growth medium for 20 minutes at 37°C prior to plating BT549 or MCF-10A cells. Cells were incubated for 48 or 96 hours on the gels prior to lysis with 100-125µl of 2X sample buffer with β-mercaptoethanol (BME, room temperature). Cells were lysed using a cell scraper and lysates were collected into 1.5-mL eppy tubes containing glass cotton wool. Lysates were pulsed at 5-10 second intervals at 1000-2000rpm in a tabletop microcentrifuge to separate the lysate, BME and

gel components. Lysates were boiled for 10 minutes prior to loading and separating on an 8% SDS-PAGE gel.

6.10 Statistical analysis

Two-tailed Student's *t* tests were used for the pair-wise comparison of two experimental groups. A Kruskal-Wallis one-way ANOVA and Dunn's Multiple Comparison post-test were used to compare multiple experimental groups.

APPENDIX 1: Potential regulation of signaling pathways downstream of epidermal growth factor receptor by BCAR3 and Cas

A1.1 Introduction

Integrin- and growth factor receptor-mediated signaling cascades frequently converge within tumor cells to promote cell motility, proliferation and survival [114, 198]. BCAR3 and Cas are two examples of adaptor proteins positioned in adhesions downstream of integrins that are capable of regulating cellular responses to growth factor stimulation. More specifically, FAK and Src can phosphorylate Cas downstream of ligand-bound integrins and growth factor receptor tyrosine kinases. These phosphorylated residues on Cas serve as docking sites for additional adaptors and kinases, such as Crk, Grb2 and PI3K, which in turn drive signaling cascades that lead to cell invasion, proliferation and survival, respectively (reviewed in [114]). Furthermore, in this thesis, we demonstrate that BCAR3 controls actin cytoskeletal and adhesion remodeling in invasive breast cancer cells in response to EGF stimulation (**Chapter 2**).

Upon ligand binding, the EGF receptor homo- or heterodimerizes, which activates its intrinsic kinase activity [17]. This results in the auto-phosphorylation of several key tyrosine residues, including tyrosine 1068 (Y1068), within the cytoplasmic tails of the receptor [17]. Notable pathways activated downstream of EGFR include the well-established PI3K/AKT and mitogen-activated protein kinase (MAPK, simply referred to herein as ERK) signaling cascades, which play central roles in tumor cell survival and proliferation, respectively (reviewed in [17]).

In addition to pro-survival and pro-proliferative signaling networks being activated downstream of EGFR, tumor cells undergo marked changes in actin cytoskeletal remodeling in response to EGF stimulation. As discussed in **Chapter 1**, one of the

major signaling pathways downstream of EGFR that regulates actin reorganization in breast tumor cells is the cofilin pathway. In response to EGF, cofilin severs stress fibers to produce small actin fragments that support dendritic nucleation and actin polymerization at the leading edge of the cell [65]. LIMK negatively regulates cofilin by phosphorylating it on serine 3 (pSer3). When cofilin is phosphorylated on serine 3, it is considered inactive and its ability to sever stress fibers is inhibited. It is important to note that a delicate balance between Rac/Rho GTPase signaling is also critical for cytoskeletal rearrangement in response to EGF stimulation. Interestingly, we have previously demonstrated that BCAR3 functions as a positive regulator of cytoskeletal remodeling in invasive breast cancer cells by promoting Rac1 activity (**Chapter 2**, [47]). It remains to be determined whether BCAR3 actively suppresses RhoA (e.g. via activation of a Rho GAP) in addition to promoting Rac1 activity.

In this current study, we explore the roles of BCAR3 and Cas in regulating ligand-induced EGFR auto-phosphorylation and various signaling cascades downstream of EGFR in invasive breast cancer cells. Specifically, we examine whether EGFR, AKT, ERK and cofilin activity are dependent upon BCAR3 and/or Cas expression. Using an siRNA-mediated approach, we selectively depleted BCAR3 and Cas protein in MDA-MB-231 breast cancer cells and measured phosphorylation levels of EGFR, AKT, ERK and cofilin in response to EGF stimulation. Furthermore, we assessed whether BCAR3 suppresses RhoA by activating a well-established Rho GAP, p190RhoGAP, downstream of EGFR. Despite high variability between experiments, our preliminary data indicate that Cas, but not BCAR3, may promote EGFR auto-phosphorylation at Y1068 in invasive breast cancer cells. Furthermore, BCAR3 and Cas may regulate temporal activation of AKT, but not ERK, signaling downstream of EGFR. Finally, data addressing whether

cofilin or p190RhoGAP activity were dependent upon BCAR3 were inconclusive. Future studies will be necessary to eliminate variability between experiments.

A1.2 Results

A1.2.1 Cas may regulate ligand-induced EGFR auto-phosphorylation, while both BCAR3 and Cas may regulate AKT, but not ERK, signaling downstream of EGFR

To determine whether BCAR3 or Cas regulates EGFR, AKT or ERK activation in invasive breast cancer cells in response to EGF stimulation, MDA-MB-231 cells were transfected with control (non-targeting, siCtl), BCAR3-specific (siB3) or Cas-specific (siCas) siRNA oligonucleotides and then incubated for 24 hours in normal growth medium. Cells were serum-starved for 16-18 hours, stimulated with 100ng/ml EGF for 0 or 30 minutes, then lysed and immunoblotted with the designated antibodies (**Fig A1.1**). BCAR3 protein levels were consistently reduced by greater than 90% in cells transfected with siB3 (panel H, lanes 3 and 4). While a high proportion of Cas was depleted in siCas-treated cells, the upper, highly phosphorylated band of Cas was selectively retained (panel I, lanes 5 and 6). In control cells, EGF stimulation resulted in a robust increase in EGF receptor auto-phosphorylation (as indicated by phosphorylation at tyrosine residue 1068, abbreviated pY1068), consistent with EGFR activation (panel A, compare lanes 1 and 2). Compared to control cells, depletion of Cas appeared to decrease ligand-induced EGFR auto-phosphorylation, while depletion of BCAR3 had no effect (panel A, compare lanes 2, 4 and 6). Interestingly, tyrosine 845 (Y845) of EGFR, a well-established substrate of Src, was only phosphorylated in control cells following EGF stimulation and not in BCAR3- or Cas-depleted MDA-MB-231 cells (panel B, compare lanes 2, 4 and 6). This is consistent with data reported from our lab and others showing that Src kinase activity is greatly reduced upon loss of BCAR3 [129, 130], and

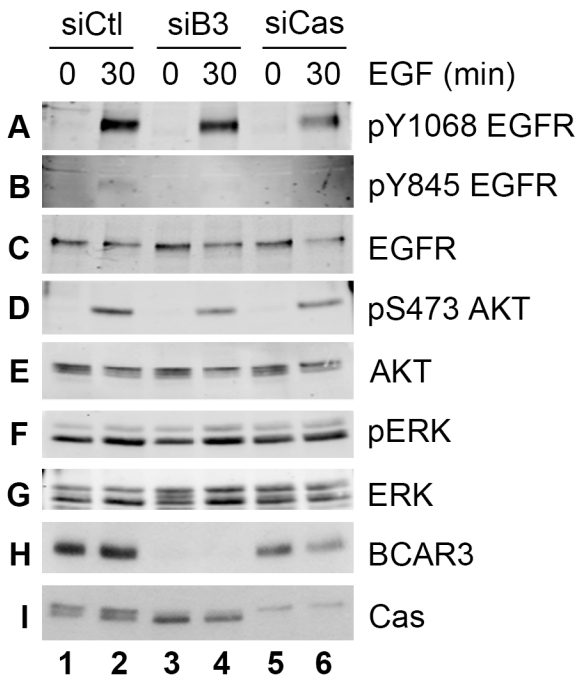
siCtl
siB3
siCas
0 30 0 30 0 30
EGF (min)
A
pY1068 EGFR
B
pY845 EGFR
C
EGFR
D
pS473 AKT
E
AKT
F
pERK
G
ERK
H
BCAR3
I
Cas
1 2 3 4 5 6

Figure A1.1. Effect of Cas and BCAR3 on EGFR signaling pathways; 30-minute EGF stimulation. MDA-MB-231 cells were transfected with control (non-targeting, siCtl), BCAR3-specific (siB3) or Cas-specific (siCas) siRNA oligonucleotides and then incubated for 24 hours in normal growth medium. Cells were serum-starved for 16-18 hours, stimulated with 100ng/ml EGF for 0 or 30 minutes, and then lysed and immunoblotted with the designated antibodies as described in the methods. Data represent one independent experiment.

that Cas binding to the SH3/2 domains of Src promotes Src kinase activity by releasing its auto-inhibitory conformation [96, 102]. Therefore, under conditions where Cas is depleted, Src may not be fully activated.

We next measured activation of AKT and ERK downstream of EGFR as indicated by AKT phosphorylation at serine 473 (pS473 AKT) and phosphorylation of ERK1/2 (pERK). Control cells exhibited a robust increase in pS473 AKT after 30 minutes of EGF stimulation (panel D, lanes 1 and 2). Loss of either BCAR3 or Cas appeared to result in a modest decrease in pS473 AKT in response to EGF (panel D, compare lanes 2, 4 and 6). However, total AKT levels may also be reduced under these conditions (panel E, compare lanes 3-6). EGF stimulation did not appear to induce activation of ERK at 30 minutes post-EGF stimulation under any condition (panel F). This is surprising because others have reported that levels of pERK are increased in MDA-MB-231 breast cancer cells following EGF stimulation [199]. Together, these data indicate that Cas may positively regulate ligand-induced EGFR auto-phosphorylation, and both BCAR3 and Cas may play roles in promoting activation of AKT, but not ERK, downstream of EGFR. It is important to note that these data are preliminary and are representative of only one experiment.

Considering signaling pathways downstream of EGFR can be activated very quickly, within seconds to minutes, we repeated the experiment described above and, instead, examined EGFR auto-phosphorylation, pS473 AKT and pERK after only 15 minutes of EFG stimulation (compared to 30 minutes) (**Fig A1.2**). Again, BCAR3 protein levels were nearly undetectable when cells were transfected with siB3 (Panel G, lanes 3 and 4), while the upper, hyper-phosphorylated form of Cas remained in MDA-MB-231 cells transfected with siCas oligonucleotides (Panel H, lanes 5 and 6). In this experiment, depletion of Cas also appeared to decrease ligand-induced EGFR auto-

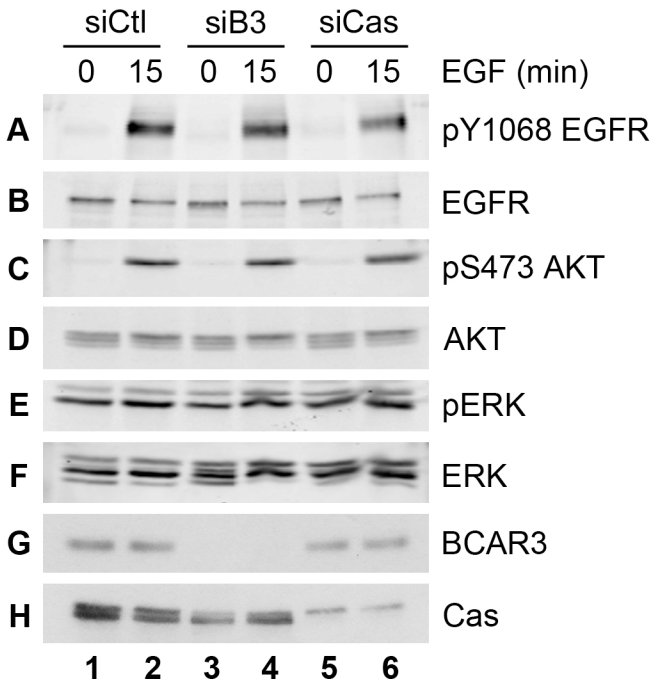
siCtl
siB3
siCas
0 15 0 15 0 15
EGF (min)
A
pY1068 EGFR
B
EGFR
C
pS473 AKT
D
AKT
E
pERK
F
ERK
G
BCAR3
H
Cas
1 2 3 4 5 6

Figure A1.2. Effect of Cas and BCAR3 on EGFR signaling pathways; 15-minute EGF stimulation. MDA-MB-231 cells were transfected with control (non-targeting, siCtl), BCAR3-specific (siB3) or Cas-specific (siCas) siRNA oligonucleotides and then incubated for 24 hours in normal growth medium. Cells were serum-starved for 16-18 hours, stimulated with 100ng/ml EGF for 0 or 15 minutes, and then lysed and immunoblotted with the designated antibodies as described in the methods. Data represent one independent experiment.

phosphorylation compared to control cells (panel A, compare lanes 2 and 6). However, unlike the first experiment, the EGF-dependent increase in pS473 AKT levels seemed comparable across all conditions (Panel C, compare lanes 2, 4 and 6). Lastly, in agreement with the previous experiment, EGF stimulation did not appear to have any effect on pERK levels in control, BCAR3- or Cas-depleted MDA-MB-231 breast cancer cells, nor were there any noticeable differences in ERK activation between conditions (panel E).

Considering the variability in results between the two experiments, we next measured EGFR, AKT and ERK phosphorylation over a broader time course in order to gain a better understanding of when BCAR3 or Cas may be regulating activation of these signaling molecules. MDA-MB-231 cells were transfected with control (non-targeting, siCtl), BCAR3-specific (siB3) or Cas-specific (siCas) siRNA oligonucleotides and then incubated for 24 hours in normal growth medium. Cells were serum-starved for 16-18 hours, stimulated with 100ng/ml EGF for 0, 5, 15 or 30 minutes, then lysed and immunoblotted with the designated antibodies (**Fig A1.3**). Similar knockdown of BCAR3 and Cas were achieved as observed in previous experiments (Panels G and H). In control cells, an increase in EGFR auto-phosphorylation was observed after only 5 minutes of EGF stimulation and these levels remained high throughout the 30-minute time course (Panel A, compare lanes 1-4). Cas depletion greatly reduced EGFR pY1068 auto-phosphorylation at all time points in response to EGF stimulation compared to control cells (Panel A, compare lanes 1-4 and 9-12). However, total EGFR protein levels were reduced under these conditions in this experiment as well (Panel B, lanes 1-4 and 9-12). Again, loss of BCAR3 appeared to have no effect on EGFR auto-phosphorylation compared to control cells (Panel A, compare lanes 1-4 and 5-8). While no differences were observed in ERK activation between conditions (Panels E and F),

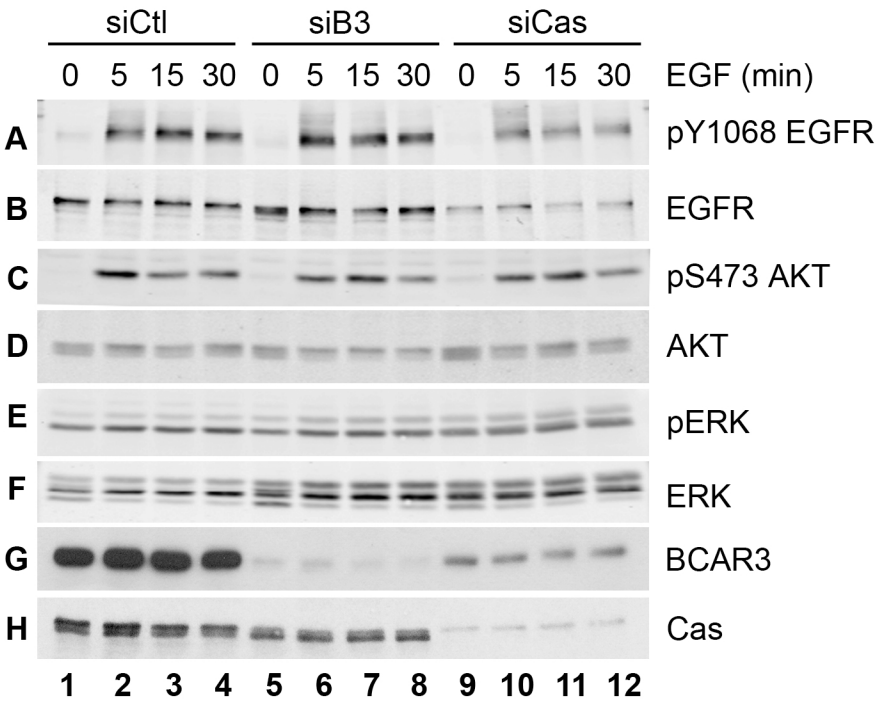
siCtl
siB3
siCas
0 5 15 30 0 5 15 30 0 5 15 30
EGF (min)
A
pY1068 EGFR
B
EGFR
C
pS473 AKT
D
AKT
E
pERK
F
ERK
G
BCAR3
H
Cas
1 2 3 4 5 6 7 8 9 10 11 12

Figure A1.3. Effect of Cas and BCAR3 on EGFR signaling pathways; 5-30 minute EGF stimulation. MDA-MB-231 cells were transfected with control (non-targeting, siCtl), BCAR3-specific (siB3) or Cas-specific (siCas) siRNA oligonucleotides and then incubated for 24 hours in normal growth medium. Cells were serum-starved for 16-18 hours, stimulated with 100ng/ml EGF for 0, 5, 15 or 30 minutes, and then lysed and immunoblotted with the designated antibodies as described in the methods. Data represent one independent experiment.

there were differences observed in pS473 AKT (Panel C). Specifically, in control cells, a robust increase in pS473 AKT levels was observed after only 5 minutes of EGF stimulation, and these levels seemed to taper off by 15 minutes (Panel C, compares lanes 1-4). Under conditions where BCAR3 or Cas was depleted, there appeared to be a temporal delay in activation of AKT. Specifically, the highest levels of pS473 AKT were not observed in BCAR3- or Cas-depleted cells until 15 minutes post-EGF stimulation, and even then, levels were not quite as high as that observed in control cells at 5 minutes post-EGF stimulation (Panel C).

Finally, considering Cas was not fully depleted in all three of the experiments described above, we repeated the time course experiment after performing a double Cas knockdown instead (i.e. cells were transfected twice with siCas oligonucleotides prior to EGF stimulation). More specifically, MDA-MB-231 cells were transfected with Cas-specific (siCas) siRNA oligonucleotides and then incubated for 24 hours in normal growth medium. Twenty-four hours later, Cas-depleted cells were transfected a second time with siCas oligonucleotides. MDA-MB-231 breast cancer cells were also singly transfected with either control (non-targeting, siCtl) or BCAR3-specific (siB3) siRNA oligonucleotides. All cells were incubated for 24 hours in normal growth medium following transfection and then serum-starved for 16-18 hours. Cells were then stimulated with 100ng/ml EGF for 0, 5, 15 or 30 minutes, lysed and immunoblotted with the designated antibodies (**Fig A1.4**). Cas protein levels were nearly undetectable after double Cas knockdown (Panel F, lanes 9-12). BCAR3 protein was also lost upon knockdown of Cas (Panel E, lanes 9-12), which has been observed by our lab group previously (Dr. Michael Guerrero, *personal communication*). Elena Pasquale's group has demonstrated BCAR3/Cas interaction is required for their reciprocal stability [132], which may help to explain why BCAR3 protein is less stable in the absence of Cas, and

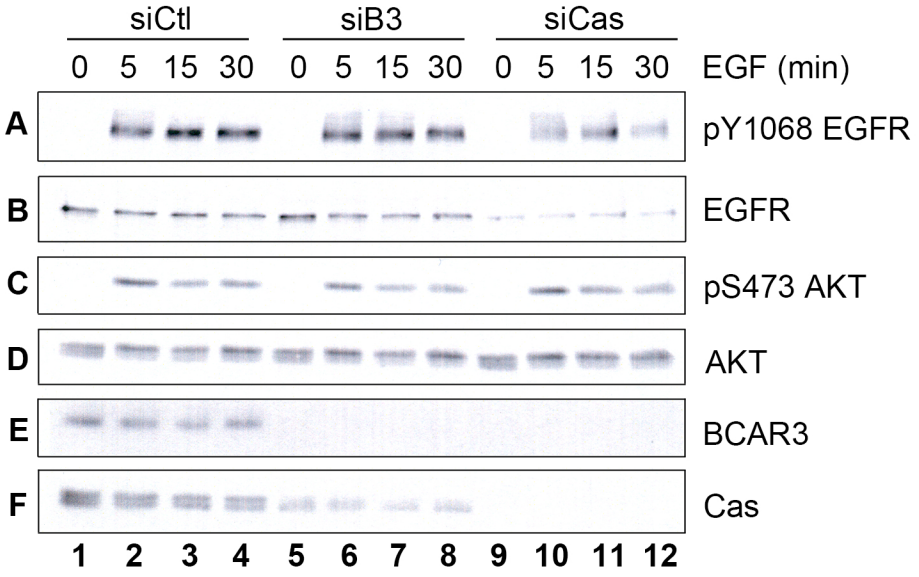
siCtl
siB3
siCas
0 5 15 30 0 5 15 30 0 5 15 30
EGF (min)
A
pY1068 EGFR
B
EGFR
C
pS473 AKT
D
AKT
E
BCAR3
F
Cas
1 2 3 4 5 6 7 8 9 10 11 12

Figure A1.4. Effect of Cas and BCAR3 on EGFR signaling pathways; 5-30 minute EGF stimulation with double Cas knockdown. MDA-MB-231 cells were transfected with Cas-specific (siCas) siRNA oligonucleotides and then incubated for 24 hours in normal growth medium. Twenty-four hours later, Cas-depleted cells were transfected a second time with siCas oligonucleotides. MDA-MB-231 breast cancer cells were also singly transfected with either control (non-targeting, siCtl) or BCAR3-specific (siB3) siRNA oligonucleotides. All cells were incubated for 24 hours in normal growth medium following transfection and then serum-starved for 16-18 hours. Cells were stimulated with 100ng/ml EGF for 0, 5, 15 or 30 minutes, and then lysed and immunoblotted with the designated antibodies as described in the methods. Data represent one independent experiment.

why Cas protein levels are reduced in BCAR3-depleted cells compared to control cells (Panel F, compare lanes 1-4 and 5-8). We are currently working to understand the mechanism of this regulation. Under conditions where greater Cas depletion was achieved, we observed less EGFR auto-phosphorylation in response to EGF stimulation compared to control cells (Panel A, compare lanes 1-4 and 9-12). However, similar to the previous experiment, total EGFR levels were also reduced upon loss of Cas (Panel B, compare lanes 1-4 and 9-12). Again, loss of BCAR3 appeared to have no effect on EGFR auto-phosphorylation compared to control cells (Panel A, compare lanes 1-4 and 5-8). Finally, the delay in AKT activation seen in **Fig A1.3** was not observed in this experiment, as evidenced by roughly equivalent increases in pS473 AKT seen upon EGF stimulation between control, BCAR3- or Cas-depleted cells (Panel C). We did not examine ERK activation under these conditions because we had not observed any noticeable changes in pERK in previous experiments.

Taken together, the above experiments suggest that Cas may regulate ligand-induced EGFR auto-phosphorylation, although the concomitant and selective decrease in total EGFR levels upon Cas knockdown makes interpretation of these data more difficult. Additionally, both Cas and BCAR3 may play roles in mediating AKT activation, but not ERK, downstream of EGFR. It is important to note that these preliminary experiments were each performed one time, and different variables were optimized in each case (i.e. EGF time points, Cas knockdown). Future work will be necessary to determine whether BCAR3 and/or Cas regulate EGF-mediated signaling pathways.

A1.2.2 BCAR3 may regulate cofilin activity in invasive breast cancer cells

We have previously demonstrated that BCAR3 controls actin cytoskeletal remodeling in invasive breast cancer cells in response to EGF (refer to **Chapter 2**).

Specifically, upon EGF stimulation, BCAR3-expressing MDA-MB-231 breast cancer cells exhibited a robust EGF response characterized by a loss of stress fibers and the development of broad, actin-rich protrusions. Conversely, upon BCAR3 depletion, MDA-MB-231 cells failed to undergo stress fiber dissolution. Based on these data, we hypothesized that, upon loss of BCAR3, cofilin activity would be decreased in response to EGF (as indicated by an increase in pSer3 on cofilin), leading to a stabilization of stress fibers. To test this, MDA-MB-231 invasive breast cancer cells were transfected with control (siCtl) or BCAR3-specific (siB3) siRNA oligonucleotides and then incubated for 24 hours in normal growth medium. Cells were serum-starved for 16-18 hours, stimulated with 100ng/ml EGF for 0, 30 seconds or 2 minutes, then lysed and immunoblotted with the designated antibodies (**Fig A1.5**). The reason for the shorter time points is because cofilin-mediated actin severing can occur very rapidly downstream of EGFR (i.e. in less than 2 minutes) [200]. Again, transfection of cells with siB3 resulted in undetectable levels of BCAR3 protein (Panel F, lanes 4-6). Despite EGF stimulation and EGFR activation (Panel C), pSer3 cofilin levels appeared to remain relatively constant in control cells (Panel A, lanes 1-3). Interestingly, compared to control cells, BCAR3-depleted cells had elevated basal levels of Ser3 cofilin phosphorylation prior to EGF stimulation (Panel A, compare lanes 1 and 4), indicating that BCAR3 may regulate cofilin activity under basal conditions. However, upon EGF stimulation, control and BCAR3-depleted cells expressed similar levels of pSer3 cofilin (Panel A, compare lanes 2-3 and 5-6). We further explored AKT activation under these conditions. Surprisingly, onset of AKT phosphorylation (pS473) appeared to be delayed in control cells post-EGF stimulation compared to BCAR3-depleted cells (Panel D, compare lanes 1-3 and 4-6). This contradicts our previous finding demonstrating a delay in AKT phosphorylation in BCAR3-depleted cells compared to control cells (**Fig A1.3**),

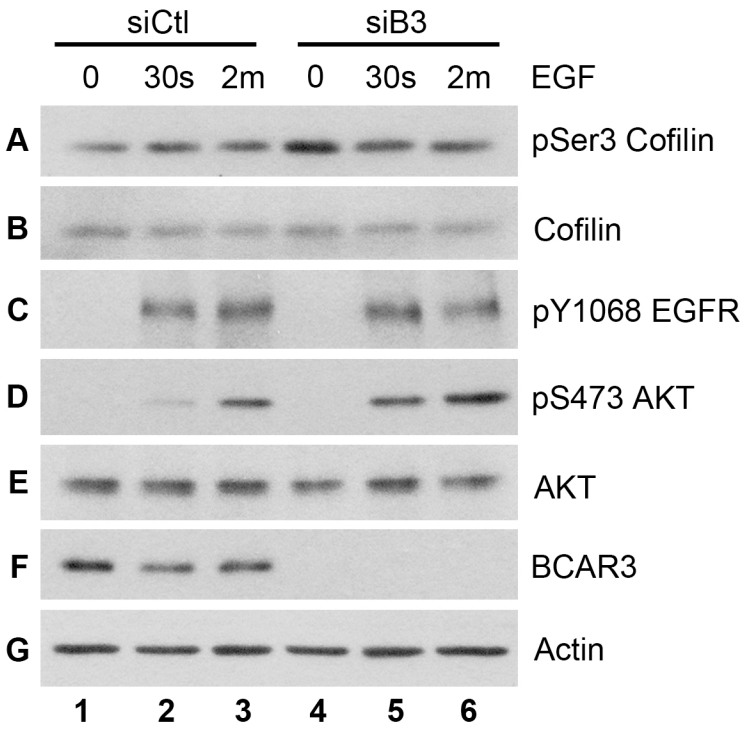
siCtl
siB3
0
30s
2m
0
30s
2m
EGF
A
pSer3 Cofilin
B
Cofilin
C
pY1068 EGFR
D
pS473 AKT
E
AKT
F
BCAR3
G
Actin
1
2
3
4
5
6

Figure A1.5. BCAR3 may regulate cofilin activity in invasive breast cancer cells. MDA-MB-231 invasive breast cancer cells were transfected with control (siCtl) or BCAR3-specific (siB3) siRNA oligonucleotides and then incubated for 24 hours in normal growth medium. Cells were serum-starved for 16-18 hours, stimulated with 100ng/ml EGF for 0, 30 seconds or 2 minutes, and then lysed and immunoblotted with the designated antibodies as described in the methods. Data represent one independent experiment.

but may be explained by the different time courses examined between experiments. Future work is necessary to distinguish between these inconsistent findings.

A1.2.3 BCAR3 may regulate p190RhoGAP phosphorylation in invasive breast cancer cells

As discussed in **Chapter 2** (Section 2.3), the BCAR3-dependent Rac1 activity observed in invasive breast cancer cells may be due to BCAR3 actively suppressing RhoA signaling, leading indirectly to Rac1 activation. This active suppression of RhoA by BCAR3 could arise from its ability to positively regulate a Rho GAP. p190RhoGAP is positively regulated by Src, which makes it a potentially attractive downstream target of BCAR3 signaling. More specifically, in response to EGF stimulation, Src phosphorylates and activates p190RhoGAP downstream of EGFR [104]. To test whether BCAR3 promotes p190RhoGAP (p190) phosphorylation, MDA-MB-231 invasive breast cancer cells were transfected with control (siCtl) or BCAR3-specific (siB3) siRNA oligonucleotides and then incubated for 24 hours in normal growth medium. Cells were serum-starved for 16-18 hours, stimulated with 100ng/ml EGF for 0, 30 seconds or 2 minutes, and then lysed. p190 immune complexes were isolated from cells and levels of phosphorylation were assessed by immunoblot using a phospho-tyrosine-specific antibody (pTyr) (**Fig A1.6**, top panels). Compared to control cells, p190 phosphorylation appeared to be slightly decreased in BCAR3-depleted cells, irrespective of EGF stimulation (compare lanes 1-3 and 4-6). This finding is consistent with data reported from our lab and others that demonstrate that Src kinase activity is greatly reduced upon loss of BCAR3 [129, 130]. This suggests that p190RhoGAP may be less active in BCAR3-depleted cells, which may ultimately lead to the elevated levels of RhoA activity seen upon loss of BCAR3 (**Chapter 2**). However, it was challenging to draw any

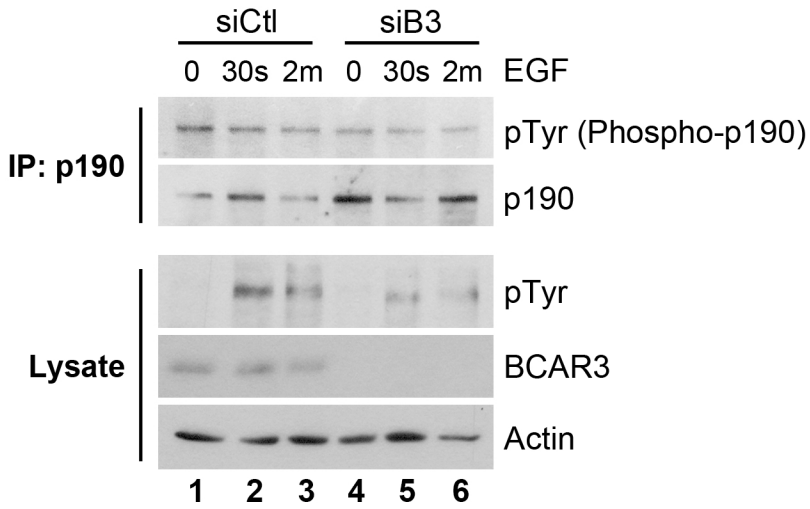
siCtl
siB3
0 30s 2m 0 30s 2m EGF
IP: p190
pTyr (Phospho-p190)
p190
Lysate
pTyr
BCAR3
Actin
1 2 3 4 5 6

Figure A1.6. BCAR3 may regulate p190RhoGAP phosphorylation in invasive breast cancer cells. MDA-MB-231 invasive breast cancer cells were transfected with control (siCtl) or BCAR3-specific (siB3) siRNA oligonucleotides and then incubated for 24 hours in normal growth medium. Cells were serum-starved for 16-18 hours, stimulated with 100ng/ml EGF for 0, 30 seconds or 2 minutes, and then lysed. p190RhoGAP (p190) immune complexes were isolated from cells as described in the methods, and levels of phosphorylation were assessed by immunoblot using a phospho-tyrosine-specific antibody (pTyr) (top panels). BCAR3 knockdown was confirmed by immunoblotting cell lysates with a BCAR3-specific antibody (bottom panels). Actin was used as a loading control. Data represent one independent experiment.

conclusions from this preliminary experiment considering total p190 protein levels were highly variable between conditions (compare lanes 1-6). Future work will be necessary to determine whether BCAR3 positively regulates p190RhoGAP phosphorylation.

A1.3 Discussion

Importantly, the data presented in this appendix are preliminary and represent single, independent experiments. For each experiment, different parameters were optimized, including the timing of EGF stimulation and transfection of siCas oligonucleotides in invasive breast cancer cells. Due to this optimization, results were variable between experiments, which made it challenging to draw any solid conclusions. Future work will aim to improve reproducibility by minimizing the inconsistencies between experimental parameters.

Nevertheless, our data indicate that Cas, but not BCAR3, may promote ligand-induced EGFR auto-phosphorylation on tyrosine 1068 in invasive breast cancer cells. This finding supports an earlier study by Paola Defilippi's group, which reported that Cas and Src are required for integrin-mediated phosphorylation of EGFR on Y1068 in response to cell adhesion [201]. Yet, in a majority of our experiments, selective depletion of Cas also significantly reduced total levels of EGFR expression. This is not surprising, however, given that depletion of Cas in A431 epidermal cancer cells has been shown to enhance EGFR internalization (i.e. endocytosis), which is thought to downregulate EGFR expression [202]. Future work will be necessary to determine whether this type of regulation occurs in invasive breast cancer cells.

Despite inconsistent results, BCAR3 and Cas may play important roles in controlling AKT activation downstream of EGFR. While some experiments indicated a delay in phosphorylation of AKT at S473 in BCAR3- or Cas-depleted cells compared to

control cells, other experiments did not reproduce this finding. However, our studies consistently showed that levels of ERK phosphorylation remained relatively constant despite EGF stimulation and were not affected by depletion of Cas or BCAR3. Again, this result is surprising because others have reported that levels of pERK are increased in MDA-MB-231 breast cancer cells following anywhere from 5 to 120 minutes of EGF stimulation [199]. While we are currently unsure why we did not observe any changes in ERK activity post-EGF stimulation, it is clear that this result was reproducible.

In the case of normal BCAR3-expressing MDA-MB-231 breast cancer cells, we expected EGF stimulation to result in an increase in cofilin activity (as indicated by a decrease in pSer3 levels), coincident with the dissolution of stress fibers and acquisition of actin-rich membrane protrusions upon EGF stimulation that we previously reported in these cells. However, EGF stimulation did not appear to have any influence on cofilin phosphorylation in control cells. This is perhaps less surprising in light of work from John Condeelis and Robert Eddy's group, which showed that EGF stimulation does not necessarily induce cofilin dephosphorylation. In fact, levels of pSer3 cofilin were shown to increase in MTLn3 rat carcinoma cells in response to EGF [200]. They propose that cofilin activity is unlikely to be regulated by phosphorylation, and alternatively suggest that cofilin is regulated by a different mechanism involving the phospholipid PIP_2 [203]. More specifically, cofilin is sequestered by membrane-bound PIP_2, which prevents it from severing actin filaments in the cytosol. John Condeelis' group demonstrated that, upon EGF stimulation, phospholipase C-gamma (PLCγ) hydrolyzes PIP_2 to diacylglycerol (DAG) and inositol triphosphate (IP_3); this action releases cofilin and allows it to bind and sever actin filaments [65, 203]. Based on these findings, it is interesting to speculate that BCAR3 may control cofilin activity by mediating PLCγ and/or cofilin release from the plasma membrane. While we did observe elevated levels of

pSer3 cofilin in BCAR3-depleted breast cancer cells compared to control cells under basal conditions, future work will be necessary to determine whether this result holds true and whether or not it is reflective of decreased basal levels of cofilin activity in the absence of BCAR3.

Finally, our preliminary results indicate that, upon loss of BCAR3, p190RhoGAP activity may be decreased, which may ultimately lead to the elevated levels of RhoA activity seen in the absence of BCAR3 (**Chapter 2**). However, total levels of p190 protein were highly variable between conditions, which made it difficult to draw conclusions. Future work is necessary to reduce variability between experimental conditions. If we indeed discover that BCAR3 promotes p190RhoGAP activity, this will provide the first evidence that BCAR3 negatively regulates Rho signaling in invasive breast cancer cells via a Rho GAP.

LIST OF REFERENCES

1. Hansen, R.K. and Bissell, M.J. 2000. Tissue architecture and breast cancer: the role of extracellular matrix and steroid hormones. *Endocr Relat Cancer* **7**:95-113.
2. Bertos, N.R. and Park, M. 2011. Breast cancer - one term, many entities? *J Clin Invest* **121**:3789-3796.
3. Figueroa, J.D., Pfeiffer, R.M., Patel, D.A., Linville, L., Brinton, L.A., Gierach, G.L., Yang, X.R., Papathomas, D., Visscher, D., Mies, C., Degnim, A.C., Anderson, W.F., Hewitt, S., Khodr, Z.G., Clare, S.E., Storniolo, A.M., and Sherman, M.E. 2014. Terminal duct lobular unit involution of the normal breast: implications for breast cancer etiology. *J Natl Cancer Inst* **106**.
4. Nelson, C.M. and Bissell, M.J. 2005. Modeling dynamic reciprocity: engineering three-dimensional culture models of breast architecture, function, and neoplastic transformation. *Semin Cancer Biol* **15**:342-352.
5. Weigelt, B. and Bissell, M.J. 2008. Unraveling the microenvironmental influences on the normal mammary gland and breast cancer. *Semin Cancer Biol* **18**:311-321.
6. Huang, B., Warner, M., and Gustafsson, J.A. 2014. Estrogen receptors in breast carcinogenesis and endocrine therapy. *Mol Cell Endocrinol*.
7. Mehta, R.G., Hawthorne, M., Mehta, R.R., Torres, K.E., Peng, X., Mccormick, D.L., and Kopelovich, L. 2014. Differential roles of ERalpha and ERbeta in normal and neoplastic development in the mouse mammary gland. *PLoS One* **9**:e113175.
8. Musgrove, E.A. and Sutherland, R.L. 2009. Biological determinants of endocrine resistance in breast cancer. *Nat Rev Cancer* **9**:631-643.
9. Beckmann, M.W., Niederacher, D., Schnurch, H.G., Gusterson, B.A., and Bender, H.G. 1997. Multistep carcinogenesis of breast cancer and tumour heterogeneity. *J Mol Med (Berl)* **75**:429-439.
10. Lin, E.Y., Jones, J.G., Li, P., Zhu, L., Whitney, K.D., Muller, W.J., and Pollard, J.W. 2003. Progression to malignancy in the polyoma middle T oncoprotein mouse breast cancer model provides a reliable model for human diseases. *Am J Pathol* **163**:2113-2126.
11. Hartmann, L.C., Degnim, A.C., Santen, R.J., Dupont, W.D., and Ghosh, K. 2015. Atypical hyperplasia of the breast--risk assessment and management options. *N Engl J Med* **372**:78-89.
12. Weigelt, B., Peterse, J.L., and Van 'T Veer, L.J. 2005. Breast cancer metastasis: markers and models. *Nat Rev Cancer* **5**:591-602.
13. Edge, S.B. and Compton, C.C. 2010. The American Joint Committee on Cancer: the 7th edition of the AJCC cancer staging manual and the future of TNM. *Ann Surg Oncol* **17**:1471-1474.
14. Aebi, S., Davidson, T., Gruber, G., Cardoso, F., and Group, E.G.W. 2011. Primary breast cancer: ESMO Clinical Practice Guidelines for diagnosis, treatment and follow-up. *Ann Oncol* **22 Suppl 6**:vi12-24.

15. Riggins, R.B., Schrecengost, R.S., Guerrero, M.S., and Bouton, A.H. 2007. Pathways to tamoxifen resistance. *Cancer Lett* **256**:1-24.

16. Mcinerney, J.M., Wilson, M.A., Strand, K.J., and Chrysogelos, S.A. 2001. A strong intronic enhancer element of the EGFR gene is preferentially active in high EGFR expressing breast cancer cells. *J Cell Biochem* **80**:538-549.

17. Hynes, N.E. and Lane, H.A. 2005. ERBB receptors and cancer: the complexity of targeted inhibitors. *Nat Rev Cancer* **5**:341-354.

18. Arteaga, C.L. and Engelman, J.A. 2014. ERBB receptors: from oncogene discovery to basic science to mechanism-based cancer therapeutics. *Cancer Cell* **25**:282-303.

19. Quail, D.F. and Joyce, J.A. 2013. Microenvironmental regulation of tumor progression and metastasis. *Nat Med* **19**:1423-1437.

20. Rowley, D.R. 2014. Reprogramming the tumor stroma: a new paradigm. *Cancer Cell* **26**:451-452.

21. Sabatier, R., Goncalves, A., and Bertucci, F. 2014. Personalized medicine: present and future of breast cancer management. *Crit Rev Oncol Hematol* **91**:223-233.

22. Perou, C.M., Sorlie, T., Eisen, M.B., Van De Rijn, M., Jeffrey, S.S., Rees, C.A., Pollack, J.R., Ross, D.T., Johnsen, H., Akslen, L.A., Fluge, O., Pergamenschikov, A., Williams, C., Zhu, S.X., Lonning, P.E., Borresen-Dale, A.L., Brown, P.O., and Botstein, D. 2000. Molecular portraits of human breast tumours. *Nature* **406**:747-752.

23. Hu, Z., Fan, C., Oh, D.S., Marron, J.S., He, X., Qaqish, B.F., Livasy, C., Carey, L.A., Reynolds, E., Dressler, L., Nobel, A., Parker, J., Ewend, M.G., Sawyer, L.R., Wu, J., Liu, Y., Nanda, R., Tretiakova, M., Ruiz Orrico, A., Dreher, D., Palazzo, J.P., Perreard, L., Nelson, E., Mone, M., Hansen, H., Mullins, M., Quackenbush, J.F., Ellis, M.J., Olopade, O.I., Bernard, P.S., and Perou, C.M. 2006. The molecular portraits of breast tumors are conserved across microarray platforms. *BMC Genomics* **7**:96.

24. Prat, A., Parker, J.S., Fan, C., and Perou, C.M. 2012. PAM50 assay and the three-gene model for identifying the major and clinically relevant molecular subtypes of breast cancer. *Breast Cancer Res Treat* **135**:301-306.

25. Cancer Genome Atlas, N. 2012. Comprehensive molecular portraits of human breast tumours. *Nature* **490**:61-70.

26. Sorlie, T. 2004. Molecular portraits of breast cancer: tumour subtypes as distinct disease entities. *Eur J Cancer* **40**:2667-2675.

27. Chia, S.K., Bramwell, V.H., Tu, D., Shepherd, L.E., Jiang, S., Vickery, T., Mardis, E., Leung, S., Ung, K., Pritchard, K.I., Parker, J.S., Bernard, P.S., Perou, C.M., Ellis, M.J., and Nielsen, T.O. 2012. A 50-gene intrinsic subtype classifier for prognosis and prediction of benefit from adjuvant tamoxifen. *Clin Cancer Res* **18**:4465-4472.

28. Baselga, J. and Swain, S.M. 2009. Novel anticancer targets: revisiting ERBB2 and discovering ERBB3. *Nat Rev Cancer* **9**:463-475.

29. Foulkes, W.D., Smith, I.E., and Reis-Filho, J.S. 2010. Triple-negative breast cancer. *N Engl J Med* **363**:1938-1948.

30. Perou, C.M. 2011. Molecular stratification of triple-negative breast cancers. *Oncologist* **16 Suppl 1**:61-70.

31. Prat, A., Parker, J.S., Karginova, O., Fan, C., Livasy, C., Herschkowitz, J.I., He, X., and Perou, C.M. 2010. Phenotypic and molecular characterization of the claudin-low intrinsic subtype of breast cancer. *Breast Cancer Res* **12**:R68.

32. Parker, J.S., Mullins, M., Cheang, M.C., Leung, S., Voduc, D., Vickery, T., Davies, S., Fauron, C., He, X., Hu, Z., Quackenbush, J.F., Stijleman, I.J., Palazzo, J., Marron, J.S., Nobel, A.B., Mardis, E., Nielsen, T.O., Ellis, M.J., Perou, C.M., and Bernard, P.S. 2009. Supervised risk predictor of breast cancer based on intrinsic subtypes. *J Clin Oncol* **27**:1160-1167.

33. Kleppe, M. and Levine, R.L. 2014. Tumor heterogeneity confounds and illuminates: assessing the implications. *Nat Med* **20**:342-344.

34. Magee, J.A., Piskounova, E., and Morrison, S.J. 2012. Cancer stem cells: impact, heterogeneity, and uncertainty. *Cancer Cell* **21**:283-296.

35. Wicha, M.S. 2014. Targeting self-renewal, an Achilles' heel of cancer stem cells. *Nat Med* **20**:14-15.

36. Valastyan, S. and Weinberg, R.A. 2011. Tumor metastasis: molecular insights and evolving paradigms. *Cell* **147**:275-292.

37. Kang, Y., Siegel, P.M., Shu, W., Drobnjak, M., Kakonen, S.M., Cordon-Cardo, C., Guise, T.A., and Massague, J. 2003. A multigenic program mediating breast cancer metastasis to bone. *Cancer Cell* **3**:537-549.

38. Minn, A.J., Kang, Y., Serganova, I., Gupta, G.P., Giri, D.D., Doubrovin, M., Ponomarev, V., Gerald, W.L., Blasberg, R., and Massague, J. 2005. Distinct organ-specific metastatic potential of individual breast cancer cells and primary tumors. *J Clin Invest* **115**:44-55.

39. Minn, A.J., Gupta, G.P., Siegel, P.M., Bos, P.D., Shu, W., Giri, D.D., Viale, A., Olshen, A.B., Gerald, W.L., and Massague, J. 2005. Genes that mediate breast cancer metastasis to lung. *Nature* **436**:518-524.

40. Bos, P.D., Zhang, X.H., Nadal, C., Shu, W., Gomis, R.R., Nguyen, D.X., Minn, A.J., Van De Vijver, M.J., Gerald, W.L., Foekens, J.A., and Massague, J. 2009. Genes that mediate breast cancer metastasis to the brain. *Nature* **459**:1005-1009.

41. Nguyen, D.X., Bos, P.D., and Massague, J. 2009. Metastasis: from dissemination to organ-specific colonization. *Nat Rev Cancer* **9**:274-284.

42. Franken, B., De Groot, M.R., Mastboom, W.J., Vermes, I., Van Der Palen, J., Tibbe, A.G., and Terstappen, L.W. 2012. Circulating tumor cells, disease recurrence and survival in newly diagnosed breast cancer. *Breast Cancer Res* **14**:R133.

43. Rack, B., Schindlbeck, C., Juckstock, J., Andergassen, U., Hepp, P., Zwingers, T., Friedl, T.W., Lorenz, R., Tesch, H., Fasching, P.A., Fehm, T., Schneeweiss, A., Lichtenegger, W., Beckmann, M.W., Friese, K., Pantel, K., Janni, W., and

Group, S.S. 2014. Circulating tumor cells predict survival in early average-to-high risk breast cancer patients. *J Natl Cancer Inst* **106**.

44. Bravo-Cordero, J.J., Hodgson, L., and Condeelis, J. 2012. Directed cell invasion and migration during metastasis. *Curr Opin Cell Biol* **24**:277-283.

45. Condeelis, J. and Segall, J.E. 2003. Intravital imaging of cell movement in tumours. *Nat Rev Cancer* **3**:921-930.

46. Gligorijevic, B., Bergman, A., and Condeelis, J. 2014. Multiparametric classification links tumor microenvironments with tumor cell phenotype. *PLoS Biol* **12**:e1001995.

47. Wilson, A.L., Schrecengost, R.S., Guerrero, M.S., Thomas, K.S., and Bouton, A.H. 2013. Breast cancer antiestrogen resistance 3 (BCAR3) promotes cell motility by regulating actin cytoskeletal and adhesion remodeling in invasive breast cancer cells. *PLoS One* **8**:e65678.

48. Roussos, E.T., Condeelis, J.S., and Patsialou, A. 2011. Chemotaxis in cancer. *Nat Rev Cancer* **11**:573-587.

49. Goswami, S., Sahai, E., Wyckoff, J.B., Cammer, M., Cox, D., Pixley, F.J., Stanley, E.R., Segall, J.E., and Condeelis, J.S. 2005. Macrophages promote the invasion of breast carcinoma cells via a colony-stimulating factor-1/epidermal growth factor paracrine loop. *Cancer Res* **65**:5278-5283.

50. Condeelis, J. and Pollard, J.W. 2006. Macrophages: obligate partners for tumor cell migration, invasion, and metastasis. *Cell* **124**:263-266.

51. Parsons, J.T., Horwitz, A.R., and Schwartz, M.A. 2010. Cell adhesion: integrating cytoskeletal dynamics and cellular tension. *Nat Rev Mol Cell Biol* **11**:633-643.

52. Noy, R. and Pollard, J.W. 2014. Tumor-associated macrophages: from mechanisms to therapy. *Immunity* **41**:49-61.

53. Wyckoff, J.B., Wang, Y., Lin, E.Y., Li, J.F., Goswami, S., Stanley, E.R., Segall, J.E., Pollard, J.W., and Condeelis, J. 2007. Direct visualization of macrophage-assisted tumor cell intravasation in mammary tumors. *Cancer Res* **67**:2649-2656.

54. Rohan, T.E., Xue, X., Lin, H.M., D'alfonso, T.M., Ginter, P.S., Oktay, M.H., Robinson, B.D., Ginsberg, M., Gertler, F.B., Glass, A.G., Sparano, J.A., Condeelis, J.S., and Jones, J.G. 2014. Tumor microenvironment of metastasis and risk of distant metastasis of breast cancer. *J Natl Cancer Inst* **106**.

55. Raftopoulou, M. and Hall, A. 2004. Cell migration: Rho GTPases lead the way. *Dev Biol* **265**:23-32.

56. Machacek, M., Hodgson, L., Welch, C., Elliott, H., Pertz, O., Nalbant, P., Abell, A., Johnson, G.L., Hahn, K.M., and Danuser, G. 2009. Coordination of Rho GTPase activities during cell protrusion. *Nature* **461**:99-103.

57. Ridley, A.J., Schwartz, M.A., Burridge, K., Firtel, R.A., Ginsberg, M.H., Borisy, G., Parsons, J.T., and Horwitz, A.R. 2003. Cell migration: integrating signals from front to back. *Science* **302**:1704-1709.

58. Ridley, A.J. 2011. Life at the leading edge. *Cell* **145**:1012-1022.

59. Weaver, A.M. 2006. Invadopodia: specialized cell structures for cancer invasion. *Clin Exp Metastasis* **23**:97-105.

60. Bergman, A., Condeelis, J.S., and Gligorijevic, B. 2014. Invadopodia in context. *Cell Adh Migr* **8**:273-279.

61. Chen, Z., Borek, D., Padrick, S.B., Gomez, T.S., Metlagel, Z., Ismail, A.M., Umetani, J., Billadeau, D.D., Otwinowski, Z., and Rosen, M.K. 2010. Structure and control of the actin regulatory WAVE complex. *Nature* **468**:533-538.

62. Krause, M. and Gautreau, A. 2014. Steering cell migration: lamellipodium dynamics and the regulation of directional persistence. *Nat Rev Mol Cell Biol* **15**:577-590.

63. Blanchoin, L. and Michelot, A. 2012. Actin cytoskeleton: a team effort during actin assembly. *Curr Biol* **22**:R643-645.

64. Choi, C.K., Vicente-Manzanares, M., Zareno, J., Whitmore, L.A., Mogilner, A., and Horwitz, A.R. 2008. Actin and alpha-actinin orchestrate the assembly and maturation of nascent adhesions in a myosin II motor-independent manner. *Nat Cell Biol* **10**:1039-1050.

65. Wang, W., Eddy, R., and Condeelis, J. 2007. The cofilin pathway in breast cancer invasion and metastasis. *Nat Rev Cancer* **7**:429-440.

66. Yang, N., Higuchi, O., Ohashi, K., Nagata, K., Wada, A., Kangawa, K., Nishida, E., and Mizuno, K. 1998. Cofilin phosphorylation by LIM-kinase 1 and its role in Rac-mediated actin reorganization. *Nature* **393**:809-812.

67. Desgrosellier, J.S. and Cheresh, D.A. 2010. Integrins in cancer: biological implications and therapeutic opportunities. *Nat Rev Cancer* **10**:9-22.

68. Bachir, A.I., Zareno, J., Moissoglu, K., Plow, E.F., Gratton, E., and Horwitz, A.R. 2014. Integrin-associated complexes form hierarchically with variable stoichiometry in nascent adhesions. *Curr Biol* **24**:1845-1853.

69. Calderwood, D.A., Zent, R., Grant, R., Rees, D.J., Hynes, R.O., and Ginsberg, M.H. 1999. The Talin head domain binds to integrin beta subunit cytoplasmic tails and regulates integrin activation. *J Biol Chem* **274**:28071-28074.

70. Harburger, D.S., Bouaouina, M., and Calderwood, D.A. 2009. Kindlin-1 and -2 directly bind the C-terminal region of beta integrin cytoplasmic tails and exert integrin-specific activation effects. *J Biol Chem* **284**:11485-11497.

71. Moser, M., Legate, K.R., Zent, R., and Fassler, R. 2009. The tail of integrins, talin, and kindlins. *Science* **324**:895-899.

72. Calderwood, D.A., Campbell, I.D., and Critchley, D.R. 2013. Talins and kindlins: partners in integrin-mediated adhesion. *Nat Rev Mol Cell Biol* **14**:503-517.

73. Nanda, S.Y., Hoang, T., Patel, P., and Zhang, H. 2014. Vinculin regulates assembly of talin: beta3 integrin complexes. *J Cell Biochem* **115**:1206-1216.

74. Carisey, A., Tsang, R., Greiner, A.M., Nijenhuis, N., Heath, N., Nazgiewicz, A., Kemkemer, R., Derby, B., Spatz, J., and Ballestrem, C. 2013. Vinculin regulates the recruitment and release of core focal adhesion proteins in a force-dependent manner. *Curr Biol* **23**:271-281.

75. Webb, D.J., Donais, K., Whitmore, L.A., Thomas, S.M., Turner, C.E., Parsons, J.T., and Horwitz, A.F. 2004. FAK-Src signalling through paxillin, ERK and MLCK regulates adhesion disassembly. *Nat Cell Biol* **6**:154-161.

76. Broussard, J.A., Webb, D.J., and Kaverina, I. 2008. Asymmetric focal adhesion disassembly in motile cells. *Curr Opin Cell Biol* **20**:85-90.

77. Vicente-Manzanares, M., Ma, X., Adelstein, R.S., and Horwitz, A.R. 2009. Non-muscle myosin II takes centre stage in cell adhesion and migration. *Nat Rev Mol Cell Biol* **10**:778-790.

78. Sawada, Y., Tamada, M., Dubin-Thaler, B.J., Cherniavskaya, O., Sakai, R., Tanaka, S., and Sheetz, M.P. 2006. Force sensing by mechanical extension of the Src family kinase substrate p130Cas. *Cell* **127**:1015-1026.

79. Del Rio, A., Perez-Jimenez, R., Liu, R., Roca-Cusachs, P., Fernandez, J.M., and Sheetz, M.P. 2009. Stretching single talin rod molecules activates vinculin binding. *Science* **323**:638-641.

80. Roca-Cusachs, P., Del Rio, A., Puklin-Faucher, E., Gauthier, N.C., Biais, N., and Sheetz, M.P. 2013. Integrin-dependent force transmission to the extracellular matrix by alpha-actinin triggers adhesion maturation. *Proc Natl Acad Sci U S A* **110**:E1361-1370.

81. Oakes, P.W., Beckham, Y., Stricker, J., and Gardel, M.L. 2012. Tension is required but not sufficient for focal adhesion maturation without a stress fiber template. *J Cell Biol* **196**:363-374.

82. Chesarone, M.A., Dupage, A.G., and Goode, B.L. 2010. Unleashing formins to remodel the actin and microtubule cytoskeletons. *Nat Rev Mol Cell Biol* **11**:62-74.

83. Mseka, T. and Cramer, L.P. 2011. Actin depolymerization-based force retracts the cell rear in polarizing and migrating cells. *Curr Biol* **21**:2085-2091.

84. Cramer, L.P. 2013. Mechanism of cell rear retraction in migrating cells. *Curr Opin Cell Biol* **25**:591-599.

85. Guilluy, C., Garcia-Mata, R., and Burridge, K. 2011. Rho protein crosstalk: another social network? *Trends Cell Biol* **21**:718-726.

86. Abreu-Blanco, M.T., Verboon, J.M., and Parkhurst, S.M. 2014. Coordination of Rho family GTPase activities to orchestrate cytoskeleton responses during cell wound repair. *Curr Biol* **24**:144-155.

87. Parsons, J.T. 2003. Focal adhesion kinase: the first ten years. *J Cell Sci* **116**:1409-1416.

88. Lahlou, H., Sanguin-Gendreau, V., Zuo, D., Cardiff, R.D., Mclean, G.W., Frame, M.C., and Muller, W.J. 2007. Mammary epithelial-specific disruption of the focal adhesion kinase blocks mammary tumor progression. *Proc Natl Acad Sci U S A* **104**:20302-20307.

89. Provenzano, P.P., Inman, D.R., Eliceiri, K.W., Beggs, H.E., and Keely, P.J. 2008. Mammary epithelial-specific disruption of focal adhesion kinase retards tumor formation and metastasis in a transgenic mouse model of human breast cancer. *Am J Pathol* **173**:1551-1565.

90. Luo, M., Fan, H., Nagy, T., Wei, H., Wang, C., Liu, S., Wicha, M.S., and Guan, J.L. 2009. Mammary epithelial-specific ablation of the focal adhesion kinase suppresses mammary tumorigenesis by affecting mammary cancer stem/progenitor cells. *Cancer Res* **69**:466-474.

91. Ashton, G.H., Morton, J.P., Myant, K., Phesse, T.J., Ridgway, R.A., Marsh, V., Wilkins, J.A., Athineos, D., Muncan, V., Kemp, R., Neufeld, K., Clevers, H., Brunton, V., Winton, D.J., Wang, X., Sears, R.C., Clarke, A.R., Frame, M.C., and Sansom, O.J. 2010. Focal adhesion kinase is required for intestinal regeneration and tumorigenesis downstream of Wnt/c-Myc signaling. *Dev Cell* **19**:259-269.

92. Sulzmaier, F.J., Jean, C., and Schlaepfer, D.D. 2014. FAK in cancer: mechanistic findings and clinical applications. *Nat Rev Cancer* **14**:598-610.

93. Jean, C., Chen, X.L., Nam, J.O., Tancioni, I., Uryu, S., Lawson, C., Ward, K.K., Walsh, C.T., Miller, N.L., Ghassemian, M., Turowski, P., Dejana, E., Weis, S., Cheresh, D.A., and Schlaepfer, D.D. 2014. Inhibition of endothelial FAK activity prevents tumor metastasis by enhancing barrier function. *J Cell Biol* **204**:247-263.

94. Deakin, N.O. and Turner, C.E. 2008. Paxillin comes of age. *J Cell Sci* **121**:2435-2444.

95. Nayal, A., Webb, D.J., Brown, C.M., Schaefer, E.M., Vicente-Manzanares, M., and Horwitz, A.R. 2006. Paxillin phosphorylation at Ser273 localizes a GIT1-PIX-PAK complex and regulates adhesion and protrusion dynamics. *J Cell Biol* **173**:587-589.

96. Yeatman, T.J. 2004. A renaissance for SRC. *Nat Rev Cancer* **4**:470-480.

97. Deakin, N.O. and Turner, C.E. 2011. Distinct roles for paxillin and Hic-5 in regulating breast cancer cell morphology, invasion, and metastasis. *Mol Biol Cell* **22**:327-341.

98. Ottenhoff-Kalff, A.E., Rijksen, G., Van Beurden, E.A., Hennipman, A., Michels, A.A., and Staal, G.E. 1992. Characterization of protein tyrosine kinases from human breast cancer: involvement of the c-src oncogene product. *Cancer Res* **52**:4773-4778.

99. Biscardi, J.S., Tice, D.A., and Parsons, S.J. 1999. c-Src, receptor tyrosine kinases, and human cancer. *Adv Cancer Res* **76**:61-119.

100. Huang, F., Reeves, K., Han, X., Fairchild, C., Platero, S., Wong, T.W., Lee, F., Shaw, P., and Clark, E. 2007. Identification of candidate molecular markers predicting sensitivity in solid tumors to dasatinib: rationale for patient selection. *Cancer Res* **67**:2226-2238.

101. Moulder, S., Yan, K., Huang, F., Hess, K.R., Liedtke, C., Lin, F., Hatzis, C., Hortobagyi, G.N., Symmans, W.F., and Pusztai, L. 2010. Development of candidate genomic markers to select breast cancer patients for dasatinib therapy. *Mol Cancer Ther* **9**:1120-1127.

102. Reynolds, A.B., Kanner, S.B., Bouton, A.H., Schaller, M.D., Weed, S.A., Flynn, D.C., and Parsons, J.T. 2014. SRChing for the substrates of Src. *Oncogene* **33**:4537-4547.

103. Huveneers, S. and Danen, E.H. 2009. Adhesion signaling - crosstalk between integrins, Src and Rho. *J Cell Sci* **122**:1059-1069.

104. Chang, J.H., Gill, S., Settleman, J., and Parsons, S.J. 1995. c-Src regulates the simultaneous rearrangement of actin cytoskeleton, p190RhoGAP, and p120RasGAP following epidermal growth factor stimulation. *J Cell Biol* **130**:355-368.

105. Dorssers, L.C., Van Agthoven, T., Dekker, A., Van Agthoven, T.L., and Kok, E.M. 1993. Induction of antiestrogen resistance in human breast cancer cells by random insertional mutagenesis using defective retroviruses: identification of bcar-1, a common integration site. *Mol Endocrinol* **7**:870-878.

106. Brinkman, A., Van Der Flier, S., Kok, E.M., and Dorssers, L.C. 2000. BCAR1, a human homologue of the adapter protein p130Cas, and antiestrogen resistance in breast cancer cells. *J Natl Cancer Inst* **92**:112-120.

107. Wallez, Y., Mace, P.D., Pasquale, E.B., and Riedl, S.J. 2012. NSP-CAS Protein Complexes: Emerging Signaling Modules in Cancer. *Genes Cancer* **3**:382-393.

108. Tornillo, G., Defilippi, P., and Cabodi, S. 2014. Cas proteins: dodgy scaffolding in breast cancer. *Breast Cancer Res* **16**:443.

109. Pylayeva, Y., Gillen, K.M., Gerald, W., Beggs, H.E., Reichardt, L.F., and Giancotti, F.G. 2009. Ras- and PI3K-dependent breast tumorigenesis in mice and humans requires focal adhesion kinase signaling. *J Clin Invest* **119**:252-266.

110. Van Der Flier, S., Brinkman, A., Look, M.P., Kok, E.M., Meijer-Van Gelder, M.E., Klijn, J.G., Dorssers, L.C., and Foekens, J.A. 2000. Bcar1/p130Cas protein and primary breast cancer: prognosis and response to tamoxifen treatment. *J Natl Cancer Inst* **92**:120-127.

111. Dorssers, L.C., Grebenchtchikov, N., Brinkman, A., Look, M.P., Van Broekhoven, S.P., De Jong, D., Peters, H.A., Portengen, H., Meijer-Van Gelder, M.E., Klijn, J.G., Van Tienoven, D.T., Geurts-Moespot, A., Span, P.N., Foekens, J.A., and Sweep, F.C. 2004. The prognostic value of BCAR1 in patients with primary breast cancer. *Clin Cancer Res* **10**:6194-6202.

112. Cabodi, S., Tinnirello, A., Di Stefano, P., Bisaro, B., Ambrosino, E., Castellano, I., Sapino, A., Arisio, R., Cavallo, F., Forni, G., Glukhova, M., Silengo, L., Altruda, F., Turco, E., Tarone, G., and Defilippi, P. 2006. p130Cas as a new regulator of mammary epithelial cell proliferation, survival, and HER2-neu oncogene-dependent breast tumorigenesis. *Cancer Res* **66**:4672-4680.

113. Guerrero, M.S., Parsons, J.T., and Bouton, A.H. 2012. Cas and NEDD9 Contribute to Tumor Progression through Dynamic Regulation of the Cytoskeleton. *Genes Cancer* **3**:371-381.

114. Cabodi, S., Del Pilar Camacho-Leal, M., Di Stefano, P., and Defilippi, P. 2010. Integrin signalling adaptors: not only figurants in the cancer story. *Nat Rev Cancer* **10**:858-870.

115. Janostiak, R., Brabek, J., Auernheimer, V., Tatarova, Z., Lautscham, L.A., Dey, T., Gemperle, J., Merkel, R., Goldmann, W.H., Fabry, B., and Rosel, D. 2014. CAS directly interacts with vinculin to control mechanosensing and focal adhesion dynamics. *Cell Mol Life Sci* **71**:727-744.

116. Klemke, R.L., Leng, J., Molander, R., Brooks, P.C., Vuori, K., and Cheresh, D.A. 1998. CAS/Crk coupling serves as a "molecular switch" for induction of cell migration. *J Cell Biol* **140**:961-972.

117. Akakura, S., Kar, B., Singh, S., Cho, L., Tibrewal, N., Sanokawa-Akakura, R., Reichman, C., Ravichandran, K.S., and Birge, R.B. 2005. C-terminal SH3 domain of CrkII regulates the assembly and function of the DOCK180/ELMO Rac-GEF. *J Cell Physiol* **204**:344-351.

118. Vervoort, V.S., Roselli, S., Oshima, R.G., and Pasquale, E.B. 2007. Splice variants and expression patterns of SHEP1, BCAR3 and NSP1, a gene family involved in integrin and receptor tyrosine kinase signaling. *Gene* **391**:161-170.

119. Schrecengost, R.S., Riggins, R.B., Thomas, K.S., Guerrero, M.S., and Bouton, A.H. 2007. Breast cancer antiestrogen resistance-3 expression regulates breast cancer cell migration through promotion of p130Cas membrane localization and membrane ruffling. *Cancer Res* **67**:6174-6182.

120. Near, R.I., Zhang, Y., Makkinje, A., Vanden Borre, P., and Lerner, A. 2007. AND-34/BCAR3 differs from other NSP homologs in induction of anti-estrogen resistance, cyclin D1 promoter activation and altered breast cancer cell morphology. *J Cell Physiol* **212**:655-665.

121. Lu, Y., Brush, J., and Stewart, T.A. 1999. NSP1 defines a novel family of adaptor proteins linking integrin and tyrosine kinase receptors to the c-Jun N-terminal kinase/stress-activated protein kinase signaling pathway. *J Biol Chem* **274**:10047-10052.

122. Cai, D., Clayton, L.K., Smolyar, A., and Lerner, A. 1999. AND-34, a novel p130Cas-binding thymic stromal cell protein regulated by adhesion and inflammatory cytokines. *J Immunol* **163**:2104-2112.

123. Gotoh, T., Cai, D., Tian, X., Feig, L.A., and Lerner, A. 2000. p130Cas regulates the activity of AND-34, a novel Ral, Rap1, and R-Ras guanine nucleotide exchange factor. *J Biol Chem* **275**:30118-30123.

124. Cai, D., Iyer, A., Felekkis, K.N., Near, R.I., Luo, Z., Chernoff, J., Albanese, C., Pestell, R.G., and Lerner, A. 2003. AND-34/BCAR3, a GDP exchange factor whose overexpression confers antiestrogen resistance, activates Rac, PAK1, and the cyclin D1 promoter. *Cancer Res* **63**:6802-6808.

125. Mace, P.D., Wallez, Y., Dobaczewska, M.K., Lee, J.J., Robinson, H., Pasquale, E.B., and Riedl, S.J. 2011. NSP-Cas protein structures reveal a promiscuous interaction module in cell signaling. *Nat Struct Mol Biol* **18**:1381-1387.

126. Near, R.I., Smith, R.S., Toselli, P.A., Freddo, T.F., Bloom, A.B., Vanden Borre, P., Seldin, D.C., and Lerner, A. 2009. Loss of AND-34/BCAR3 expression in mice results in rupture of the adult lens. *Mol Vis* **15**:685-699.

127. Van Agthoven, T., Van Agthoven, T.L., Dekker, A., Van Der Spek, P.J., Vreede, L., and Dorssers, L.C. 1998. Identification of BCAR3 by a random search for genes involved in antiestrogen resistance of human breast cancer cells. *EMBO J* **17**:2799-2808.

128. Felekkis, K.N., Narsimhan, R.P., Near, R., Castro, A.F., Zheng, Y., Quilliam, L.A., and Lerner, A. 2005. AND-34 activates phosphatidylinositol 3-kinase and induces

anti-estrogen resistance in a SH2 and GDP exchange factor-like domain-dependent manner. *Mol Cancer Res* **3**:32-41.

129. Schuh, N.R., Guerrero, M.S., Schrecengost, R.S., and Bouton, A.H. 2010. BCAR3 regulates Src/p130 Cas association, Src kinase activity, and breast cancer adhesion signaling. *J Biol Chem* **285**:2309-2317.

130. Sun, G., Cheng, S.Y., Chen, M., Lim, C.J., and Pallen, C.J. 2012. Protein tyrosine phosphatase alpha phosphotyrosyl-789 binds BCAR3 to position Cas for activation at integrin-mediated focal adhesions. *Mol Cell Biol* **32**:3776-3789.

131. Riggins, R.B., Thomas, K.S., Ta, H.Q., Wen, J., Davis, R.J., Schuh, N.R., Donelan, S.S., Owen, K.A., Gibson, M.A., Shupnik, M.A., Silva, C.M., Parsons, S.J., Clarke, R., and Bouton, A.H. 2006. Physical and functional interactions between Cas and c-Src induce tamoxifen resistance of breast cancer cells through pathways involving epidermal growth factor receptor and signal transducer and activator of transcription 5b. *Cancer Res* **66**:7007-7015.

132. Wallez, Y., Riedl, S.J., and Pasquale, E.B. 2014. Association of the breast cancer antiestrogen resistance protein 1 (BCAR1) and BCAR3 scaffolding proteins in cell signaling and antiestrogen resistance. *J Biol Chem* **289**:10431-10444.

133. Van Agthoven, T., Sieuwerts, A.M., Meijer-Van Gelder, M.E., Look, M.P., Smid, M., Veldscholte, J., Sleijfer, S., Foekens, J.A., and Dorssers, L.C. 2009. Relevance of breast cancer antiestrogen resistance genes in human breast cancer progression and tamoxifen resistance. *J Clin Oncol* **27**:542-549.

134. Sieuwerts, A.M., Lyng, M.B., Meijer-Van Gelder, M.E., De Weerd, V., Sweep, F.C., Foekens, J.A., Span, P.N., Martens, J.W., and Ditzel, H.J. 2014. Evaluation of the ability of adjuvant tamoxifen-benefit gene signatures to predict outcome of hormone-naive estrogen receptor-positive breast cancer patients treated with tamoxifen in the advanced setting. *Mol Oncol* **8**:1679-1689.

135. Guo, J., Canaff, L., Rajadurai, C., Fils-Aime, N., Tian, J., Dai, M., Korah, J., Villatoro, M., Park, M., Ali, S., and Lebrun, J.J. 2014. Breast Cancer Anti-Estrogen Resistance-3 inhibits transforming growth factor-ss/Smad signaling and associates with favorable breast cancer disease outcomes. *Breast Cancer Res* **16**:476.

136. Ridley, A.J., Paterson, H.F., Johnston, C.L., Diekmann, D., and Hall, A. 1992. The small GTP-binding protein rac regulates growth factor-induced membrane ruffling. *Cell* **70**:401-410.

137. Nobes, C.D. and Hall, A. 1995. Rho, rac, and cdc42 GTPases regulate the assembly of multimolecular focal complexes associated with actin stress fibers, lamellipodia, and filopodia. *Cell* **81**:53-62.

138. Burridge, K. and Chrzanowska-Wodnicka, M. 1996. Focal adhesions, contractility, and signaling. *Annu Rev Cell Dev Biol* **12**:463-518.

139. Vega, F.M. and Ridley, A.J. 2008. Rho GTPases in cancer cell biology. *FEBS Lett* **582**:2093-2101.

140. Cho, S.Y. and Klemke, R.L. 2002. Purification of pseudopodia from polarized cells reveals redistribution and activation of Rac through assembly of a CAS/Crk scaffold. *J Cell Biol* **156**:725-736.

141. Brugnera, E., Haney, L., Grimsley, C., Lu, M., Walk, S.F., Tosello-Trampont, A.C., Macara, I.G., Madhani, H., Fink, G.R., and Ravichandran, K.S. 2002. Unconventional Rac-GEF activity is mediated through the Dock180-ELMO complex. *Nat Cell Biol* **4**:574-582.

142. Makkinje, A., Vanden Borre, P., Near, R.I., Patel, P.S., and Lerner, A. 2012. Breast cancer anti-estrogen resistance 3 (BCAR3) protein augments binding of the c-Src SH3 domain to Crk-associated substrate (p130cas). *J Biol Chem* **287**:27703-27714.

143. Vanden Borre, P., Near, R.I., Makkinje, A., Mostoslavsky, G., and Lerner, A. 2011. BCAR3/AND-34 can signal independent of complex formation with CAS family members or the presence of p130Cas. *Cell Signal* **23**:1030-1040.

144. Burnham, M.R., Bruce-Staskal, P.J., Harte, M.T., Weidow, C.L., Ma, A., Weed, S.A., and Bouton, A.H. 2000. Regulation of c-SRC activity and function by the adapter protein CAS. *Mol Cell Biol* **20**:5865-5878.

145. Guilluy, C., Swaminathan, V., Garcia-Mata, R., O'brien, E.T., Superfine, R., and Burridge, K. 2011. The Rho GEFs LARG and GEF-H1 regulate the mechanical response to force on integrins. *Nat Cell Biol* **13**:722-727.

146. Ishizawar, R. and Parsons, S.J. 2004. c-Src and cooperating partners in human cancer. *Cancer Cell* **6**:209-214.

147. Finn, R.S. 2008. Targeting Src in breast cancer. *Ann Oncol* **19**:1379-1386.

148. Carey, L., Winer, E., Viale, G., Cameron, D., and Gianni, L. 2010. Triple-negative breast cancer: disease entity or title of convenience? *Nat Rev Clin Oncol* **7**:683-692.

149. Riggins, R.B., Quilliam, L.A., and Bouton, A.H. 2003. Synergistic promotion of c-Src activation and cell migration by Cas and AND-34/BCAR3. *J Biol Chem* **278**:28264-28273.

150. Corkery, B., Crown, J., Clynes, M., and O'donovan, N. 2009. Epidermal growth factor receptor as a potential therapeutic target in triple-negative breast cancer. *Ann Oncol* **20**:862-867.

151. Wyckoff, J., Wang, W., Lin, E.Y., Wang, Y., Pixley, F., Stanley, E.R., Graf, T., Pollard, J.W., Segall, J., and Condeelis, J. 2004. A paracrine loop between tumor cells and macrophages is required for tumor cell migration in mammary tumors. *Cancer Res* **64**:7022-7029.

152. Waterman-Storer, C. 2002. Fluorescent speckle microscopy (FSM) of microtubules and actin in living cells. *Curr Protoc Cell Biol* **Chapter 4**:Unit 4 10.

153. Elsberger, B., Tan, B.A., Mitchell, T.J., Brown, S.B., Mallon, E.A., Tovey, S.M., Cooke, T.G., Brunton, V.G., and Edwards, J. 2009. Is expression or activation of Src kinase associated with cancer-specific survival in ER-, PR- and HER2-negative breast cancer patients? *Am J Pathol* **175**:1389-1397.

154. Bellamy, C.O., Mcdonald, C., Salter, D.M., Chetty, U., and Anderson, T.J. 1993. Noninvasive ductal carcinoma of the breast: the relevance of histologic categorization. *Hum Pathol* **24**:16-23.

155. Levental, K.R., Yu, H., Kass, L., Lakins, J.N., Egeblad, M., Erler, J.T., Fong, S.F., Csiszar, K., Giaccia, A., Weninger, W., Yamauchi, M., Gasser, D.L., and Weaver, V.M. 2009. Matrix crosslinking forces tumor progression by enhancing integrin signaling. *Cell* **139**:891-906.

156. Lu, P., Weaver, V.M., and Werb, Z. 2012. The extracellular matrix: a dynamic niche in cancer progression. *J Cell Biol* **196**:395-406.

157. Butcher, D.T., Alliston, T., and Weaver, V.M. 2009. A tense situation: forcing tumour progression. *Nat Rev Cancer* **9**:108-122.

158. Tilghman, R.W., Cowan, C.R., Mih, J.D., Koryakina, Y., Gioeli, D., Slack-Davis, J.K., Blackman, B.R., Tschumperlin, D.J., and Parsons, J.T. 2010. Matrix rigidity regulates cancer cell growth and cellular phenotype. *PLoS One* **5**:e12905.

159. Espina, V. and Liotta, L.A. 2011. What is the malignant nature of human ductal carcinoma in situ? *Nat Rev Cancer* **11**:68-75.

160. Kilker, R.L. and Planas-Silva, M.D. 2006. Cyclin D1 is necessary for tamoxifen-induced cell cycle progression in human breast cancer cells. *Cancer Res* **66**:11478-11484.

161. Rudas, M., Lehnert, M., Huynh, A., Jakesz, R., Singer, C., Lax, S., Schippinger, W., Dietze, O., Greil, R., Stiglbauer, W., Kwasny, W., Grill, R., Stierer, M., Gnant, M.F., Filipits, M., Austrian, B., and Colorectal Cancer Study, G. 2008. Cyclin D1 expression in breast cancer patients receiving adjuvant tamoxifen-based therapy. *Clin Cancer Res* **14**:1767-1774.

162. Burandt, E., Grunert, M., Lebeau, A., Choschzick, M., Quaas, A., Janicke, F., Muller, V., Scholz, U., Bokemeyer, C., Petersen, C., Geist, S., Paluchowski, P., Wilke, C., Heilenkotter, U., Simon, R., Sauter, G., and Wilczak, W. 2014. Cyclin D1 gene amplification is highly homogeneous in breast cancer. *Breast Cancer*.

163. Husemann, Y., Geigl, J.B., Schubert, F., Musiani, P., Meyer, M., Burghart, E., Forni, G., Eils, R., Fehm, T., Riethmuller, G., and Klein, C.A. 2008. Systemic spread is an early step in breast cancer. *Cancer Cell* **13**:58-68.

164. Pape-Zambito, D., Jiang, Z., Wu, H., Devarajan, K., Slater, C.M., Cai, K.Q., Patchefsky, A., Daly, M.B., and Chen, X. 2014. Identifying a highly-aggressive DCIS subgroup by studying intra-individual DCIS heterogeneity among invasive breast cancer patients. *PLoS One* **9**:e100488.

165. Kang, Y. and Pantel, K. 2013. Tumor cell dissemination: emerging biological insights from animal models and cancer patients. *Cancer Cell* **23**:573-581.

166. Gauthier, M.L., Berman, H.K., Miller, C., Kozakeiwicz, K., Chew, K., Moore, D., Rabban, J., Chen, Y.Y., Kerlikowske, K., and Tlsty, T.D. 2007. Abrogated response to cellular stress identifies DCIS associated with subsequent tumor events and defines basal-like breast tumors. *Cancer Cell* **12**:479-491.

167. Harunaga, J.S. and Yamada, K.M. 2011. Cell-matrix adhesions in 3D. *Matrix Biol* **30**:363-368.

168. Fraley, S.I., Feng, Y., Krishnamurthy, R., Kim, D.H., Celedon, A., Longmore, G.D., and Wirtz, D. 2010. A distinctive role for focal adhesion proteins in three-dimensional cell motility. *Nat Cell Biol* **12**:598-604.

169. Kubow, K.E. and Horwitz, A.R. 2011. Reducing background fluorescence reveals adhesions in 3D matrices. *Nat Cell Biol* **13**:3-5; author reply 5-7.

170. Jayo, A. and Parsons, M. 2012. Imaging of cell adhesion events in 3D matrix environments. *Eur J Cell Biol* **91**:824-833.

171. Kubow, K.E., Conrad, S.K., and Horwitz, A.R. 2013. Matrix microarchitecture and myosin II determine adhesion in 3D matrices. *Curr Biol* **23**:1607-1619.

172. Deakin, N.O., Ballestrem, C., and Turner, C.E. 2012. Paxillin and Hic-5 interaction with vinculin is differentially regulated by Rac1 and RhoA. *PLoS One* **7**:e37990.

173. Karpova, T.S., Baumann, C.T., He, L., Wu, X., Grammer, A., Lipsky, P., Hager, G.L., and Mcnally, J.G. 2003. Fluorescence resonance energy transfer from cyan to yellow fluorescent protein detected by acceptor photobleaching using confocal microscopy and a single laser. *J Microsc* **209**:56-70.

174. Day, R.N. and Davidson, M.W. 2012. Fluorescent proteins for FRET microscopy: monitoring protein interactions in living cells. *Bioessays* **34**:341-350.

175. Conway, J.R., Carragher, N.O., and Timpson, P. 2014. Developments in preclinical cancer imaging: innovating the discovery of therapeutics. *Nat Rev Cancer* **14**:314-328.

176. Johnsson, A.K., Dai, Y., Nobis, M., Baker, M.J., Mcghee, E.J., Walker, S., Schwarz, J.P., Kadir, S., Morton, J.P., Myant, K.B., Huels, D.J., Segonds-Pichon, A., Sansom, O.J., Anderson, K.I., Timpson, P., and Welch, H.C. 2014. The Rac-FRET mouse reveals tight spatiotemporal control of Rac activity in primary cells and tissues. *Cell Rep* **6**:1153-1164.

177. Timpson, P., Mcghee, E.J., Morton, J.P., Von Kriegsheim, A., Schwarz, J.P., Karim, S.A., Doyle, B., Quinn, J.A., Carragher, N.O., Edward, M., Olson, M.F., Frame, M.C., Brunton, V.G., Sansom, O.J., and Anderson, K.I. 2011. Spatial regulation of RhoA activity during pancreatic cancer cell invasion driven by mutant p53. *Cancer Res* **71**:747-757.

178. Murphy, D.A. and Courtneidge, S.A. 2011. The 'ins' and 'outs' of podosomes and invadopodia: characteristics, formation and function. *Nat Rev Mol Cell Biol* **12**:413-426.

179. Gligorijevic, B., Wyckoff, J., Yamaguchi, H., Wang, Y., Roussos, E.T., and Condeelis, J. 2012. N-WASP-mediated invadopodium formation is involved in intravasation and lung metastasis of mammary tumors. *J Cell Sci* **125**:724-734.

180. Beaty, B.T. and Condeelis, J. 2014. Digging a little deeper: the stages of invadopodium formation and maturation. *Eur J Cell Biol* **93**:438-444.

181. Moshfegh, Y., Bravo-Cordero, J.J., Miskolci, V., Condeelis, J., and Hodgson, L. 2014. A Trio-Rac1-Pak1 signalling axis drives invadopodia disassembly. *Nat Cell Biol* **16**:574-586.

182. Magalhaes, M.A., Larson, D.R., Mader, C.C., Bravo-Cordero, J.J., Gil-Henn, H., Oser, M., Chen, X., Koleske, A.J., and Condeelis, J. 2011. Cortactin phosphorylation regulates cell invasion through a pH-dependent pathway. *J Cell Biol* **195**:903-920.

183. Stroka, K.M., Gu, Z., Sun, S.X., and Konstantopoulos, K. 2014. Bioengineering paradigms for cell migration in confined microenvironments. *Curr Opin Cell Biol* **30**:41-50.

184. Kedrin, D., Gligorijevic, B., Wyckoff, J., Verkhusha, V.V., Condeelis, J., Segall, J.E., and Van Rheenen, J. 2008. Intravital imaging of metastatic behavior through a mammary imaging window. *Nat Methods* **5**:1019-1021.

185. Charras, G. and Sahai, E. 2014. Physical influences of the extracellular environment on cell migration. *Nat Rev Mol Cell Biol* **15**:813-824.

186. Hung, W.C., Chen, S.H., Paul, C.D., Stroka, K.M., Lo, Y.C., Yang, J.T., and Konstantopoulos, K. 2013. Distinct signaling mechanisms regulate migration in unconfined versus confined spaces. *J Cell Biol* **202**:807-824.

187. Jenkins, D.E., Oei, Y., Hornig, Y.S., Yu, S.F., Dusich, J., Purchio, T., and Contag, P.R. 2003. Bioluminescent imaging (BLI) to improve and refine traditional murine models of tumor growth and metastasis. *Clin Exp Metastasis* **20**:733-744.

188. Rodriguez-Paredes, M. and Esteller, M. 2011. Cancer epigenetics reaches mainstream oncology. *Nat Med* **17**:330-339.

189. Gilkes, D.M., Xiang, L., Lee, S.J., Chaturvedi, P., Hubbi, M.E., Wirtz, D., and Semenza, G.L. 2014. Hypoxia-inducible factors mediate coordinated RhoA-ROCK1 expression and signaling in breast cancer cells. *Proc Natl Acad Sci U S A* **111**:E384-393.

190. Thiery, J.P. and Sleeman, J.P. 2006. Complex networks orchestrate epithelial-mesenchymal transitions. *Nat Rev Mol Cell Biol* **7**:131-142.

191. Wirtz, D., Konstantopoulos, K., and Searson, P.C. 2011. The physics of cancer: the role of physical interactions and mechanical forces in metastasis. *Nat Rev Cancer* **11**:512-522.

192. Thiery, J.P., Acloque, H., Huang, R.Y., and Nieto, M.A. 2009. Epithelial-mesenchymal transitions in development and disease. *Cell* **139**:871-890.

193. Abate-Shen, C. 2002. Deregulated homeobox gene expression in cancer: cause or consequence? *Nat Rev Cancer* **2**:777-785.

194. Nero, T.L., Morton, C.J., Holien, J.K., Wielens, J., and Parker, M.W. 2014. Oncogenic protein interfaces: small molecules, big challenges. *Nat Rev Cancer* **14**:248-262.

195. Cierpicki, T. and Grembecka, J. 2015. Targeting protein-protein interactions in hematologic malignancies: still a challenge or a great opportunity for future therapies? *Immunol Rev* **263**:279-301.

196. Bouton, A.H. and Burnham, M.R. 1997. Detection of distinct pools of the adapter protein p130CAS using a panel of monoclonal antibodies. *Hybridoma* **16**:403-411.

197. Wang, Y.L. and Pelham, R.J., Jr. 1998. Preparation of a flexible, porous polyacrylamide substrate for mechanical studies of cultured cells. *Methods Enzymol* **298**:489-496.

198. Schwartz, M.A. and Ginsberg, M.H. 2002. Networks and crosstalk: integrin signalling spreads. *Nat Cell Biol* **4**:E65-68.

199. Hu, Z., Xu, R., Liu, J., Zhang, Y., Du, J., Li, W., Zhang, W., Li, Y., Zhu, Y., and Gu, L. 2013. GEP100 regulates epidermal growth factor-induced MDA-MB-231 breast cancer cell invasion through the activation of Arf6/ERK/uPAR signaling pathway. *Exp Cell Res* **319**:1932-1941.

200. Song, X., Chen, X., Yamaguchi, H., Mouneimne, G., Condeelis, J.S., and Eddy, R.J. 2006. Initiation of cofilin activity in response to EGF is uncoupled from cofilin phosphorylation and dephosphorylation in carcinoma cells. *J Cell Sci* **119**:2871-2881.

201. Moro, L., Dolce, L., Cabodi, S., Bergatto, E., Boeri Erba, E., Smeriglio, M., Turco, E., Retta, S.F., Giuffrida, M.G., Venturino, M., Godovac-Zimmermann, J., Conti, A., Schaefer, E., Beguinot, L., Tacchetti, C., Gaggini, P., Silengo, L., Tarone, G., and Defilippi, P. 2002. Integrin-induced epidermal growth factor (EGF) receptor activation requires c-Src and p130Cas and leads to phosphorylation of specific EGF receptor tyrosines. *J Biol Chem* **277**:9405-9414.

202. Kang, Y.S., Kim, W., Huh, Y.H., Bae, J., Kim, J.S., and Song, W.K. 2011. P130Cas attenuates epidermal growth factor (EGF) receptor internalization by modulating EGF-triggered dynamin phosphorylation. *PLoS One* **6**:e20125.

203. Van Rheenen, J., Song, X., Van Roosmalen, W., Cammer, M., Chen, X., Desmarais, V., Yip, S.C., Backer, J.M., Eddy, R.J., and Condeelis, J.S. 2007. EGF-induced PIP2 hydrolysis releases and activates cofilin locally in carcinoma cells. *J Cell Biol* **179**:1247-1259.